

UCSF

UC San Francisco Electronic Theses and Dissertations

Title

Spectral and Image-guided Laser Ablation for Dental Applications

Permalink

<https://escholarship.org/uc/item/55f1j69q>

Author

Chan, Kenneth Henry

Publication Date

2018

Peer reviewed|Thesis/dissertation

Spectral and Image-guided Laser Ablation for Dental Applications

by
Kenneth Henry Chan

DISSERTATION

Submitted in partial satisfaction of the requirements for degree of
DOCTOR OF PHILOSOPHY

in

Oral and Craniofacial Sciences

in the

GRADUATE DIVISION

of the

UNIVERSITY OF CALIFORNIA, SAN FRANCISCO

Approved:

DocuSigned by:

Daniel Fried

Daniel Fried

A5D635A9DBEF486...

Chair

DocuSigned by:

Cynthia Darling

Cynthia Darling

DocuSigned by:36...

Michal Staninec

Michal Staninec

DocuSigned by:422...

Duygu Tosun-Turgut

Duygu Tosun-Turgut

A2C3822F2671486...

Committee Members

Copyright 2018

by

Kenneth Henry Chan

DEDICATION

To my family and friends. Thank you.

ACKNOWLEDGMENTS

This work was supported by NIH/NIDCR grants F31-DE026350, R01-DE19631, R01-DE14698, and T32-DE-07306.

Foremost, I would like to acknowledge and thank my dissertation advisor and mentor, Dr. Daniel Fried. His support, encouragement, patience, knowledge, and guidance have led me to finally finish my degree and complete my work. Thank you!

Besides my mentor, I would like to thank members of my dissertation and qualifying exam committee: Drs. Cynthia Darling, Michal Staninec, Duygu Tosun-Turgut, Xiaojuan Li, and Arthur Miller. Their expertise and knowledge have helped further my knowledge and dissertation.

I would also like to thank the current and past members of Dr. Daniel Fried's biophotonics lab, whom of which have assisted me in my projects and Drs. Hobin Kang, Robert CS Lee, Andrew T Jang, Jonathan Stahl, as well as the previous staff research associates, Henry Tom, Daniel Saltiel, and William A Fried. I would like to also acknowledge contributions made by Grace Nonomura and Charles Le. Much of my experimental work could not have been accomplished without their support.

Thank you to my graduate program advisor and Oral and Craniofacial Sciences program co-director, Dr. Pamela DenBesten and her co-director Dr. Ralph Marcucio for their guidance and training support. I would also like to acknowledge and thank Roger Mraz, Kathryn Gabriel, Arabella Teng, and Tran Luu, with whom made it possible for my fellowship award funding this very project.

Finally, I would like to acknowledge the following scientific journals and their publishers for their permission to use the following publications within this dissertation.

Chapter II

Used with permission from Lasers in Surgery and Medicine:

Chan, K.H., Hirasuna, K., and Fried, D. (2011). Selective removal of composite from tooth surfaces with a 9.3 μm CO_2 laser using spectral feedback. LSM 43:824-832.

Chapter III

Used with permission from Photonics Lasers Medicine:

Chan, K.H., Hirasuna, K., and Fried, D. (2014). Analysis of enamel surface damage after selective laser ablation of composite from tooth surfaces. Phot. Lasers Med. 3(1): 37-45.

Chapter IV

Used with permission from Lasers in Surgery and Medicine:

Jang, A.T., Chan, K.H., and Fried, D. (2017). Automated ablation of dental composite using an IR pulsed laser coupled to a plume emission spectral feedback system. LSM 49:658-665.

Chapter V

Used with permission from Journal of Biophotonics:

Chan, K.H., Chan, A.C., Fried, W.A., Simon, J.C., Darling, C.L., and Fried, D. (2015). Use of 2D images of depth and integrated reflectivity to represent the severity of demineralization in cross-polarization optical coherence tomography. J. Biophotonics 8(0): 36-45.

Chapter VI

Used with permission from Journal of Biomedical Optics Express:

Chan, K.H., and Fried D. (2018). Multispectral cross-polarization reflectance measurements suggest high contrast of demineralization on tooth surfaces at wavelengths beyond 1300 nm due to reduced light scattering in sound enamel. J. Biomed. Opt. 23(6):1-4.

Chapter VII

Used with permission from Lasers in Surgery and Medicine:

Chan, K.H., and Fried, D. (2018) Selective ablation of dental caries using coaxial CO_2 (9.3- μm) and near-IR (1880-nm) lasers. LSM (in press)

Spectral and Image-guided Laser Ablation for Dental Applications

Kenneth Henry Chan

Abstract

Although there has been progress in reducing the incidence of dental decay, dental caries remains a significant health problem and a new approach towards the treatment of dental caries with an emphasis on early detection and minimal intervention would be a significant step forward. Systems that can rapidly and selectively remove caries and/or composite from tooth surfaces while minimizing the inadvertent removal of healthy tooth structure would be a significant improvement over current methods. These fundamental studies will significantly advance our overall knowledge of laser-tissue interactions and facilitate the development of safer and more efficient laser systems for the removal of dental caries and restorative materials.

The overall objective of this proposed research is to develop laser-based methods for the selective removal of dental caries and composite restorative materials using an integrated approach of computer-controlled laser-scanning coupled with methods of feedback. In addition to eliminating unpleasant noise and vibration associated with conventional dental handpieces, lasers deliver unparalleled precision, and sterilize tissue. The objective of this proposal will be achieved through the following two specific aims: (1) Test the hypothesis that near-IR imaging systems can be combined with IR laser systems for the image-guided selective ablation of carious lesions; and (2) Test the hypothesis that spectral analysis can be used with a pulsed CO₂ laser system for the selective removal of dental composites and sealants. These fundamental studies will significantly further our knowledge of the interaction of laser radiation with dental hard

tissues and aid the development of safer and more effective feedback-guided laser systems over existing methods for the removal of dental caries and restorative materials. Furthermore, laser feedback systems have the potential to globally advance the standard of healthcare with increased conservative care for cavity preparations and dental restoration replacement procedures.

TABLE OF CONTENTS

CHAPTER I INTRODUCTION.....	1
1.1 DISSERTATION MOTIVATION AND SIGNIFICANCE.....	2
1.2 DENTAL CARIES AND RESTORATIONS	4
1.3 LASERS	5
1.4 FEEDBACK MECHANISMS	6
1.4.1 Near – infrared imaging	7
1.4.2 Plume spectroscopy	8
1.5 SELECTIVITY ANALYSIS	8
1.5.1 Polarized light microscopy	8
1.5.2 Polarization – sensitive optical coherence tomography	9
1.6 OBJECTIVE	10
1.7 FIGURES AND FIGURE LEGENDS.....	12
1.8 REFERENCES	14
CHAPTER II SPECTRAL GUIDANCE LASER REMOVAL OF COMPOSITE.....	19
2.1 SUMMARY	20
2.2 INTRODUCTION	21
2.3 MATERIALS AND METHODS.....	24
2.3.1 Sample Preparation and Simulated Lesion Models.....	24
2.3.2 Tissue Irradiation and Laser Parameters.....	24
2.3.3 Plume Emission Spectroscopy	25
2.3.4 Ablation Rate Measurements	26
2.3.5 Heat Accumulation Measurements	27

2.3.6	Optical Microscopy	27
2.3.7	Optical Feedback and Selective Removal	28
2.4	RESULTS.....	30
2.5	DISCUSSION	32
2.6	FIGURES AND FIGURE LEGENDS.....	37
2.7	REFERENCES	45
CHAPTER III ANALYSIS OF ENAMEL SURFACE DAMAGE AFTER SELECTIVE		
LASER ABLATION OF COMPOSITE FROM TOOTH SURFACES		
		49
3.1	SUMMARY	50
3.2	INTRODUCTION	51
3.3	MATERIALS AND METHODS.....	54
3.3.1	Tooth Samples.....	54
3.3.2	Laser System.....	55
3.3.3	Computer-controlled Laser Scanning System with Spectral Feedback.....	55
3.3.4	Composite Ablation Rate Measurements	56
3.3.5	Measurements of Heat Accumulation and the Time Required for Removal.	57
3.3.6	Measurements of Enamel Loss and Volume of Composite/Enamel Removed (Groups #2 and #3)	58
3.3.7	Statistical Analysis	60
3.4	RESULTS.....	60
3.4.1	Composite Ablation Rate Measurements	60
3.4.2	Measurements of Heat Accumulation for Removal (Group #1)	61

3.4.3 Measurements of Enamel Loss and Volume of Composite/Enamel Removed (Groups #2 and #3)	61
3.5 DISCUSSION	63
3.6 FIGURES AND FIGURE LEGENDS	66
3.7 REFERENCES	73
 CHAPTER IV DEVELOPING AND ASSESSING AN INTEGRATED SPECTRAL GUIDED LASER SYSTEM FOR AUTOMATED COMPOSITE REMOVAL	
4.1 SUMMARY	77
4.2 INTRODUCTION	77
4.3 MATERIALS AND METHODS	80
4.3.1 Tooth Samples	80
4.3.2 Clinical Laser Scanning System for Composite Removal	81
4.3.3 Cross Polarization Optical Coherence Tomography (CP-OCT) System	82
4.3.4 Volumetric Analysis	83
4.4 RESULTS	84
4.4.1 Plume Emission Analysis	84
4.4.2 Volumetric Measurements	84
4.4.3 Clinical Handpiece Results	84
4.5 DISCUSSION	85
4.6 FIGURES AND FIGURE LEGENDS	89
4.7 REFERENCES	96
 CHAPTER V 2D VISUALIZATION AND DETECTION OF DENTAL LESION SEVERITY	
	100

5.1 SUMMARY	101
5.2 INTRODUCTION	101
5.3 MATERIALS AND METHODS.....	108
5.3.1 Samples and Lesion Preparation.....	108
5.3.2 Polarization Sensitive Optical Coherence Tomography (PS-OCT) System	110
5.3.3 Image Analysis	111
5.4 RESULTS AND DISCUSSION.....	112
5.5 FIGURES AND FIGURE LEGENDS.....	119
5.6 REFERENCES	128
 CHAPTER VI MULTISPECTRAL CROSS-POLARIZATION REFLECTANCE	
MEASUREMENTS OF DEMINERALIZATION ON TOOTH SURFACES	131
6.1 SUMMARY	132
6.2 INTRODUCTION.....	132
6.3 MATERIALS AND METHODS.....	135
6.3.1 Sample Preparation	135
6.3.2 Near-Infrared Reflectance Imaging System and Laser Sources	136
6.3.3 NIR Reflectance Image Acquisition and Analysis.....	137
6.4 RESULTS.....	137
6.5 DISCUSSION	138
6.6 FIGURES AND FIGURE LEGENDS.....	140
6.7 REFERENCES	144
 CHAPTER VII SELECTIVE ABLATION OF DENTAL CARIES USING COAXIAL CO₂	
AND NEAR-INFRARED LASERS	147

7.1 SUMMARY	148
7.2 INTRODUCTION	148
7.3 MATERIALS AND METHODS.....	152
7.3.1 Sample Preparation	152
7.3.2 Coaxial NIR/CO ₂ Laser System	153
7.3.3 Lesion Segmentation and Removal.....	154
7.3.4 Polarization Sensitive – Optical Coherence Tomography (PS-OCT)	156
7.3.5 Processing of PS-OCT Images and Analysis of Selectivity	157
7.3.6 Digital Microscopy.....	159
7.4 RESULTS.....	159
7.5 DISCUSSION	161
7.6 FIGURES AND FIGURE LEGENDS.....	165
7.7 REFERENCES	171
8.1.1 Spectral – guided composite ablation.....	176
8.1.2 Near – Infrared image guided caries ablation.....	177
8.2 FUTURE WORK.....	178
8.3 REFERENCES	179

LIST OF FIGURES

CHAPTER I:

Figure 1.1.....	12
Figure 1.2.....	13

CHAPTER II:

Figure 2.1.....	37
Figure 2.2.....	38
Figure 2.3.....	39
Figure 2.4.....	40
Figure 2.5.....	41
Figure 2.6.....	42
Figure 2.7.....	43
Figure 2.8.....	44

CHAPTER III:

Figure 3.1.....	66
Figure 3.2.....	67
Figure 3.3.....	68
Figure 3.4.....	69
Figure 3.5.....	70
Figure 3.6.....	71
Figure 3.7.....	72

CHAPTER IV:

Figure 4.1.....89
Figure 4.2.....90
Figure 4.3.....91
Figure 4.4.....92
Figure 4.5.....93
Figure 4.6.....94
Figure 4.7.....95

CHAPTER V:

Figure 5.1.....119
Figure 5.2.....120
Figure 5.3.....121
Figure 5.4.....122
Figure 5.5.....123
Figure 5.6.....124
Figure 5.7.....125
Figure 5.8.....126
Figure 5.9.....127

CHAPTER VI:

Figure 6.1.....140
Figure 6.2.....141
Figure 6.3.....142
Figure 6.4.....143

CHAPTER VII:

Figure 7.1.....165
Figure 7.2.....166
Figure 7.3.....167
Figure 7.4.....168
Figure 7.5.....169
Figure 7.6.....170

CHAPTER I
INTRODUCTION

1.1 DISSERTATION MOTIVATION AND SIGNIFICANCE

Lasers can be used by dental clinicians to provide a number of unique and effective treatment options in dentistry, including: soft tissue vaporization with hemostasis, removal (ablation) of carious and noncarious dental hard tissues, preventive laser-treatment on enamel surfaces to inhibit caries, and surface conditioning for improved adhesion to composite restorative materials (Miserendino & Pick, 1995; Stern & Sognnaes, 1964; H. A. Wigdor et al., 1995). New and more sensitive optical methods for caries detection are now available that allow acquisition of 2 and 3-dimensional (3D) images of caries' location, depth, and severity on tooth surfaces. Such imaging systems are ideally suited for the integration with computer controlled laser scanning systems for the precise removal of dental caries and composite restorative materials.

Lasers are ideally suited for the conservative and selective removal of carious tissue in the pits and fissures of occlusal tooth surfaces and for the thermal sterilization of such surfaces (R. Hibst, Graser, Udart, & Stock, 2010; Leco-Berrocal, Martinez-Gonzalez, Donado-Rodriguez, & Lopez-Carriches, 2006). Such surfaces are often filled with composite sealants and the same lasers can also be used to selectively remove that composite with minimal loss of sound enamel (Chan, Hirasuna, & Fried, 2011; T. M. Louie, Jones, Sarma, & Fried, 2005). Dentists spend more time replacing existing restorations that fail due to microleakage and secondary caries than placing new restorations (Bernardo et al., 2007; Gordan et al., 2009). Tooth colored restorations are a challenge to differentiate from the surrounding tooth structure, particularly near the interfaces of the restoration. All of the existing composite from a restoration must be removed to ensure proper bonding of new composite to the tooth structure, since new

composite does not bond well to residual composite. Hence, clinicians frequently remove excessive amounts of healthy tooth structure to ensure complete removal of the composite (Hong & Lew, 1995; R G Oliver, 1988). Therefore, a system that can rapidly and selectively remove composite from tooth surfaces while minimizing the inadvertent removal of healthy tooth structure would be a significant improvement over current methods. The use of highly selective laser systems for the removal of dental caries and dental composites is likely to lead to the practice of more conservative dental procedures that will reduce the amount of healthy tissue loss that is generally associated with conventional cavity preparations and the repair of existing composite restorations.

New caries diagnostics can be used to identify early carious lesions before they have spread extensively into the underlying dentin. By taking an early preventive laser treatment approach, the dentist can intervene in a conservative manner before the lesion has progressed to the point that more invasive surgical intervention is necessary. Furthermore, under the appropriate irradiation conditions are met, the walls will have enhanced resistance to acid dissolution and improved adhesion properties for bonding (Konishi, Fried, Featherstone, & Staninec, 1999; Young, Fried, & Featherstone, 2000). However, 3D caries detection systems are highly time and resource intensive to be used practically with lasers and the *a priori* data of the 3D lesion structure cannot be reliably positioned with the laser alone for precise removal, thus an integrated laser scanning system coupled with a real-time feedback mechanism is necessary. The spectral and image-guided approaches developed in this dissertation offer an innovative and practical method to selectively ablate carious lesions and composites.

1.2 DENTAL CARIES AND RESTORATIONS

Although there has been progress in reducing the incidence of dental decay, dental caries remains a significant public health problem. Tooth decay or dental caries is a disease that afflicts over 91% of the adult population in the US (B. Dye, Thornton-Evans, Li, & Iafolla, 2015). A new approach towards the treatment of dental caries with an emphasis on early detection and minimal intervention would be a significant step forward (Anusavice, 1995; Harris & Garcia-Godoy, 1999).

Several developments are driving the shift to more conservative approaches to restorative dentistry and these include: new and more sensitive methods of caries detection, the development of new effective adhesive restorative materials, and the public's demand for more aesthetic restorations. Over the past 50 years, the nature of dental caries has changed with 90% of new lesions forming in high-risk pits and fissures (occlusal surfaces) of posterior teeth (Harris & Garcia-Godoy, 1999; Mertz-Fairhurst, 1992). The quality of sealant placement depends on the condition of fissure surfaces. Incomplete removal of demineralized carious tissue or cariogenic bacteria in the fissure can harbor an active biofilm (Fejerskov & Kidd, 2003) and can reduce the adhesive properties (Hevinga, Opdam, Frencken, Bronkhorst, & Truin, 2007, 2008; Kidd, 2004). Dental caries is the demineralization of tooth structure due to acids made by bacteria. Cariogenic bacteria metabolize fermentable carbohydrates to organic acids which dissolve tooth structure, namely enamel and dentin (John D. B. Featherstone, Le, Hsu, Manesh, & Fried, 2008). Enamel and dentin are comprised of a hydroxyapatite mineral that contain defects and impurities, including carbonated hydroxyapatite, which is highly soluble and more susceptible to demineralization (John D. B. Featherstone et al., 2008).

Dental restorations are used to restore the structural and functional integrity of the missing tooth structure caused from dental caries. However, dental restorations are not permanent and need to be replaced. Dentists spend more time replacing restorations than applying new ones. Studies have shown that teeth in which restorations are replaced lose a significant amount of healthy tooth structure (Gordan, 2001; Gordan, Mondragon, & Shen, 2002). This becomes problematic since dental restorations require existing sound tooth structure and over time, a dental restoration cannot be replaced. New tools are necessary for minimizing the inadvertent removal of sound tissue.

1.3 LASERS

Lasers offer the potential for minimally invasive surgery and reducing the amount of sound tissue removed. Lasers can also be used to target specific tissues by choosing a wavelength coincident with its high absorption. As of now, there are only three lasers that are FDA cleared for treatment of dental hard tissues: the erbium-doped yttrium scandium gallium garnet (Er:YSGG) which operates at 2.79; erbium-doped yttrium aluminium garnet laser (Er:YAG) at 2.94 μm ; and the carbon dioxide laser (CO_2) operating between 9.4 – 10.6 μm . These lasers are well suited for dental hard tissue ablation, however they remove tissues with different mechanisms (Figure 1.1) (J. D. B. Featherstone & Fried, 2001). The output of Er:YSGG and Er:YAG lasers is highly absorbed by the interstitial water between enamel prisms and creates a sudden water expansion that removes dental tissue, whereas the CO_2 laser is highly absorbed by the phosphate group in hydroxyapatite (Figure 1.1). Previous studies have suggested that the CO_2 laser operating at a non-ablative fluence can alter the chemical composition of enamel crystal (J. D. B. Featherstone, Barrett-Vespone, Fried, Kantorowitz, &

Lofthouse, 1998). Irradiated carbonated hydroxyapatite has been demonstrated to thermally decompose into a purer phase of hydroxyapatite thus becoming more acid resistant and preventing further tooth decay/demineralization from occurring. Studies have also been done to assess the clinical safety of using a high-speed scanning ablation of dental hard tissues using the CO₂ laser and demonstrated that enamel and dentin surfaces can be rapidly ablated by short-pulsed CO₂ lasers with minimal peripheral thermal and mechanical damage and without excessive heat accumulation (Nguyen et al., 2011).

1.4 FEEDBACK MECHANISMS

The precision and benefits of using lasers for dentistry cannot be fully utilized with current conventional caries detection. Current caries detection involves visual and tactile techniques which are subject to clinician bias: namely the examiners' visual acuity, differences in tactile sensitivity, direct/indirect lighting, the use of magnifying eyewear, patient position, instrument used for assessment, and interactions between the clinician and patient can alter the diagnosis of caries lesion (K. Ekstrand, Qvist, & Thylstrup, 1987; K. R. Ekstrand, Zero, Martignon, & Pitts, 2009). Conventional X-rays are not sensitive for detecting enamel demineralization and in most cases, lesions that are radiographically detected are lesions that have progressed well into the dentin. Furthermore, the mineral content of demineralized enamel is highly variable and accurately predicting the amount of laser pulses for precise lesion removal is not ideal. Thus a scanning system coupled with a real-time feedback mechanism is necessary for selective caries removal. Transverse microradiography (TMR) and polarized light microscopy (PLM) are both gold standard methods for detecting caries, however they

require the destruction of the tooth making both methods unsuitable for *in vivo*. Novel minimally invasive feedback mechanisms need to be developed for precisely guiding lasers to ablate areas of demineralization or for removing preexisting restorations.

1.4.1 Near – infrared imaging

Near-infrared (NIR) imaging wavelengths of light are highly transmissible through dental hard tissues. At longer NIR wavelengths, the scattering coefficient of enamel decreases, allowing deeper light penetration and decreased backscattered light in sound enamel structure. The light scattering in sound enamel decreases as $1/\lambda^3$ with increasing wavelength from 400 to 1300 nm (Figure 1.2) (D. Fried et al., 1995). Wavelengths beyond 1300 nm may continue to have decreased light scattering and yield higher lesion contrast, but at these wavelengths, light absorption is difficult to measure and warrants investigation. Additionally, wavelengths coincident with water absorption bands, namely 1450, 1880, and 1950-nm have high water absorption (29, 31, and 113-cm^{-1} , respectively) (Hale & Querry, 1973). Interstitial water trapped between enamel prisms and water within the underlying dentin highly absorb these wavelengths and cause sound enamel to appear opaque. In contrast, light scattering appears in the lesion body deriving from the porous structure of the demineralization. This can be exploited to acquire high contrast areas of lesion activity for laser removal (Chung, Fried, Staninec, & Darling, 2011; Simon, Chan, Darling, & Fried, 2014). In addition, NIR imaging is advantageous over conventional techniques since stains which normally confound caries diagnosis do not interfere in the NIR range (Buhler, Ngaotheppitak, & Fried, 2005; Chung et al., 2011; R. S. Jones, G. D. Huynh, G. C. Jones, & D. Fried, 2003; Simon et al., 2014; Staninec, Lee, Darling, & Fried, 2010; Wu & Fried, 2009;

Zakian, Pretty, & Ellwood, 2009). Thus, NIR reflectance imaging is well suited for guiding selective caries laser ablation.

1.4.2 Plume spectroscopy

During ablation, a distinct emission plume that is characteristic of the ablated tissue's atomic and molecular emission lines is visible and can be used to determine the composition of the target. Studies have demonstrated that the spectra of tooth ablation can be discriminated from that of composite ablation by the strong calcium emission lines in the tooth ablation plume, which are not present in conventional composite ablation plume (Alexander & Fried, 2001; T Dumore & D Fried, 2000). By using a CO₂ laser, plume emission spectra can be collected over the tooth surface and composite restorations can be identified and removed in a sequential process without excessive damage to the underlying enamel.

1.5 SELECTIVITY ANALYSIS

New tools are also needed for quantifying selective lesion removal. There are now technologies that are capable of rendering 3D images of the tooth and quantifying the lesion volume *in vivo*. Image processing techniques can be applied to these 3D data sets for accurately determining the volume of the lesion body prior to removal and of the sound tissue after removal.

1.5.1 Polarized light microscopy

Sound enamel prisms are highly ordered and naturally birefringent. When polarized light is transmitted through a thin slice of sound enamel, this causes a rotation in the phase of polarized light but not complete light attenuation. On the other hand, demineralized enamel is highly scattering due to its porous nature and scrambles the incident

polarized light and attenuates the path of light. This can be used for detecting demineralization and measuring the lesion depth. However this process requires the destruction of the tooth and is not ideal for determining the selectivity of lesion removal.

1.5.2 Polarization – sensitive optical coherence tomography

Polarization – sensitive optical coherence tomography (PS-OCT) is a non-invasive technique that is based on a Michelson white light interferometer and creates 3D data of the internal structure. Polarization sensitivity is essential for resolving the early caries lesions from sound tooth structure. As previously mentioned, enamel is transparent at 1300-nm, however dental caries causes an increase in the scattering coefficient by 1-2 orders of magnitude at this wavelength (Darling, Huynh, & Fried, 2006). This causes strong reflective intensities in the orthogonal polarization state that can be measured and quantified as the lesion volume (M. H. Le, Darling, & Fried, 2010). Studies have shown that the lesion reflectivity derived from orthogonally polarized optical coherence tomography is analogous to the integrated mineral loss, ΔZ , through comparison with transverse microradiography (Arends, Ruben, & Inaba, 1997; Jones, Darling, Featherstone, & Fried, 2006; P Ngaotheppitak, C L Darling, & D Fried, 2005). Surface reflections that normally mask the lesion reflectivity are omitted in orthogonally polarized optical coherence tomographic scans, but are present in the parallel polarized scans. These surface reflections can be processed to acquire the 3D surface structure of the tooth and can be registered before and after lesion removal to quantify the removal volume. Comparing the removal volume with the lesion volume can elucidate the selectivity of lesion removal.

1.6 OBJECTIVE

Current tools now exist that can improve conservative care in dentistry. Minimally invasive procedures can prolong the tooth's lifetime and decrease the need for highly invasive and costly procedures such as dental implants and prosthetics. Lasers are ubiquitously used in medicine and its therapeutic safety has been thoroughly investigated. The overall objective is to develop laser-based methods for dentistry, namely the selective removal of dental caries and composite restorative materials using an integrated approach of computer-controlled laser – scanning coupled with methods of feedback. The objective of this dissertation will be achieved through the following two specific aims: (1) Test the hypothesis that spectral analysis can be used with a pulsed CO₂ laser system for the selective removal of dental composites and sealants (**Chapters II-IV**); and (2) Test the hypothesis that near-IR imaging systems can be combined with IR laser systems for the image-guided selective ablation of carious lesions (**Chapters V-VII**). Previous studies have demonstrated that the optical emission spectra can be used to differentiate between enamel (T Dumore & D Fried, 2000), and a spectral-guided feedback system was developed in **Chapter II** and its safety and the irradiated surface evaluated in **Chapter III**. This system was later miniaturized and optimized using fiber optic probes and the selectivity of composite removal was determined in **Chapter IV**. Previous studies have shown that lasers can be guided by high contrast lesion images for subsequent removal (Chan & Fried, 2012), however assessing their selectivity remained a challenge. **Chapter V** outlines a method for analyzing lesion depth and surface morphology using optical coherence tomography to be used for analyzing the selectivity of laser removal. **Chapter VI** explored using longer

wavelengths for determining the best wavelength for imaging dental lesions. **Chapter VII** describes development of an image-guided laser system using this wavelength and analyzed the selective removal with optical coherence tomography. These fundamental studies will significantly further our knowledge of the interaction of laser radiation with dental hard tissues and aid the development of safer and more effective feedback-guided laser systems over existing methods for the removal of dental caries and restorative materials. Furthermore, laser feedback systems have the potential to globally advance the standard of healthcare with increased conservative care for cavity preparations and dental restoration replacement procedures.

1.7 FIGURES AND FIGURE LEGENDS

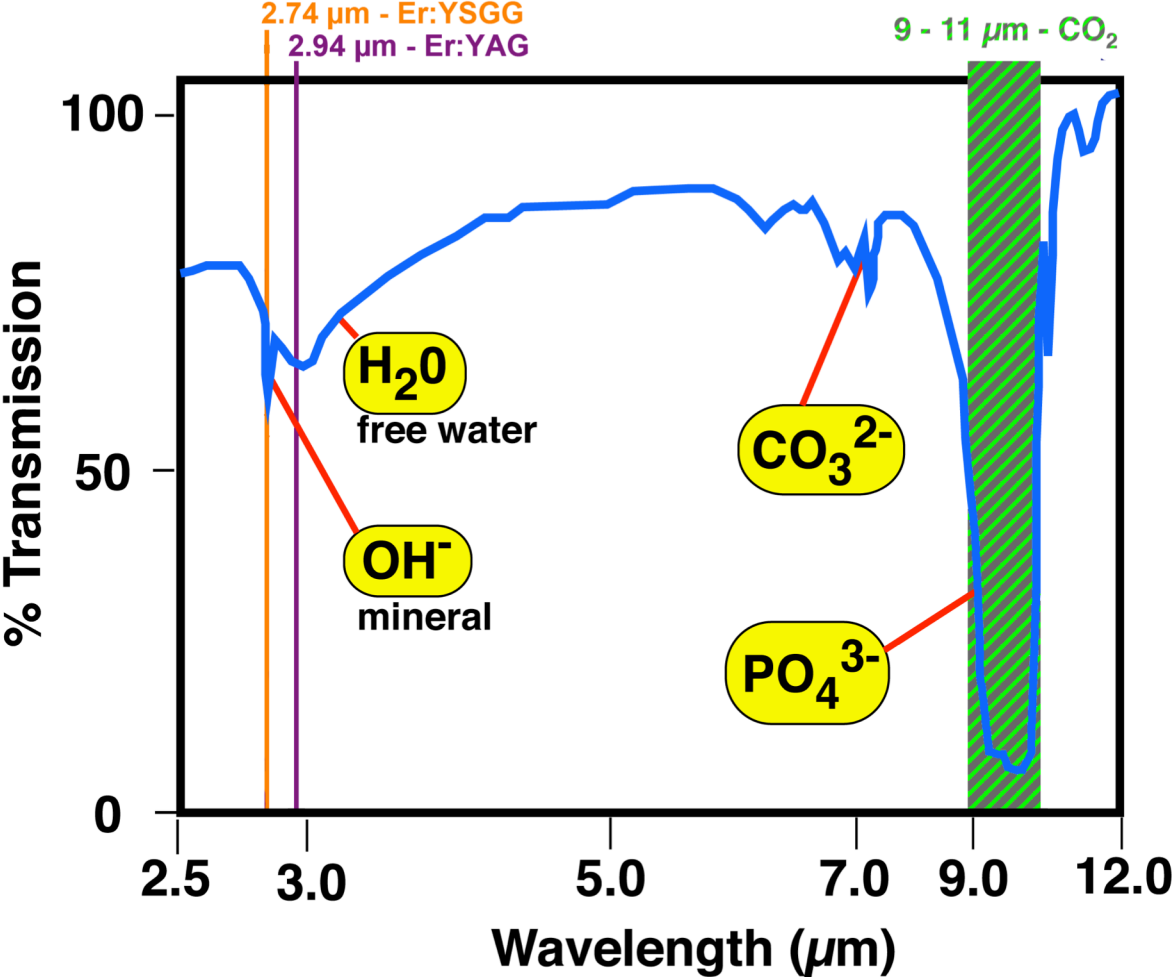


Figure 1.1: Infrared transmission spectrum of dental hard tissues. Note the low transmittance/high absorption of the phosphate group found in hydroxyapatite by the CO₂ laser.

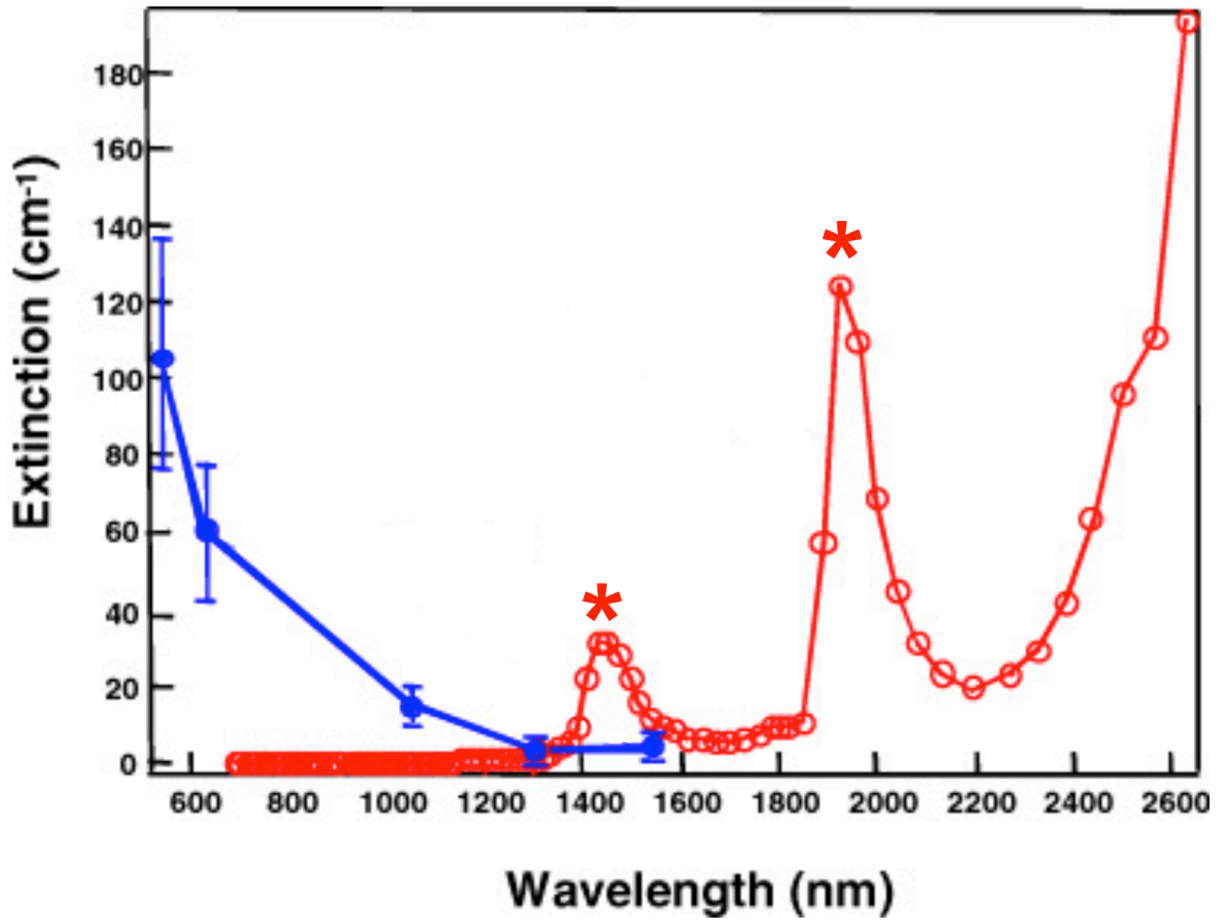


Figure 1.2: Enamel attenuation spectra (blue) and water absorption spectra (red). Notable water absorption peaks are found at 1450 and 1940 nm (28.6 and 119 cm^{-1} , respectively).

1.8 REFERENCES

Alexander, R., & Fried, D. (2001). Selective Removal of Orthodontic Composite using 355-nm Q-switched Laser Pulses, *Lasers in Surgery and Medicine*, 30 240-245 (2002). *Lasers in Surg. Med.*, 30, 240-245.

Anusavice, K. J. (1995). Treatment regimens in preventive and restorative dentistry. *JADA*, 126, 727-743.

Arends, J., Ruben, J. L., & Inaba, D. (1997). Major topics in quantitative microradiography of enamel and dentin: R parameter, mineral distribution visualization, and hyper-remineralization. *Adv Dent Res*, 11(4), 403-414.

Bernardo, M., Luis, H., Martin, M. D., Leroux, B. G., Rue, T., Leitao, J., & DeRouen, T. A. (2007). Survival and reasons for failure of amalgam versus composite posterior restorations placed in a randomized clinical trial. *Journal of the American Dental Association*, 138(6), 775-783.

Buhler, C., Ngaotheppitak, P., & Fried, D. (2005). Imaging of occlusal dental caries (decay) with near-IR light at 1310-nm. *Optics Express*, 13(2), 573-582.

Chan, K. H., Hirasuna, K., & Fried, D. (2011). Rapid and Selective Removal of Composite from Tooth Surfaces with a 9.3- μ m CO₂ Laser using Spectral Feedback. *Lasers in Surgery and Medicine*, 43(8), 824-832.

Chung, S., Fried, D., Staninec, M., & Darling, C. L. (2011). Multispectral near-IR reflectance and transillumination imaging of teeth. *Biomedical Optics Express*, 2(10), 2804-2814.

Darling, C. L., Huynh, G. D., & Fried, D. (2006). Light scattering properties of natural and artificially demineralized dental enamel at 1310 nm. *Journal of Biomedical Optics*, 11(3), 34023.

Dumore, T., & Fried, D. (2000). Selective Ablation of Orthodontic Composite using Sub-microsecond IR laser pulses with Optical Feedback. *Lasers Surg. Med.*, 27(2), 103-110.

Dye, B., Thornton-Evans, G., Li, X., & Iafolla, T. (2015). Dental caries and tooth loss in adults in the United States, 2011-2012. *NCHS Data Brief*(197), 197.

Ekstrand, K., Qvist, V., & Thylstrup, A. (1987). Light microscope study of the effect of probing in occlusal surfaces. *Caries Res*, 21(4), 368-374.

Ekstrand, K. R., Zero, D. T., Martignon, S., & Pitts, N. B. (2009). Lesion activity assessment. *Monographs in oral science*, 21, 63-90.

Featherstone, J. D. B., Barrett-Vespone, N. A., Fried, D., Kantorowitz, Z., & Lofthouse, J. (1998). CO₂ laser inhibition of artificial caries-like lesion progression in dental enamel. *J Dent Res*, 77(6), 1397-1403.

Featherstone, J. D. B., & Fried, D. (2001). Fundamental Interactions of Lasers with Dental hard Tissue. *Med. Laser Appl*, 16, 181-195.

Featherstone, J. D. B., Le, C. Q., Hsu, D., Manesh, S., & Fried, D. (2008). *Changes in acid resistance of dentin irradiated by a CW 10.6 μm CO₂ laser*. Paper presented at the Dental Materials, San Jose, CA, USA.

Fejerskov, O., & Kidd, E. (Eds.). (2003). *Dental Caries: The Disease and its Clinical Management*. Oxford: Blackwell.

Fried, D., Glana, R. E., Featherstone, J. D., & Seka, W. (1995). Nature of light scattering in dental enamel and dentin at visible and near-infrared wavelengths. *Applied optics*, 34(7), 1278-1285.

Gordan, V. V. (2001). Clinical evaluation of replacement of class V resin based composite restorations. *J Dent*, 29(7), 485-488.

Gordan, V. V., Garvan, C. W., Richman, J. S., Fellows, J. L., Rindal, D. B., Qvist, V., . . . Gilbert, G. H. (2009). How dentists diagnose and treat defective restorations: evidence from the dental practice-based research network. *Operative dentistry*, 34(6), 664-673.

Gordan, V. V., Mondragon, E., & Shen, C. (2002). Replacement of resin-based composite: evaluation of cavity design, cavity depth, and shade matching. *Quintessence Int*, 33(4), 273-278.

Hale, G. M., & Querry, M. R. (1973). Optical constants of water in the 200-nm to 200-μm wavelength region. *Appl. Optics*, 12, 555-563.

Harris, N., & Garcia-Godoy, F. (1999). *Primary Preventive Dentistry* (5th ed.). Stamford, CT: Appleton & Lange.

CHAPTER I
INTRODUCTION

1.1 DISSERTATION MOTIVATION AND SIGNIFICANCE

Lasers can be used by dental clinicians to provide a number of unique and effective treatment options in dentistry, including: soft tissue vaporization with hemostasis, removal (ablation) of carious and noncarious dental hard tissues, preventive laser-treatment on enamel surfaces to inhibit caries, and surface conditioning for improved adhesion to composite restorative materials (Miserendino & Pick, 1995; Stern & Sognnaes, 1964; H. A. Wigdor et al., 1995). New and more sensitive optical methods for caries detection are now available that allow acquisition of 2 and 3-dimensional (3D) images of caries' location, depth, and severity on tooth surfaces. Such imaging systems are ideally suited for the integration with computer controlled laser scanning systems for the precise removal of dental caries and composite restorative materials.

Lasers are ideally suited for the conservative and selective removal of carious tissue in the pits and fissures of occlusal tooth surfaces and for the thermal sterilization of such surfaces (R. Hibst, Graser, Udart, & Stock, 2010; Leco-Berrocal, Martinez-Gonzalez, Donado-Rodriguez, & Lopez-Carriches, 2006). Such surfaces are often filled with composite sealants and the same lasers can also be used to selectively remove that composite with minimal loss of sound enamel (Chan, Hirasuna, & Fried, 2011; T. M. Louie, Jones, Sarma, & Fried, 2005). Dentists spend more time replacing existing restorations that fail due to microleakage and secondary caries than placing new restorations (Bernardo et al., 2007; Gordan et al., 2009). Tooth colored restorations are a challenge to differentiate from the surrounding tooth structure, particularly near the interfaces of the restoration. All of the existing composite from a restoration must be removed to ensure proper bonding of new composite to the tooth structure, since new

composite does not bond well to residual composite. Hence, clinicians frequently remove excessive amounts of healthy tooth structure to ensure complete removal of the composite (Hong & Lew, 1995; R G Oliver, 1988). Therefore, a system that can rapidly and selectively remove composite from tooth surfaces while minimizing the inadvertent removal of healthy tooth structure would be a significant improvement over current methods. The use of highly selective laser systems for the removal of dental caries and dental composites is likely to lead to the practice of more conservative dental procedures that will reduce the amount of healthy tissue loss that is generally associated with conventional cavity preparations and the repair of existing composite restorations.

New caries diagnostics can be used to identify early carious lesions before they have spread extensively into the underlying dentin. By taking an early preventive laser treatment approach, the dentist can intervene in a conservative manner before the lesion has progressed to the point that more invasive surgical intervention is necessary. Furthermore, under the appropriate irradiation conditions are met, the walls will have enhanced resistance to acid dissolution and improved adhesion properties for bonding (Konishi, Fried, Featherstone, & Staninec, 1999; Young, Fried, & Featherstone, 2000). However, 3D caries detection systems are highly time and resource intensive to be used practically with lasers and the *a priori* data of the 3D lesion structure cannot be reliably positioned with the laser alone for precise removal, thus an integrated laser scanning system coupled with a real-time feedback mechanism is necessary. The spectral and image-guided approaches developed in this dissertation offer an innovative and practical method to selectively ablate carious lesions and composites.

1.2 DENTAL CARIES AND RESTORATIONS

Although there has been progress in reducing the incidence of dental decay, dental caries remains a significant public health problem. Tooth decay or dental caries is a disease that afflicts over 91% of the adult population in the US (B. Dye, Thornton-Evans, Li, & Iafolla, 2015). A new approach towards the treatment of dental caries with an emphasis on early detection and minimal intervention would be a significant step forward (Anusavice, 1995; Harris & Garcia-Godoy, 1999).

Several developments are driving the shift to more conservative approaches to restorative dentistry and these include: new and more sensitive methods of caries detection, the development of new effective adhesive restorative materials, and the public's demand for more aesthetic restorations. Over the past 50 years, the nature of dental caries has changed with 90% of new lesions forming in high-risk pits and fissures (occlusal surfaces) of posterior teeth (Harris & Garcia-Godoy, 1999; Mertz-Fairhurst, 1992). The quality of sealant placement depends on the condition of fissure surfaces. Incomplete removal of demineralized carious tissue or cariogenic bacteria in the fissure can harbor an active biofilm (Fejerskov & Kidd, 2003) and can reduce the adhesive properties (Hevinga, Opdam, Frencken, Bronkhorst, & Truin, 2007, 2008; Kidd, 2004). Dental caries is the demineralization of tooth structure due to acids made by bacteria. Cariogenic bacteria metabolize fermentable carbohydrates to organic acids which dissolve tooth structure, namely enamel and dentin (John D. B. Featherstone, Le, Hsu, Manesh, & Fried, 2008). Enamel and dentin are comprised of a hydroxyapatite mineral that contains defects and impurities, including carbonated hydroxyapatite, which is highly soluble and more susceptible to demineralization (John D. B. Featherstone et al., 2008).

Dental restorations are used to restore the structural and functional integrity of the missing tooth structure caused from dental caries. However, dental restorations are not permanent and need to be replaced. Dentists spend more time replacing restorations than applying new ones. Studies have shown that teeth in which restorations are replaced lose a significant amount of healthy tooth structure (Gordan, 2001; Gordan, Mondragon, & Shen, 2002). This becomes problematic since dental restorations require existing sound tooth structure and over time, a dental restoration cannot be replaced. New tools are necessary for minimizing the inadvertent removal of sound tissue.

1.3 LASERS

Lasers offer the potential for minimally invasive surgery and reducing the amount of sound tissue removed. Lasers can also be used to target specific tissues by choosing a wavelength coincident with its high absorption. As of now, there are only three lasers that are FDA cleared for treatment of dental hard tissues: the erbium-doped yttrium scandium gallium garnet (Er:YSGG) which operates at 2.79; erbium-doped yttrium aluminium garnet laser (Er:YAG) at 2.94 μm ; and the carbon dioxide laser (CO_2) operating between 9.4 – 10.6 μm . These lasers are well suited for dental hard tissue ablation, however they remove tissues with different mechanisms (Figure 1.1) (J. D. B. Featherstone & Fried, 2001). The output of Er:YSGG and Er:YAG lasers is highly absorbed by the interstitial water between enamel prisms and creates a sudden water expansion that removes dental tissue, whereas the CO_2 laser is highly absorbed by the phosphate group in hydroxyapatite (Figure 1.1). Previous studies have suggested that the CO_2 laser operating at a non-ablative fluence can alter the chemical composition of enamel crystal (J. D. B. Featherstone, Barrett-Vespone, Fried, Kantorowitz, &

Lofthouse, 1998). Irradiated carbonated hydroxyapatite has been demonstrated to thermally decompose into a purer phase of hydroxyapatite thus becoming more acid resistant and preventing further tooth decay/demineralization from occurring. Studies have also been done to assess the clinical safety of using a high-speed scanning ablation of dental hard tissues using the CO₂ laser and demonstrated that enamel and dentin surfaces can be rapidly ablated by short-pulsed CO₂ lasers with minimal peripheral thermal and mechanical damage and without excessive heat accumulation (Nguyen et al., 2011).

1.4 FEEDBACK MECHANISMS

The precision and benefits of using lasers for dentistry cannot be fully utilized with current conventional caries detection. Current caries detection involves visual and tactile techniques which are subject to clinician bias: namely the examiners' visual acuity, differences in tactile sensitivity, direct/indirect lighting, the use of magnifying eyewear, patient position, instrument used for assessment, and interactions between the clinician and patient can alter the diagnosis of caries lesion (K. Ekstrand, Qvist, & Thylstrup, 1987; K. R. Ekstrand, Zero, Martignon, & Pitts, 2009). Conventional X-rays are not sensitive for detecting enamel demineralization and in most cases, lesions that are radiographically detected are lesions that have progressed well into the dentin. Furthermore, the mineral content of demineralized enamel is highly variable and accurately predicting the amount of laser pulses for precise lesion removal is not ideal. Thus a scanning system coupled with a real-time feedback mechanism is necessary for selective caries removal. Transverse microradiography (TMR) and polarized light microscopy (PLM) are both gold standard methods for detecting caries, however they

require the destruction of the tooth making both methods unsuitable for *in vivo*. Novel minimally invasive feedback mechanisms need to be developed for precisely guiding lasers to ablate areas of demineralization or for removing preexisting restorations.

1.4.1 Near – infrared imaging

Near-infrared (NIR) imaging wavelengths of light are highly transmissible through dental hard tissues. At longer NIR wavelengths, the scattering coefficient of enamel decreases, allowing deeper light penetration and decreased backscattered light in sound enamel structure. The light scattering in sound enamel decreases as $1/\lambda^3$ with increasing wavelength from 400 to 1300 nm (Figure 1.2) (D. Fried et al., 1995). Wavelengths beyond 1300 nm may continue to have decreased light scattering and yield higher lesion contrast, but at these wavelengths, light absorption is difficult to measure and warrants investigation. Additionally, wavelengths coincident with water absorption bands, namely 1450, 1880, and 1950-nm have high water absorption (29, 31, and 113-cm^{-1} , respectively) (Hale & Querry, 1973). Interstitial water trapped between enamel prisms and water within the underlying dentin highly absorb these wavelengths and cause sound enamel to appear opaque. In contrast, light scattering appears in the lesion body deriving from the porous structure of the demineralization. This can be exploited to acquire high contrast areas of lesion activity for laser removal (Chung, Fried, Staninec, & Darling, 2011; Simon, Chan, Darling, & Fried, 2014). In addition, NIR imaging is advantageous over conventional techniques since stains which normally confound caries diagnosis do not interfere in the NIR range (Buhler, Ngaotheppitak, & Fried, 2005; Chung et al., 2011; R. S. Jones, G. D. Huynh, G. C. Jones, & D. Fried, 2003; Simon et al., 2014; Staninec, Lee, Darling, & Fried, 2010; Wu & Fried, 2009;

Zakian, Pretty, & Ellwood, 2009). Thus, NIR reflectance imaging is well suited for guiding selective caries laser ablation.

1.4.2 Plume spectroscopy

During ablation, a distinct emission plume that is characteristic of the ablated tissue's atomic and molecular emission lines is visible and can be used to determine the composition of the target. Studies have demonstrated that the spectra of tooth ablation can be discriminated from that of composite ablation by the strong calcium emission lines in the tooth ablation plume, which are not present in conventional composite ablation plume (Alexander & Fried, 2001; T Dumore & D Fried, 2000). By using a CO₂ laser, plume emission spectra can be collected over the tooth surface and composite restorations can be identified and removed in a sequential process without excessive damage to the underlying enamel.

1.5 SELECTIVITY ANALYSIS

New tools are also needed for quantifying selective lesion removal. There are now technologies that are capable of rendering 3D images of the tooth and quantifying the lesion volume *in vivo*. Image processing techniques can be applied to these 3D data sets for accurately determining the volume of the lesion body prior to removal and of the sound tissue after removal.

1.5.1 Polarized light microscopy

Sound enamel prisms are highly ordered and naturally birefringent. When polarized light is transmitted through a thin slice of sound enamel, this causes a rotation in the phase of polarized light but not complete light attenuation. On the other hand, demineralized enamel is highly scattering due to its porous nature and scrambles the incident

polarized light and attenuates the path of light. This can be used for detecting demineralization and measuring the lesion depth. However this process requires the destruction of the tooth and is not ideal for determining the selectivity of lesion removal.

1.5.2 Polarization – sensitive optical coherence tomography

Polarization – sensitive optical coherence tomography (PS-OCT) is a non-invasive technique that is based on a Michelson white light interferometer and creates 3D data of the internal structure. Polarization sensitivity is essential for resolving the early caries lesions from sound tooth structure. As previously mentioned, enamel is transparent at 1300-nm, however dental caries causes an increase in the scattering coefficient by 1-2 orders of magnitude at this wavelength (Darling, Huynh, & Fried, 2006). This causes strong reflective intensities in the orthogonal polarization state that can be measured and quantified as the lesion volume (M. H. Le, Darling, & Fried, 2010). Studies have shown that the lesion reflectivity derived from orthogonally polarized optical coherence tomography is analogous to the integrated mineral loss, ΔZ , through comparison with transverse microradiography (Arends, Ruben, & Inaba, 1997; Jones, Darling, Featherstone, & Fried, 2006; P Ngaotheppitak, C L Darling, & D Fried, 2005). Surface reflections that normally mask the lesion reflectivity are omitted in orthogonally polarized optical coherence tomographic scans, but are present in the parallel polarized scans. These surface reflections can be processed to acquire the 3D surface structure of the tooth and can be registered before and after lesion removal to quantify the removal volume. Comparing the removal volume with the lesion volume can elucidate the selectivity of lesion removal.

1.6 OBJECTIVE

Current tools now exist that can improve conservative care in dentistry. Minimally invasive procedures can prolong the tooth's lifetime and decrease the need for highly invasive and costly procedures such as dental implants and prosthetics. Lasers are ubiquitously used in medicine and its therapeutic safety has been thoroughly investigated. The overall objective is to develop laser-based methods for dentistry, namely the selective removal of dental caries and composite restorative materials using an integrated approach of computer-controlled laser – scanning coupled with methods of feedback. The objective of this dissertation will be achieved through the following two specific aims: (1) Test the hypothesis that spectral analysis can be used with a pulsed CO₂ laser system for the selective removal of dental composites and sealants (**Chapters II-IV**); and (2) Test the hypothesis that near-IR imaging systems can be combined with IR laser systems for the image-guided selective ablation of carious lesions (**Chapters V-VII**). Previous studies have demonstrated that the optical emission spectra can be used to differentiate between enamel (T Dumore & D Fried, 2000), and a spectral-guided feedback system was developed in **Chapter II** and its safety and the irradiated surface evaluated in **Chapter III**. This system was later miniaturized and optimized using fiber optic probes and the selectivity of composite removal was determined in **Chapter IV**. Previous studies have shown that lasers can be guided by high contrast lesion images for subsequent removal (Chan & Fried, 2012), however assessing their selectivity remained a challenge. **Chapter V** outlines a method for analyzing lesion depth and surface morphology using optical coherence tomography to be used for analyzing the selectivity of laser removal. **Chapter VI** explored using longer

wavelengths for determining the best wavelength for imaging dental lesions. **Chapter VII** describes development of an image-guided laser system using this wavelength and analyzed the selective removal with optical coherence tomography. These fundamental studies will significantly further our knowledge of the interaction of laser radiation with dental hard tissues and aid the development of safer and more effective feedback-guided laser systems over existing methods for the removal of dental caries and restorative materials. Furthermore, laser feedback systems have the potential to globally advance the standard of healthcare with increased conservative care for cavity preparations and dental restoration replacement procedures.

1.7 FIGURES AND FIGURE LEGENDS

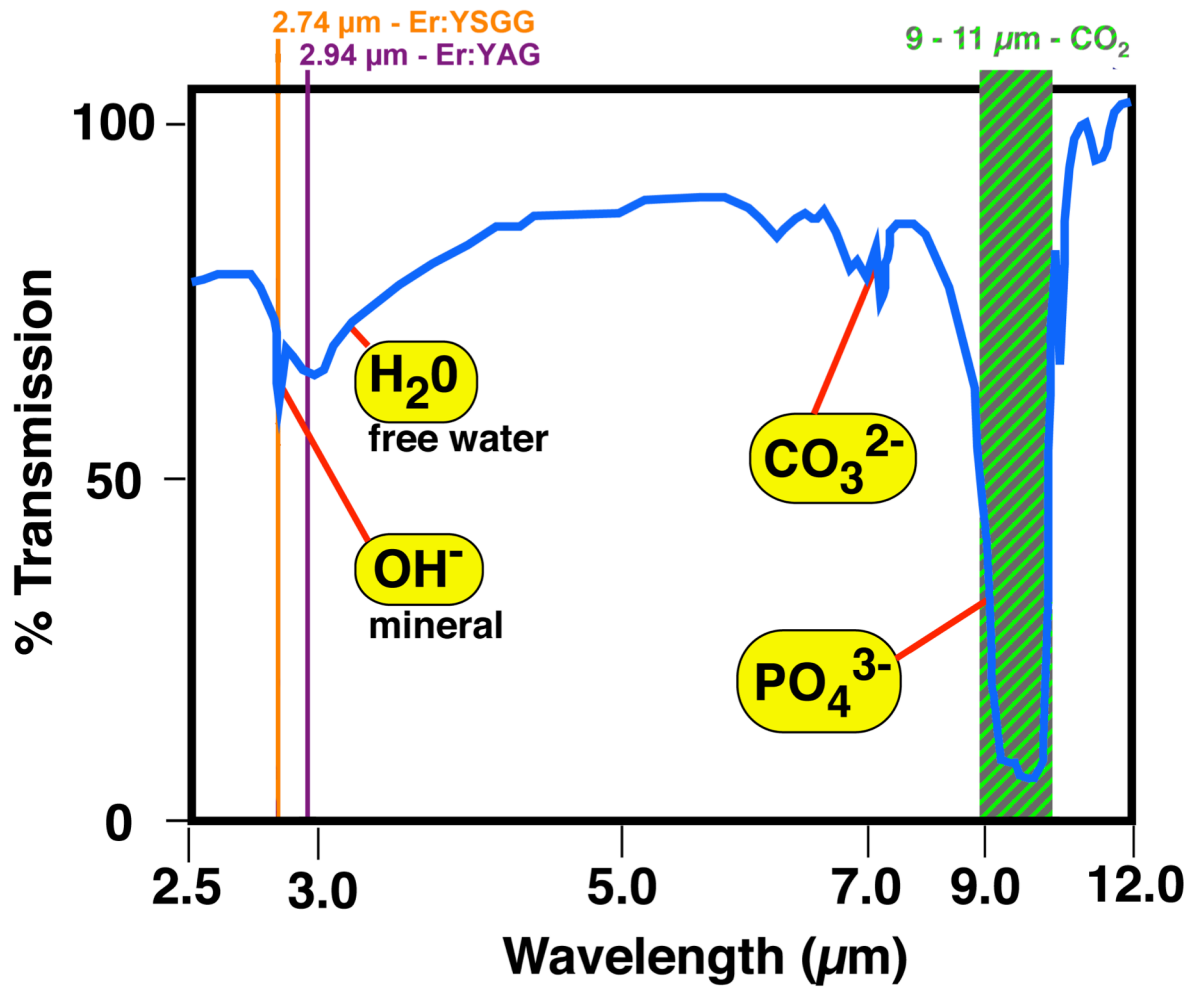


Figure 1.1: Infrared transmission spectrum of dental hard tissues. Note the low transmittance/high absorption of the phosphate group found in hydroxyapatite by the CO₂ laser.

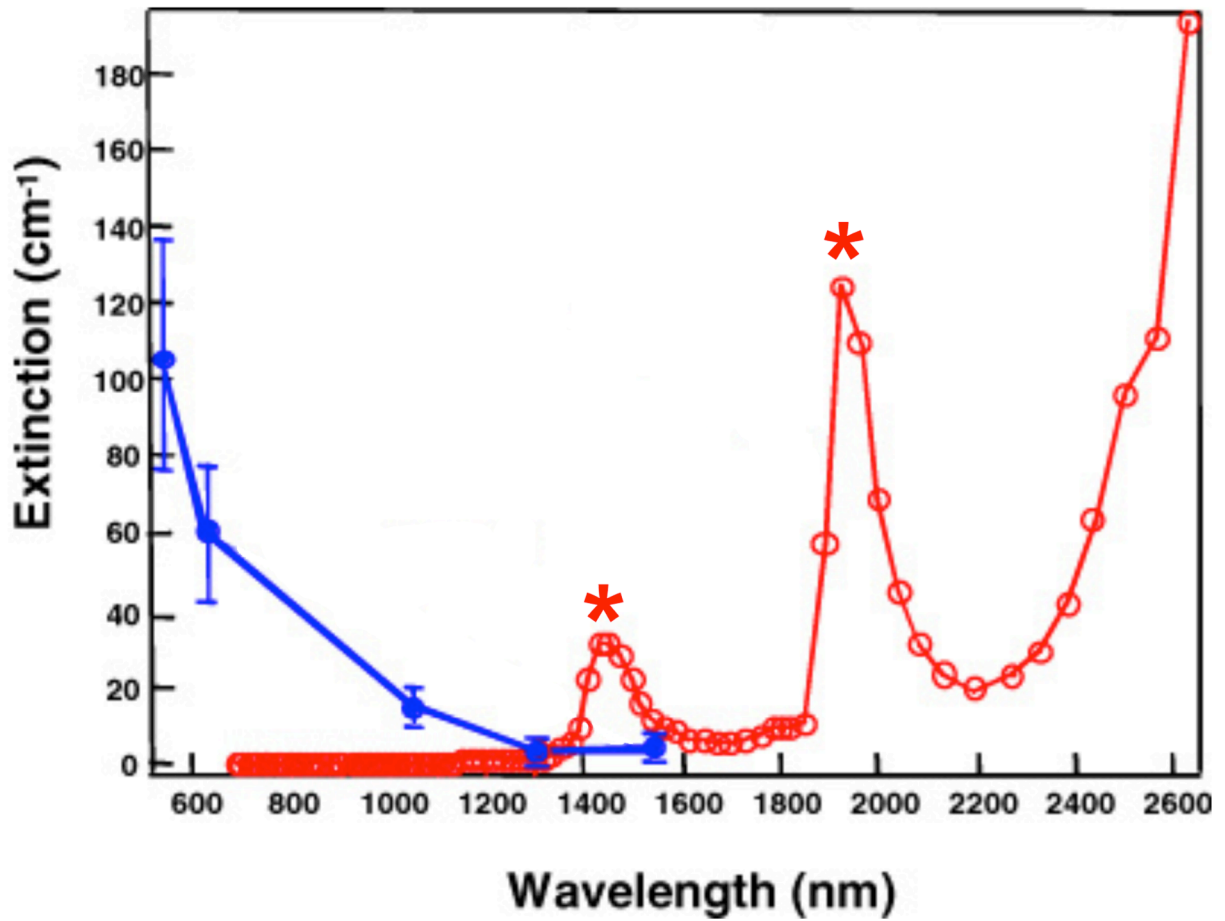


Figure 1.2: Enamel attenuation spectra (blue) and water absorption spectra (red). Notable water absorption peaks are found at 1450 and 1940 nm (28.6 and 119 cm^{-1} , respectively).

1.8 REFERENCES

- Alexander, R., & Fried, D. (2001). Selective Removal of Orthodontic Composite using 355-nm Q-switched Laser Pulses, *Lasers in Surgery and Medicine*, 30 240-245 (2002). *Lasers in Surg. Med.*, 30, 240-245.
- Anusavice, K. J. (1995). Treatment regimens in preventive and restorative dentistry. *JADA*, 126, 727-743.
- Arends, J., Ruben, J. L., & Inaba, D. (1997). Major topics in quantitative microradiography of enamel and dentin: R parameter, mineral distribution visualization, and hyper-remineralization. *Adv Dent Res*, 11(4), 403-414.
- Bernardo, M., Luis, H., Martin, M. D., Leroux, B. G., Rue, T., Leitao, J., & DeRouen, T. A. (2007). Survival and reasons for failure of amalgam versus composite posterior restorations placed in a randomized clinical trial. *Journal of the American Dental Association*, 138(6), 775-783.
- Buhler, C., Ngoatheppitak, P., & Fried, D. (2005). Imaging of occlusal dental caries (decay) with near-IR light at 1310-nm. *Optics Express*, 13(2), 573-582.
- Chan, K. H., Hirasuna, K., & Fried, D. (2011). Rapid and Selective Removal of Composite from Tooth Surfaces with a 9.3- μ m CO₂ Laser using Spectral Feedback. *Lasers in Surgery and Medicine*, 43(8), 824-832.
- Chung, S., Fried, D., Staninec, M., & Darling, C. L. (2011). Multispectral near-IR reflectance and transillumination imaging of teeth. *Biomedical Optics Express*, 2(10), 2804-2814.
- Darling, C. L., Huynh, G. D., & Fried, D. (2006). Light scattering properties of natural and artificially demineralized dental enamel at 1310 nm. *Journal of Biomedical Optics*, 11(3), 34023.
- Dumore, T., & Fried, D. (2000). Selective Ablation of Orthodontic Composite using Sub-microsecond IR laser pulses with Optical Feedback. *Lasers Surg. Med.*, 27(2), 103-110.
- Dye, B., Thornton-Evans, G., Li, X., & Iafolla, T. (2015). Dental caries and tooth loss in adults in the United States, 2011-2012. *NCHS Data Brief*(197), 197.
- Ekstrand, K., Qvist, V., & Thylstrup, A. (1987). Light microscope study of the effect of probing in occlusal surfaces. *Caries Res*, 21(4), 368-374.

Ekstrand, K. R., Zero, D. T., Martignon, S., & Pitts, N. B. (2009). Lesion activity assessment. *Monographs in oral science*, 21, 63-90.

Featherstone, J. D. B., Barrett-Vespone, N. A., Fried, D., Kantorowitz, Z., & Lofthouse, J. (1998). CO₂ laser inhibition of artificial caries-like lesion progression in dental enamel. *J Dent Res*, 77(6), 1397-1403.

Featherstone, J. D. B., & Fried, D. (2001). Fundamental Interactions of Lasers with Dental hard Tissue. *Med. Laser Appl*, 16, 181-195.

Featherstone, J. D. B., Le, C. Q., Hsu, D., Manesh, S., & Fried, D. (2008). *Changes in acid resistance of dentin irradiated by a CW 10.6 μm CO₂ laser*. Paper presented at the Dental Materials, San Jose, CA, USA.

Fejerskov, O., & Kidd, E. (Eds.). (2003). *Dental Caries: The Disease and its Clinical Management*. Oxford: Blackwell.

Fried, D., Glana, R. E., Featherstone, J. D., & Seka, W. (1995). Nature of light scattering in dental enamel and dentin at visible and near-infrared wavelengths. *Applied optics*, 34(7), 1278-1285.

Gordan, V. V. (2001). Clinical evaluation of replacement of class V resin based composite restorations. *J Dent*, 29(7), 485-488.

Gordan, V. V., Garvan, C. W., Richman, J. S., Fellows, J. L., Rindal, D. B., Qvist, V., . . . Gilbert, G. H. (2009). How dentists diagnose and treat defective restorations: evidence from the dental practice-based research network. *Operative dentistry*, 34(6), 664-673.

Gordan, V. V., Mondragon, E., & Shen, C. (2002). Replacement of resin-based composite: evaluation of cavity design, cavity depth, and shade matching. *Quintessence Int*, 33(4), 273-278.

Hale, G. M., & Querry, M. R. (1973). Optical constants of water in the 200-nm to 200-μm wavelength region. *Appl. Optics*, 12, 555-563.

Harris, N., & Garcia-Godoy, F. (1999). *Primary Preventive Dentistry* (5th ed.). Stamford, CT: Appleton & Lange.

Hevinga, M. A., Opdam, N. J., Frencken, J. E., Bronkhorst, E. M., & Truin, G. J. (2007). Microleakage and sealant penetration in contaminated carious fissures. *J Dent*, *35*(12), 909-914.

Hevinga, M. A., Opdam, N. J., Frencken, J. E., Bronkhorst, E. M., & Truin, G. J. (2008). Can Caries Fissures be Sealed as Adequately as Sound Fissures? *J Dent Res*, *87*(5), 495-498.

Hibst, R., Graser, R., Udart, M., & Stock, K. (2010). Mechanism of high-power NIR laser bacteria inactivation. *Journal of biophotonics*, *3*(5-6), 296-303.

Hong, Y. H., & Lew, K. K. (1995). Quantitative and qualitative assessment of enamel surface following five composite removal methods after bracket debonding. *Eur J Orthod*, *17*(2), 121-128.

Jones, R. S., Darling, C. L., Featherstone, J. D., & Fried, D. (2006). Imaging artificial caries on the occlusal surfaces with polarization-sensitive optical coherence tomography. *Caries research*, *40*(2), 81-89.

Jones, R. S., Huynh, G. D., Jones, G. C., & Fried, D. (2003). Near-IR Transillumination at 1310-nm for the Imaging of Early Dental Caries. *Optics Express*, *11*(18), 2259-2265.

Kidd, E. A. (2004). How 'clean' must a cavity be before restoration? *Caries Res*, *38*(3), 305-313.

Konishi, N., Fried, D., Featherstone, J. D. B., & Staninec, M. (1999). Inhibition of secondary caries by CO₂ laser treatment. *Amer. J. Dent.*, *12*(5), 213-216.

Le, M. H., Darling, C. L., & Fried, D. (2010). Automated analysis of lesion depth and integrated reflectivity in PS-OCT scans of tooth demineralization. *Lasers Surg Med*, *42*(1), 62-68.

Leco-Berrocal, M. I., Martinez-Gonzalez, J. M., Donado-Rodriguez, M., & Lopez-Carriches, C. (2006). Sterilizing effects of the Erbium:Yag laser upon dental structures: an in vitro study. *Medicina oral, patologia oral y cirugia bucal*, *11*(2), E158-161.

Louie, T. M., Jones, R. S., Sarma, A. V., & Fried, D. (2005). Selective removal of composite sealants with near-ultraviolet laser pulses of nanosecond duration. *Journal of Biomedical Optics*, *10*(1), 14001.

Mertz-Fairhurst, E. J. (1992). Pit-and-fissure sealants:A global lack of scientific transfer ? *J Dent Res*, 115, 1543-1544.

Miserendino, L. J., & Pick, R. M. (1995). *Lasers in Dentistry*. Chicago: Quintessence.

Ngaotheppitak, P., Darling, C. L., & Fried, D. (2005). Polarization Optical Coherence Tomography for the Measuring the Severity of Caries Lesions. *Lasers Surg Med*, 37(1), 78-88.

Nguyen, D., Chang, K., Hedayatollahnajafi, S., Staninec, M., Chan, K., Lee, R., & Fried, D. (2011). High-speed scanning ablation of dental hard tissues with a $\lambda=9.3 \mu\text{m}$ CO₂ laser: adhesion, mechanical strength, heat accumulation, and peripheral thermal damage. *J. Biomed. Opt.*, 16(7), 071410:071411-071418.

Oliver, R. G. (1988). The effect of different methods of bracket removal on the amount of residual adhesive. *Amer J Orthod Dentofacial Orthop*, 93(3), 196-200.

Simon, J. C., Chan, K. H., Darling, C. L., & Fried, D. (2014). Multispectral near-IR reflectance imaging of simulated early occlusal lesions: Variation of lesion contrast with lesion depth and severity. *Lasers Surg Med*, 46(3), 203-215.

Staninec, M., Lee, C., Darling, C. L., & Fried, D. (2010). In vivo near-IR imaging of approximal dental decay at 1,310 nm. *Lasers in Surgery and Medicine*, 42(4), 292-298.

Stern, R. H., & Sognnaes, R. F. (1964). Laser beam effect on hard dental tissues. *J. Dent. Res.*, 43, 873.

Wigdor, H. A., Walsh, J. T., Jr., Featherstone, J. D., Visuri, S. R., Fried, D., & Waldvogel, J. L. (1995). Lasers in dentistry. *Lasers Surg Med*, 16(2), 103-133.

Wu, J., & Fried, D. (2009). High contrast near-infrared polarized reflectance images of demineralization on tooth buccal and occlusal surfaces at $\lambda = 1310\text{-nm}$. *Lasers in Surgery and Medicine*, 41(3), 208-213.

Young, D., Fried, D., & Featherstone, J. (2000). *Treating occlusal pit and fissure surfaces by IR laser irradiation* (Vol. 3910).

Zakian, C., Pretty, I., & Ellwood, R. (2009). Near-infrared hyperspectral imaging of teeth for dental caries detection. *Journal of Biomedical Optics*, 14(6), 064047-064047.

CHAPTER II
SPECTRAL GUIDANCE LASER REMOVAL OF COMPOSITE

2.1 SUMMARY

Dental composite restorative materials are color matched to the tooth and are difficult to remove by mechanical means without excessive removal of, or damage to peripheral enamel and dentin. Lasers are ideally suited for selective ablation to minimize healthy tissue loss when replacing existing restorations, sealants, or removing composite adhesives such as residual composite left after debonding orthodontic brackets.

A carbon dioxide laser operating at 9.3- μm with a pulse duration of 10-20-microsecond and a pulse repetition rate of ~200 Hz was integrated with a galvanometer based scanner and used to selectively remove composite from tooth surfaces. Spectra of the plume emission were acquired after each laser pulse and used to differentiate between the ablation of dental enamel or composite. Microthermocouples were used to monitor the temperature rise in the pulp chamber during composite removal. The composite was placed on tooth buccal and occlusal surfaces and the carbon dioxide laser beam was scanned across the surface to selectively remove the composite without excessive damage to the underlying sound enamel. The residual composite and the damage to the underlying enamel were evaluated using optical microscopy.

The laser was able to rapidly remove composite from tooth buccal and occlusal surfaces with minimal damage to the underlying sound enamel and without excessive heat accumulation in the tooth.

This chapter demonstrates that composite can be selectively removed from tooth surfaces at clinically relevant rates using a CO₂ laser operating at 9.3- μm with high pulse repetition rates with minimal heat deposition and damage to the underlying enamel.

2.2 INTRODUCTION

Dental composites are typically color matched to the tooth for esthetic reasons and are difficult to remove by mechanical means without excessive removal of, or damage to peripheral enamel and dentin. Lasers are ideally suited for selective ablation to minimize healthy tissue loss when replacing failed restorations and sealants, removing composite adhesives such as residual composite left after debonding orthodontic brackets, and for the repair of esthetic bonding.

High ablation selectivity can be achieved by operating at laser wavelengths that ablate composite at lower ablation thresholds than dental hard tissues. Previous studies have shown that high selectivity can be achieved for short nanosecond laser pulses at 355-nm and for CO₂ laser pulses at 10.6- μ m (Alexander & Fried, 2001; T. M. Louie et al., 2005; Wheeler, Fried, Featherstone, Watanabe, & Le, 2003). Another approach is to use image guided ablation which has been carried out for selective removal of dental caries using near-IR imaging (Tao & Fried, 2009) and fluorescence (Eberhard, Eisenbeiss, Braun, Hedderich, & Jepsen, 2005) to demarcate areas of decay. Dynamic methods employing acoustic and spectral feedback are also feasible and these approaches have been demonstrated to remove both caries and dental calculus (Cheng, Fan, & Fried, 2006; Kenneth Fan & Fried, 2007; Kim, Feit, Rubenchik, Mammini, & Da, 1998; Niemz, 1994; Rechmann & Hennig, 1994; Rechmann, Hennig, von den Hoff, & Kaufmann, 1993).

Multiple studies have shown that spectral feedback or emission spectroscopy can be used effectively to discriminate between the ablation of dental composite adhesive/restorative materials and dental hard tissues (Alexander, Xie, & Fried, 2002;

T. Dumore & D. Fried, 2000; Lizarelli, Moriyama, & Bagnato, 2003; T. M. Louie, Jones, Le, & Fried, 2004; Smith, Walsh, & Taverne, 1999). During the ablation event there is a distinct luminous emission plume with characteristic atomic and molecular emission lines that can be used to determine the composition of the target materials. The plume emission is dominated by calcium atom, ion, and molecular emission lines during the ablation of dental hard tissues and bone which can be exploited for selective laser ablation. Composite restorative materials lack calcium and thus lack the calcium emission lines that are very strong between 580 and 650-nm which gives the plume a distinct red appearance. Plume emission spectroscopy or laser microprobe emission spectroscopy can be used for the identification of many materials (Adrain & Watson, 1984; Chrisey & Hubler, 1994; J. F. Ready, 1971). The method was first used to examine teeth over 40 years ago (Sherman, Ruben, & Goldman, 1965) and has been used to identify calcified plaque in arteries (Oraevsky, Jacques, Pettit, Tittel, & Henry, 1993). Over the past few years very compact fiber-optic spectrometers have become available that are relatively inexpensive and can be readily interfaced with laser ablation systems. Dumore (T. Dumore & D. Fried, 2000), Cheng (Cheng et al., 2006) and Alexander (Alexander & Fried, 2001) showed that the spectra of the tooth could be easily discriminated from composite by the strong distinctive calcium emission lines in the tooth ablation plume that are not present in the composite resin or filler material ablation plumes.

We have focused our efforts on the selective removal of composite on two laser systems, the frequency tripled Nd:YAG laser operating at 355-nm and the CO₂ laser that can be operated at several wavelengths between 9.2 and 10.6- μ m (Alexander et

al., 2002; T. M. Louie et al., 2004; Wheeler, Fried, Featherstone, Watanabe, et al., 2003). Short nanosecond laser pulses at 355-nm are well suited for selective ablation of composite from enamel surfaces and spectral feedback can be used to control the removal of residual composite (T. M. Louie et al., 2004; Suri, 2005; Wheeler, Fried, Featherstone, Watanabe, et al., 2003). However, the concern of UV exposure, limited usefulness for other dental laser procedures and the high cost of diode-pumped systems that can be operated at higher pulse repetition rates has tempered enthusiasm for this laser system.

Alexander (Alexander & Fried, 2001) and Cheng et al. (Cheng et al., 2006) showed that a transverse excited atmospheric pressure (TEA) operating at 10.6- μm can be used for selective removal of composite and that spectral feedback can be used to control removal from the occlusal surfaces. One problem with the shorter TEA CO₂ laser pulses is that the high peak power in the initial gain switched spike which is 500-ns in duration generates a plasma which shields the tail end of the laser pulse. This limits the ablation rate of dental hard tissues to a few microns per pulse and severely limits their utility for caries removal. Moreover the laser wavelengths of 9.3 and 9.6- μm are more strongly absorbed by carbonated hydroxyapatite for more efficient coupling to dental hard tissues (Duplain, Boulay, & Belanger, 1987; M. Zuerlein, D. Fried, J. Featherstone, & W. Seka, 1999). Recent studies have shown that CO₂ lasers operating at 9.3 and 9.6- μm wavelengths with longer pulse durations of 10-20-microseconds are ideally suited for the efficient ablation of dental hard tissues and for caries removal (K Fan, Bell, & Fried, 2006; D Fried et al., 2001). The longer laser pulse durations reduce the effects of plasma shielding and allow the removal of 10-20- μm per laser pulse at relatively low

incident fluence, 5-10 J/cm² and these lasers can be operated at high pulse repetition rates.

The purpose of the this study was to determine if a rapidly scanned 9.3- μ m CO₂ laser ablation system with laser pulses of 10-20-microseconds duration can safely be used for the rapid and selective removal of dental composite from enamel surfaces with minimal loss of sound enamel.

2.3 MATERIALS AND METHODS

2.3.1 Sample Preparation and Simulated Lesion Models

Sound and carious whole teeth and tooth sections taken from teeth extracted from patients in the San Francisco Bay Area were collected, cleaned, and sterilized with gamma radiation. Teeth were sectioned using a diamond saw to provide transverse sections approximately 1-2-mm thick. Composite disks were prepared from Z-250 composite (3M Minneapolis, MN) and Grengloo™ composite (Ormco, Orange, CA). The Grengloo™ composite used in this study is designed as an adhesive for metal orthodontic brackets. After removal of orthodontic brackets it is difficult to see the residual composite left on tooth buccal surfaces and the green coloration is designed to aid mechanical removal. The Grengloo™ composite was green below body temperature which made it easy to identify any residual composite missed by the laser. The ablation thresholds and ablation rates were similar for both composite materials.

2.3.2 Tissue Irradiation and Laser Parameters

An industrial marking laser, Impact 2500 from GSI Lumonics (Rugby, United Kingdom) operating at a wavelength of 9.3 μ m was used. The laser was custom modified to produce a Gaussian output beam (single spatial mode) and a pulse duration of between

10-15-microseconds. This laser is capable of high repetition rates up to 500 Hz. The laser energy output was monitored using a power meter EPM 1000, Coherent-Moletron (Santa Clara, CA), and the Joulemeter ED-200 from Gentec (Quebec, Canada). A f-theta scanning lens with a focal length of 90-mm from II-VI (Saxonburg, PA) was used to focus the beam onto the tooth surfaces. A razor blade was scanned across the beam to determine the diameter ($1/e^2$) of the laser beam. Computer-controlled XY galvanometers 6200HM series with MicroMax Series 671 from Cambridge Technology, Inc. (Cambridge) were used to scan the laser beam over sample surfaces. A low volume/low pressure air-actuated fluid spray delivery system consisting of a 780S spray valve, a Valvemate 7040 controller, and a fluid reservoir from EFD, Inc. (East Providence, RI) was used to provide a uniform spray of fine water mist onto the tooth surfaces. The setup is shown in **Figure 2.1**. The water spray was pulsed with a frequency of 0.5 Hz for a delivery rate of 10 $\mu\text{l}/\text{second}$ over an area of 5 cm^2 .

2.3.3 Plume Emission Spectroscopy

A USB2000+ fiber optic spectrometer from Ocean Optics (Dunedin, FL) incorporating a 2048 element CCD detector was used to acquire spectra. The spectrometer is equipped with a 600 g/mm grating with a blaze wavelength of 500-nm designed for 350-850-nm. No slit was used and the L2 cylindrical collection lens was installed. A 1" lens with a focal length of 50-mm positioned 6" from the plume was used to focus the plume emission into a 1-mm in diameter optical fiber. The spectra of dental composite and sealants are markedly different than that of enamel and dentin (Cheng et al., 2006). Spectra of dental enamel and composite are shown in **Figure 2.2**. The composite spectra produced using the CO_2 laser had only a single strong peak at around 580 nm,

that was identical to the spectrum of glass which we had observed previously (Cheng et al., 2006). The 580-nm peak is most probably due to sodium emission from glass/silica particles, the filler material of dental composites. This peak is also present in the spectrum of dental hard tissues which also contain some sodium. The spectral lines were identified using spectral tables (Striganov & Sventitskii, 1968). Dental hard tissues have much stronger emission with a very strong peak centered at 605-nm. Since the intensity is dependent on the position of the optical fiber, we used an imaging system that viewed the entire plume to avoid excessive variation in the spectra. The ratio and intensities of the 580 and 605-nm peaks were used to differentiate between composite and enamel. The sodium line is present in both materials while the strong 605-nm calcium emission line is only present in dental hard tissue.

2.3.4 Ablation Rate Measurements

The rate of enamel and composite removal was measured as a function of the incident fluence to determine the optimum laser irradiation intensity to be used for removal of composite. Disks of Grelgloo™ and Z250 composites were prepared along with tooth section approximately half a millimeter thick. The laser spot size was maintained at 450- μm and the laser beam was scanned in a rectangular pattern over an area roughly 3.6 x 1.5 ml with each laser spot separated by 150- μm apart with a high degree of overlap over the samples. After scanning, the depth was measured using an optical coherence tomography (OCT) system. The time-domain OCT system is described in further detail in earlier manuscripts (D. Fried et al., 2002). A high power (15-mW) polarized superluminescent diode source was used with a center wavelength of 1,317 nm and a spectral bandwidth FWHM of 84 nm to provide an axial resolution of 9- μm in air. The

laser energy/fluence was varied using CaF₂ attenuators of varying thickness. Two composite materials were explored: Z250 is a filled general purpose composite that best represents the bulk of composite materials that are likely to be encountered and Grengloo™ is also a filled orthodontic composite that expressed similar ablation rates.

2.3.5 Heat Accumulation Measurements

Type K, 36 gauge, 0.13 mm diameter, one meter length thermocouples (Omega Engineering Inc., Stamford, Connecticut) were placed coronally inside the pulp chamber of extracted human teeth to measure the temperatures in the pulp chamber. Thermally conductive paste was used to adhere the thermocouples to the inside of the pulp chamber and maintain thermal contact with the coronal surface of the pulp chamber wall. Radiographs were used to confirm accurate placement of thermocouples. A thermocouple controller, Stanford Research SR630 (Stanford Research Systems, Sunnyvale, CA), and Labview software (National Instruments, Austin, TX) were used to record the thermal data. The cooling water was at room temperature. The time required for composite removal was also recorded. Ten samples were measured. The temperature rise in the pulp chamber of each tooth was monitored until complete removal of the composite. A temperature rise of 5.5°C was considered indicative of excessive heat accumulation.

2.3.6 Optical Microscopy

In previous studies we had used OCT to assess underlying damage to the enamel surface. However, the 10-20-µm resolution of OCT is too low to measure changes that were typically less than 10-20-µm. Therefore, optical microscopy was used to analyze the samples in this study. After surface ablation, a Leitz Secolux microscope with 5, 10,

20, 50, and 100x infinity corrected fluorite objectives and BF/DF/DIC capability with a maximum magnification of 1,000 times (10x eyepieces) interfaced to a digital firewire camera, and image analysis software was used to acquire images of the underlying enamel after composite removal. Other lower magnification optical scopes were also used.

2.3.7 Optical Feedback and Selective Removal

In order to selectively remove composite, the laser beam was scanned over the area of interest while the plume was monitored with the spectrometer to differentiate between composite and enamel. The laser spot size was 750- μm and the area to be irradiated was divided into a 4-5 mm square grid with each spot on the grid separated by 150- μm . The algorithm used for selective removal of composite is derived from a closed loop feedback system. The system has a set of input variables and when the system encounters a difference in the output from a controlled variable, the system changes the input variables and reiterates through the process again until the system does not provide any new input variables. For selective removal, the laser beam was scanned across a user constructed area of interest coordinate grid, designated as a primary storage array, with one laser pulse delivered to each grid coordinate. The plume emission was acquired by the spectrometer at each coordinate and analyzed to determine if composite or enamel was ablated. The plume spectra for enamel and composite are shown in **Figure 2.2**. The spectral lines located at 580 and 605-nm were used to demarcate between composite and enamel. The spectra of ablated enamel was more intense than composite and exhibited a strong peak at approximately 605-nm, whereas both enamel and composite exhibited a less intense peak at roughly 580-nm,

as shown, respectively, as [E] and [C]. The program utilized the difference in plume emission at these two wavelengths to differentiate between composite and enamel. If the plume emission spectrum indicated composite, this grid coordinate was recorded in a secondary storage array and only these coordinates stored in that array were targeted on the next pass. This process was repeated until the program had scanned all the points in the primary array. The program then checked if the secondary storage array contained any more points, if so, the program replaced the primary storage array with the secondary array and repeated the process until the subsequent iteration's secondary array was empty and all the composite was removed. This selective ablation algorithm is shown in the flowchart of **Figure 2.3**.

The optimum fluence for composite removal is dependent on the location of the composite on the tooth. On tooth facial surfaces, the amount of enamel removed must be minimized since it is desirable to avoid changing the appearance of the enamel. Several irradiation intensities were empirically investigated to determine the maximum fluence that could be used without varying the appearance of the enamel. We chose a fluence of 3.2 J/cm^2 for which visual changes were only visible upon close inspection.

By scanning over the entire area during the initial pass, as opposed to removing composite from each individual location with multiple laser pulses, localized heat deposition is minimized. The ablation efficiency is higher since deep holes are not being drilled in the composite. The ablation rate and efficiency decreases for subsequent laser pulses as an ablation crater develops and the fluence decreases as the incident laser energy is spread over a larger area. In many cases stalling can occur, therefore it is advantageous to scan the laser beam over adjacent spots to minimize crater/hole

formation. The laser was externally triggered by the computer after analysis of each laser spot, therefore the pulse repetition rate was limited by the software and processing time. The number of spots irradiated per second fluctuated slightly between 200 and 220.

2.4 RESULTS

Figure 2.4 shows a graph of ablation rate of human enamel and Z250 dental composite for varying incident fluence. The ablation rate for composite ranged from just below 10- μm per pass at 1 J/cm^2 to 90- μm at 18 J/cm^2 . The ablation rate for enamel increased more slowly from 10- $\mu\text{m}/\text{scan}$ at 4-5 J/cm^2 to around 20- $\mu\text{m}/\text{scan}$ at 18 J/cm^2 . The respective removal rates for the Grelgloo™ composite and enamel were 12 and 8- $\mu\text{m}/\text{scan}$ at this fluence. In the occlusal surfaces damage to the underlying enamel is less critical and higher fluence rates can be used for more rapid removal of the composite.

Composite applied to tooth buccal surfaces was investigated first, since these areas are most sensitive to damage to the enamel and excessive damage would adversely affect the appearance of the tooth. **Figure 2.5** shows two samples in which a layer of composite approximately 1-mm thick was bonded to the enamel of the crown before and after the tooth surface was scanned by the laser over the right half of the composite area. As can be seen in the images the composite is cleanly removed without charring of the composite. If a water spray is not used there is discoloration and thermal damage to the composite. At a fluence of only 3.2 J/cm^2 , there is minimal removal of sound enamel. The zone of laser-irradiated enamel is shown in more detail in **Figure 2.6**. It is difficult to resolve changes in the irradiated enamel and at higher magnification it can be

seen that there were some regions of the treated area where there was some minor enamel removal. This was localized to the center of the individual laser spots where the local fluence was highest due to the Gaussian spatial profile of the laser beam. These areas of localized damage to enamel were limited to a depth of less than 20- μm . This depth was determined by scanning the image plane of the microscope to focus on both the surface and base of the craters using a calibrated micrometer. The average of two sites examined on each of the 10 teeth scanned by the laser indicated a mean depth of 16.3 ± 3.02 at the center of the Gaussian shaped laser spots. At higher magnification, **Figure 2.7**, it is obvious that the enamel irradiated by the laser has also undergone melting and recrystallization without ablation in most areas. The characteristic worm like structures indicative of laser melting and recrystallization are clearly visible (McCormack, Fried, Featherstone, Glana, & Seka, 1995).

After establishing the laser parameters that could be used effectively for composite removal on smooth surfaces, we applied composite to the pits and fissures of the occlusal surfaces of molars as shown in **Figure 2.8**. Although this appears far more challenging to remove composite from the highly convoluted topography of these surfaces, it is actually easier than removal from smooth surfaces since damage to the underlying enamel is less critical for cosmetic reasons and higher irradiation intensities are permissible. A higher fluence of 7 J/cm^2 was used for the occlusal surfaces. The higher fluence results in faster composite removal and it compensates for the topography of the fissures which lowers the effective incident fluence in those areas.

Composite was placed in the occlusal surfaces of 10 teeth and the temperature rise in the pulp chamber was monitored during composite removal. The mean temperature rise

during the removal process for nine samples was $2.1 \pm 1.4^{\circ}\text{C}$ with a mean removal time of 21.6 ± 6.4 seconds. The maximum temperature rise measured was 3.5°C . One of the samples was rejected because the removal process was interrupted before complete removal was achieved. A second pass was carried out and the composite was completely removed.

2.5 DISCUSSION

This demonstrated that composite could be rapidly removed from tooth surfaces with a high degree of selectivity with minimal heat deposition in the tooth. In previous literature, CO_2 lasers are demonstrated to be promising for selective removal of composite from tooth surfaces; however, this marks the first time to show that a CO_2 laser optimized for the efficient removal of dental hard tissue and caries, namely operating at a wavelength of $9.3\text{-}\mu\text{m}$ with a pulse duration between 10 and 20-microseconds could be used for the selective removal of composite. Moreover, this is the first study to show that composite could be removed safely at rates fast enough to be feasible for clinical use. This laser was operated at approximately 200-Hz. This rate was limited by the processing time for analyzing the plume and higher removal rates are certainly feasible. It is likely that it will not be necessary to use a spectrometer for plume analysis. A much faster and more simplistic system involving two or three photodiodes should be suitable.

At an incident fluence of 3.2 J/cm^2 , which we found optimal for smooth surfaces, removal was highly selective and damage to sound enamel was localized to the center of the individual laser spots where the local fluence was highest due to the Gaussian spatial profile of the laser beam. These areas of localized damage to enamel were limited to a depth of less than $20\text{-}\mu\text{m}$ which has a minimal impact on appearance and is

similar in magnitude to that produced during prophylaxis using a brush. Measurements of the enamel loss during a routine brush and cup prophylaxis indicated mean enamel loss ranging from 6 to 17- μm depending on the material employed (Thompson & Way, 1981). High-resolution optical microscopy showed that the underlying enamel had undergone melting and recrystallization. This surface modification is advantageous since the modified enamel has an increased resistance to acid dissolution (K. Fan & Fried, 2006; J. D. Featherstone, Barrett-Vespone, Fried, Kantorowitz, & Seka, 1998; D. Fried, Featherstone, Le, & Fan, 2006a). This surface layer with enhanced resistance to acid dissolution is also created at higher incident fluence as well (Can, Darling, Ho, & Fried, 2008; D. Fried et al., 2006a). This is an additional advantage of using the CO₂ laser for composite removal over other lasers systems such as the Er:YAG, Er:YSGG and the frequency tripled Nd:YAG laser at 355-nm.

At the time of this experiment, employing CO₂ lasers for this procedure has yet to receive FDA approval for hard tissue use, however, since 2013, Convergent Dental's Solea™ CO₂ laser has been cleared by the FDA for hard and soft tissue use.

Selective laser ablation is particularly advantageous for composite removal from the occlusal surfaces where the convoluted topography of the pits and fissures poses a challenge for composite removal by mechanical means. The occlusal pits and fissures are considered high risk surfaces for dental caries and the thermal modification of those surfaces by the CO₂ laser is desirable to render those sites more resistant to acid dissolution. One approach is to scan the CO₂ laser over the pits and fissures of the occlusal surface prior to placing sealants to further enhance the resistance to caries. If

the sealants need to be removed due to failure, the same CO₂ laser can be used to remove the sealant and any decay that needs to be removed.

In addition to the removal of composite-based adhesives used for the bonding of orthodontic brackets and dental sealants and restorations, selective laser ablation is likely to work well for the repair of esthetic restorations.

One requirement of using plume analysis for laser control is that the ablation pulses do not remove excessive amounts of sound tissue. For example, such an approach would not be suitable for use with the Er:YAG or Er:YSGG lasers that are typically used with fairly high single-pulse energies and irradiation intensities to remove dental hard tissues, namely 100-500 mJ per pulse with incident fluence ranging from 20-100 J/cm² (T. Dumore & D. Fried, 2000; R Hibst & Keller, 1991; Lizarelli et al., 2003; J. S. Nelson, Yow, Liaw, Macleay, & Zavar, 1988). Such pulses can remove up to 50-µm of enamel and 200-µm of dentin per shot (R. Hibst & Keller, 1989) producing excessive damage to the underlying tooth structure (Almeida, Vedovello Filho, Vedovello, Young, & Ramirez-Ya, 2009). Moreover, ablation is not selective at erbium wavelengths (T. Dumore & D. Fried, 2000). Optical plume analysis is better suited for femto-second and pico-second visible laser systems, UV laser systems, and TEA CO₂ laser systems operating at high pulse repetition rates with low or moderate rates of ablation. Such systems can be operated efficiently at repetition rates approaching a kHz with low ablation thresholds on composite.

We have shown in prior studies that composite ablation is more selective for 355-nm pulses from a frequency tripled Q-switch Nd:YAG laser than for the CO₂ laser and that composite can be removed with minimal damage to sound enamel without the need for

spectral feedback at 355-nm (T. M. Louie et al., 2004; Suri, 2005; Wheeler, Fried, Featherstone, & Watanabe, 2003). However, a feedback mechanism is still needed to determine whether the composite has been completely removed and spectral feedback ensures that the minimal number of laser pulses are employed to remove the composite thus minimizing the heat deposition and the time needed for removal. In addition, the CO₂ laser can be used for several applications in dentistry including hard tissue ablation, caries ablative treatments and soft tissue surgery, while it has not been established that a laser operating at 355-nm can be used for any other important dental procedures. Moreover, a diode pumped solid state laser operating at 355-nm with high pulse repetition rates is expensive to manufacture and the 355-nm photons are in the UV range, and they are considered ionizing radiation.

The heat accumulation measurements taken using microthermocouples suggest that composite can be removed rapidly without excessive heat accumulation. The mean temperature rise was less than half the 5.5°C temperature rise that is considered excessive according to the Zach and Cohen study (Zach & Cohen, 1965). It is also important to note that the teeth were isolated so that there was poor heat flow from the tooth and there was no pulpal blood flow to cool the pulp. Therefore the measured temperature rise would be expected to be less *in vivo* for vital teeth. Moreover, the cooling water was at room temperature and the tap water typically used in the dental office is significantly cooler than room temperature which would further limit temperature excursions.

Niemz (Niemz, 1994) suggests that spectral feedback can also be used to discriminate sound from decayed dental hard tissues; however, after extensive investigation of this

approach utilizing several different laser systems, we did not find spectral emission useful for discriminating between sound and demineralized dental hard tissues (Cheng et al., 2006). Hard tissue spectra are dominated by calcium emission lines and there is little difference in the chemical content between sound and demineralized dental hard tissues. There are differences in the mineral density however this only influences the overall intensity of the emission. Image guided ablation is more feasible using near-IR imaging (Tao & Fried, 2009) and fluorescence (Eberhard et al., 2005) to demarcate areas of decay. In conclusion, this study has demonstrated that composite can be selectively removed from tooth surfaces at clinically relevant rates using a CO₂ laser operating at 9.3- μ m with high pulse repetition rates with minimal heat deposition and damage to the underlying enamel.

2.6 FIGURES AND FIGURE LEGENDS

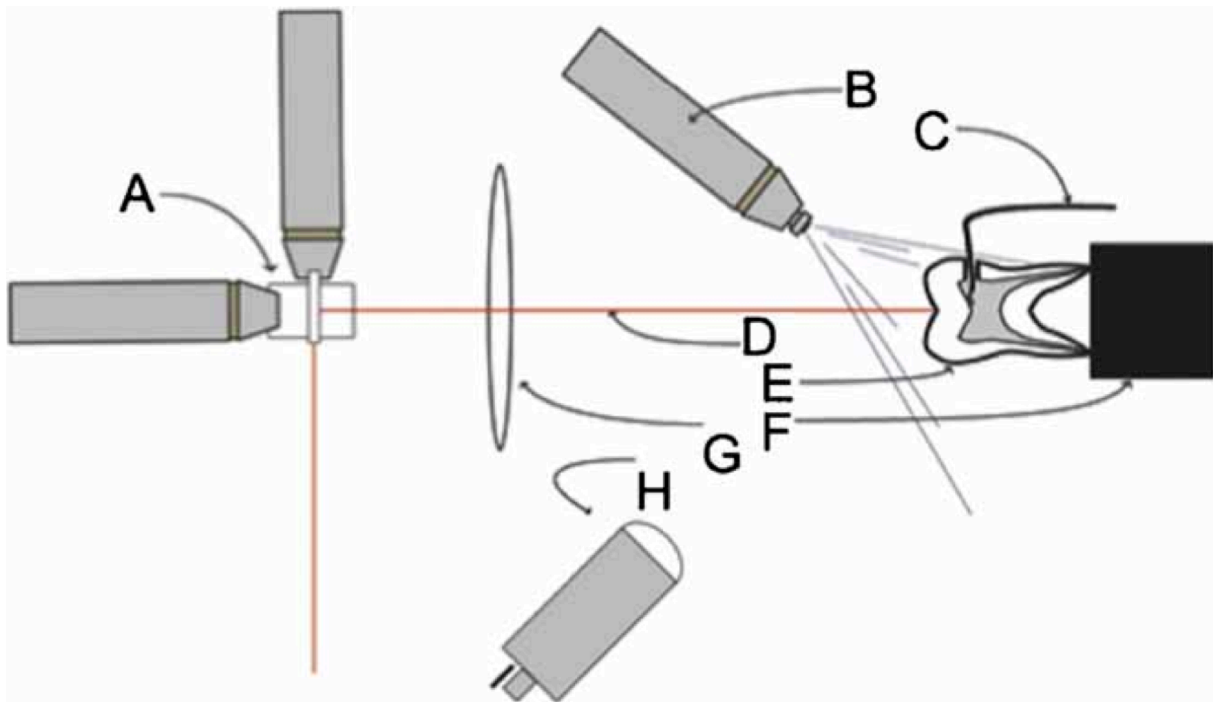


Figure 2.1: The experimental setup for selective ablation of composite consists: (A) XY galvanometers; (B) water-spray; (C) microthermocouples; (D) CO₂ laser beam; (E) tooth sample; (F) delrin sample mount; (G) ZnSe f-theta scanning lens; and (H) imaging optics for spectrometer.

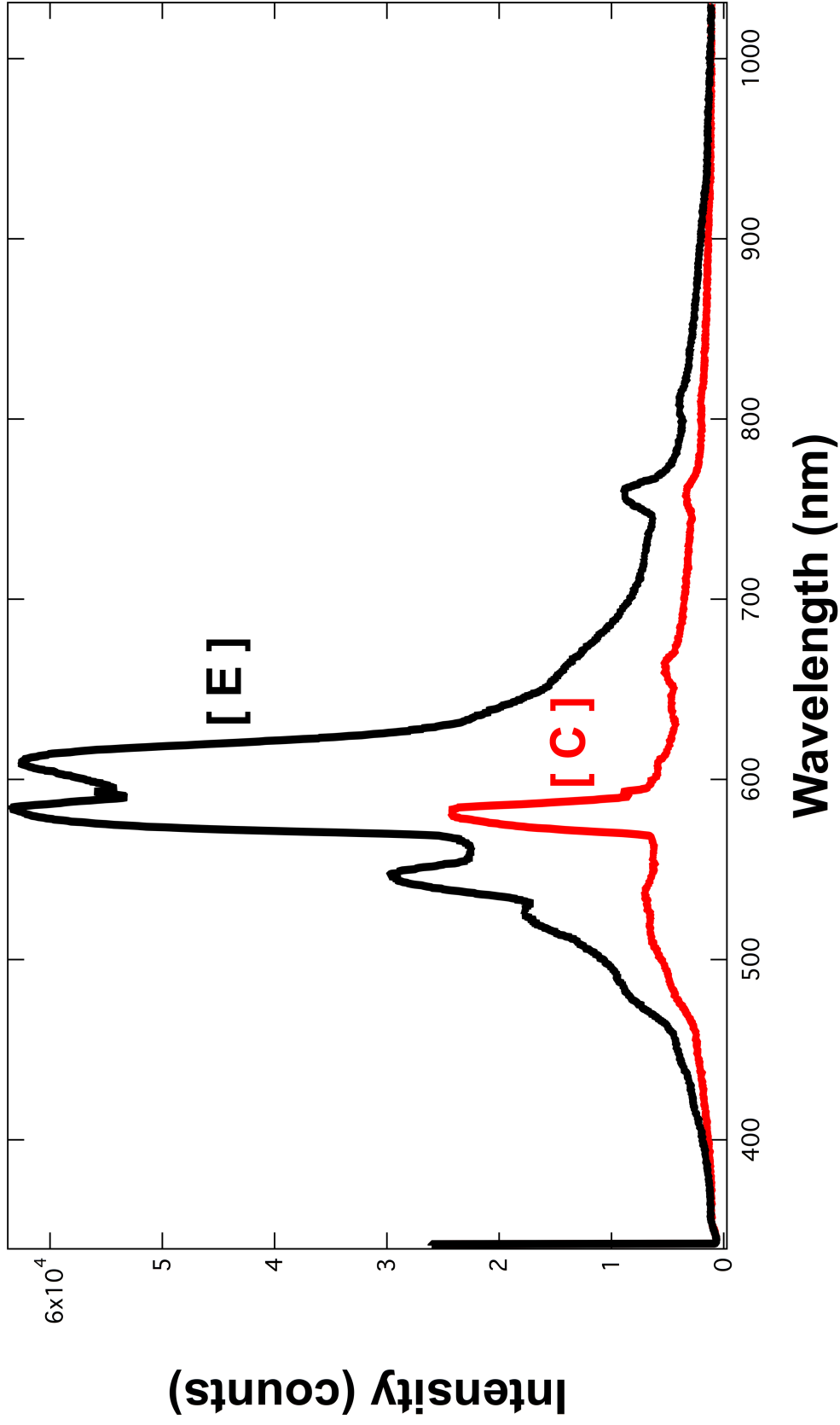


Figure 2.2: Plume emission spectra of [E] enamel and [C] composite. Note the higher intensity from enamel, the common sodium emission line at 589 nm in both spectra, and the strong calcium emission line at 605 nm in the enamel spectrum.

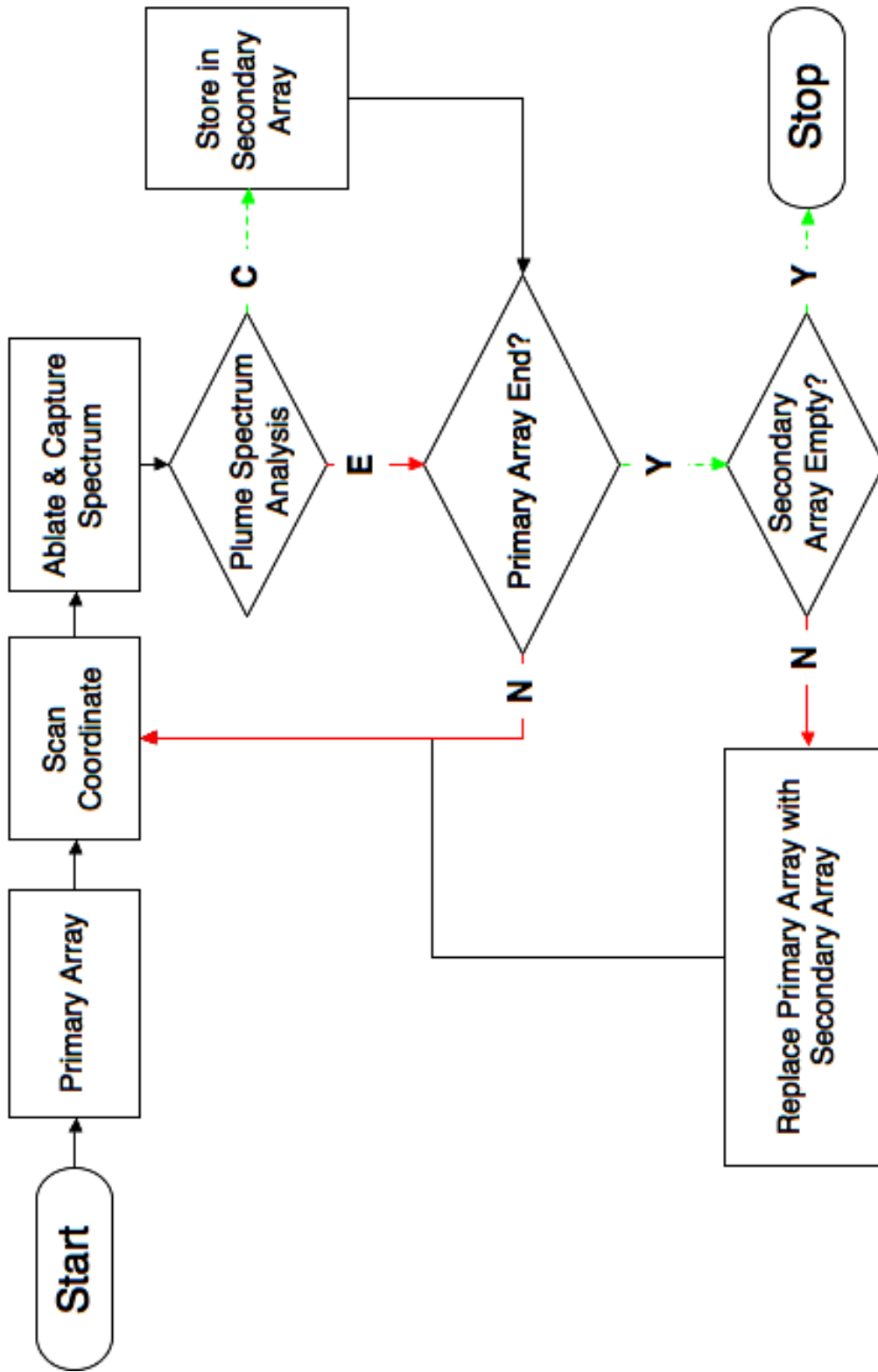


Figure 2.3: Flowchart outlining the sequence of steps required for selective ablation.

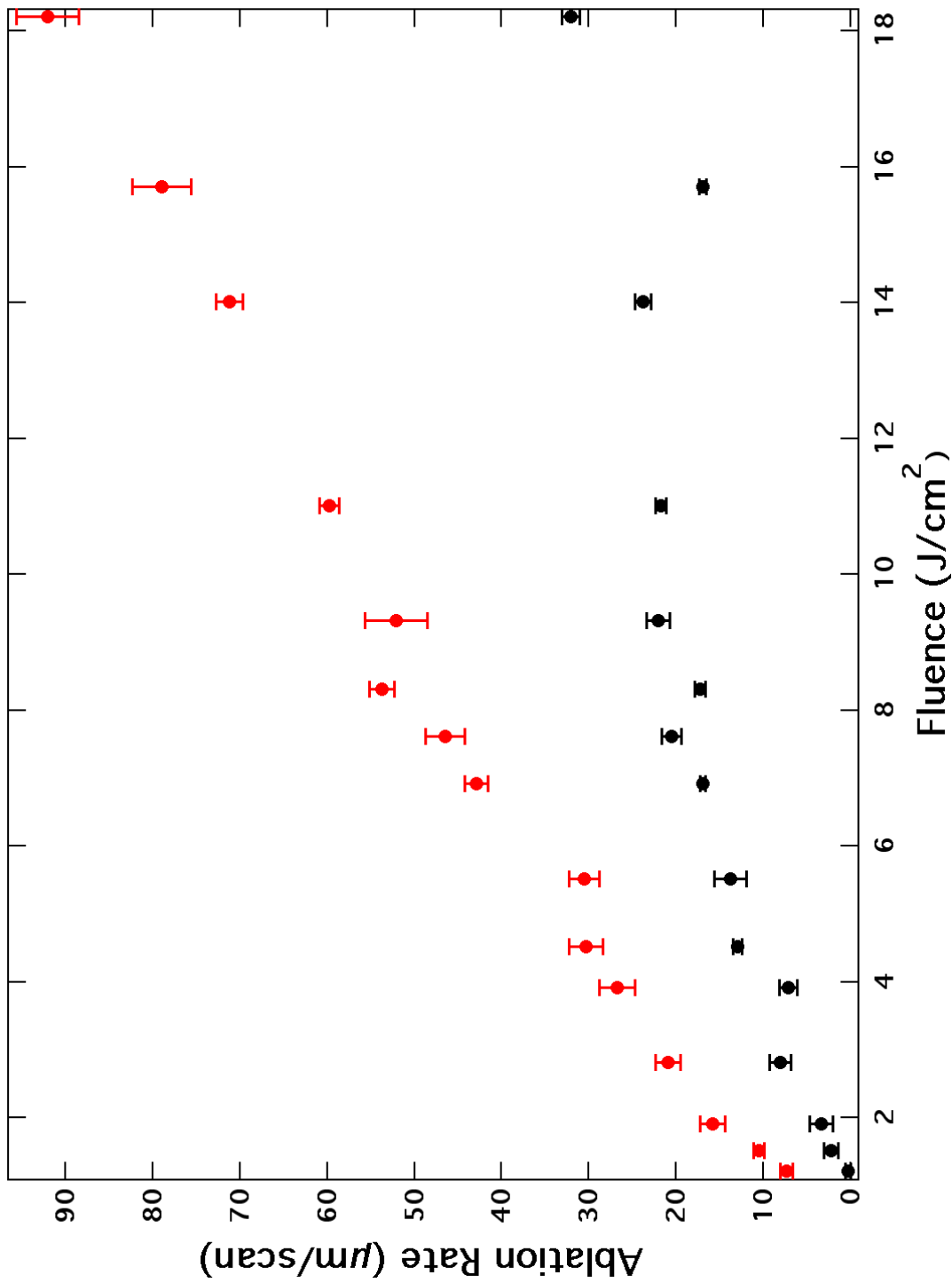


Figure 2.4: Plot of the mean ablation rate (\pm s.d.) for enamel (black circles) and composite (red circles) as a function of incident fluence.

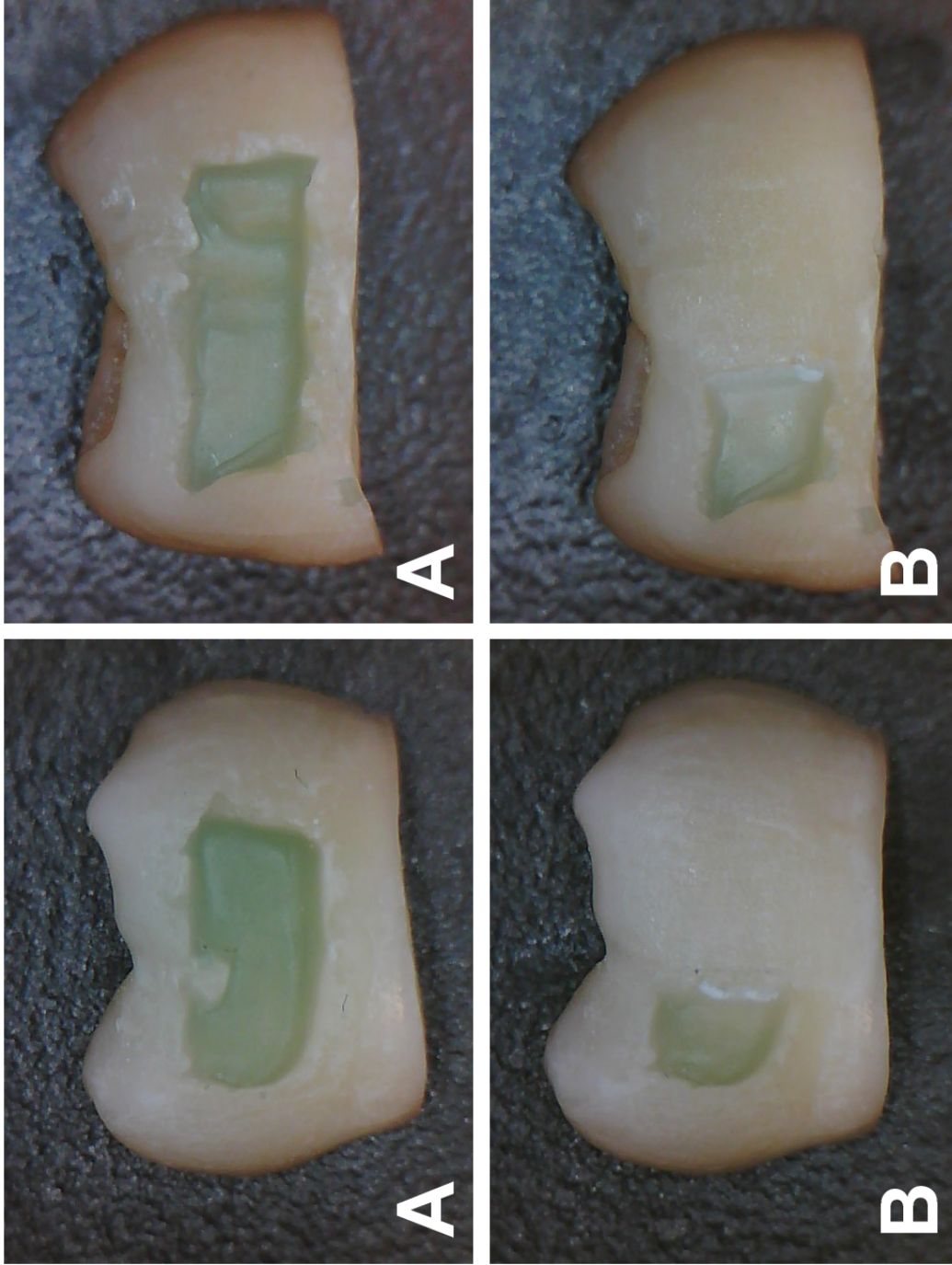


Figure 2.5: Images of two tooth samples with Grelgloo™ composite placed on smooth buccal surfaces. The right half of the composite was removed via selective laser ablation. Images are shown (A) before and (B) after laser irradiation.

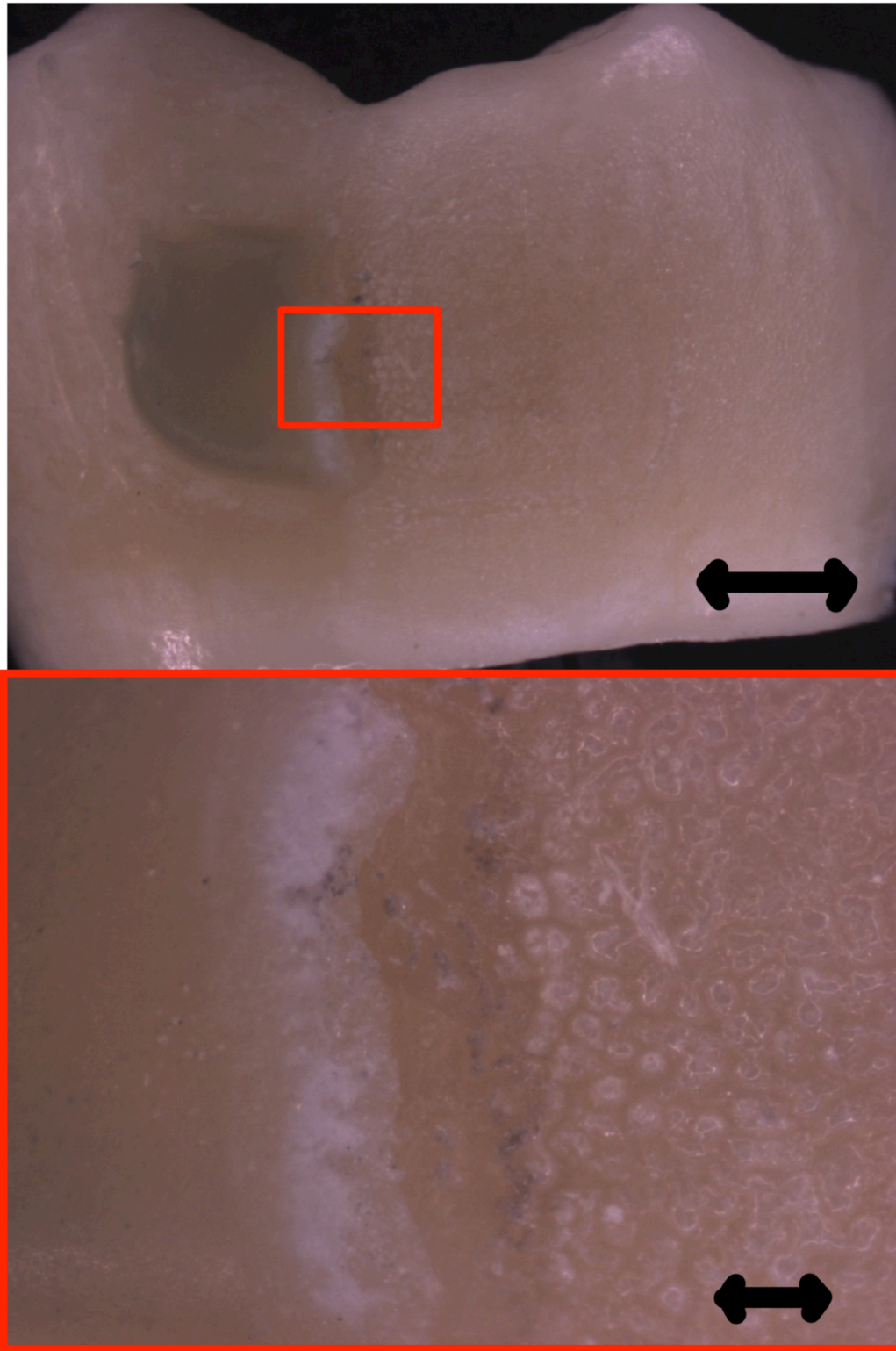


Figure 2.6: Optical microscopy images of the enamel surface after composite removal at two magnifications. The bar in the top image is 1 mm and the bar in the lower image represents 250 μm .

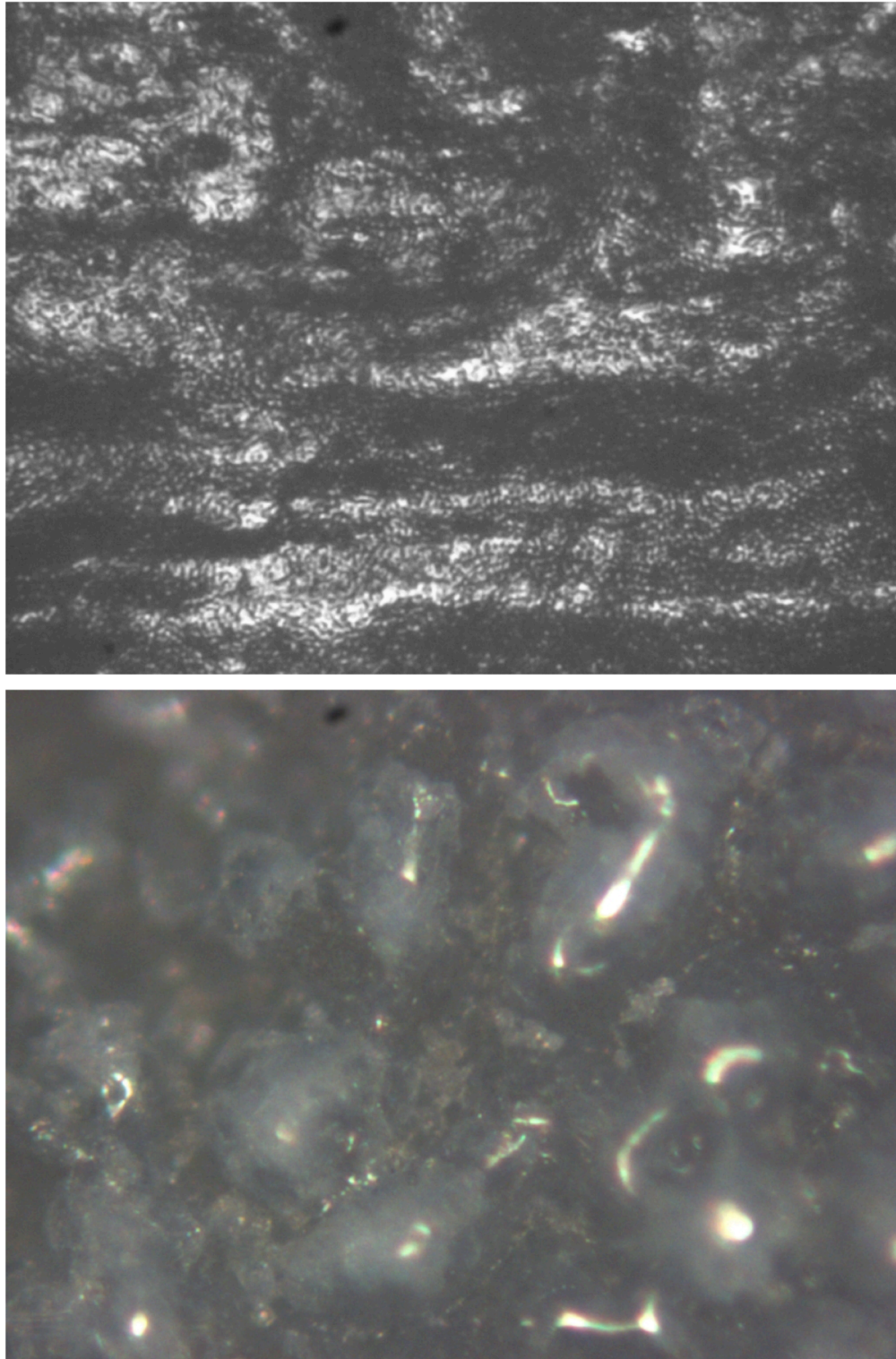


Figure 2.7: Optical microscopy images of the enamel surface (top) before and (bottom) after composite removal at 100x magnification. The enamel surfaces irradiated by the laser appear glassy with worm-like structures that are indicative of melting and recrystallization.

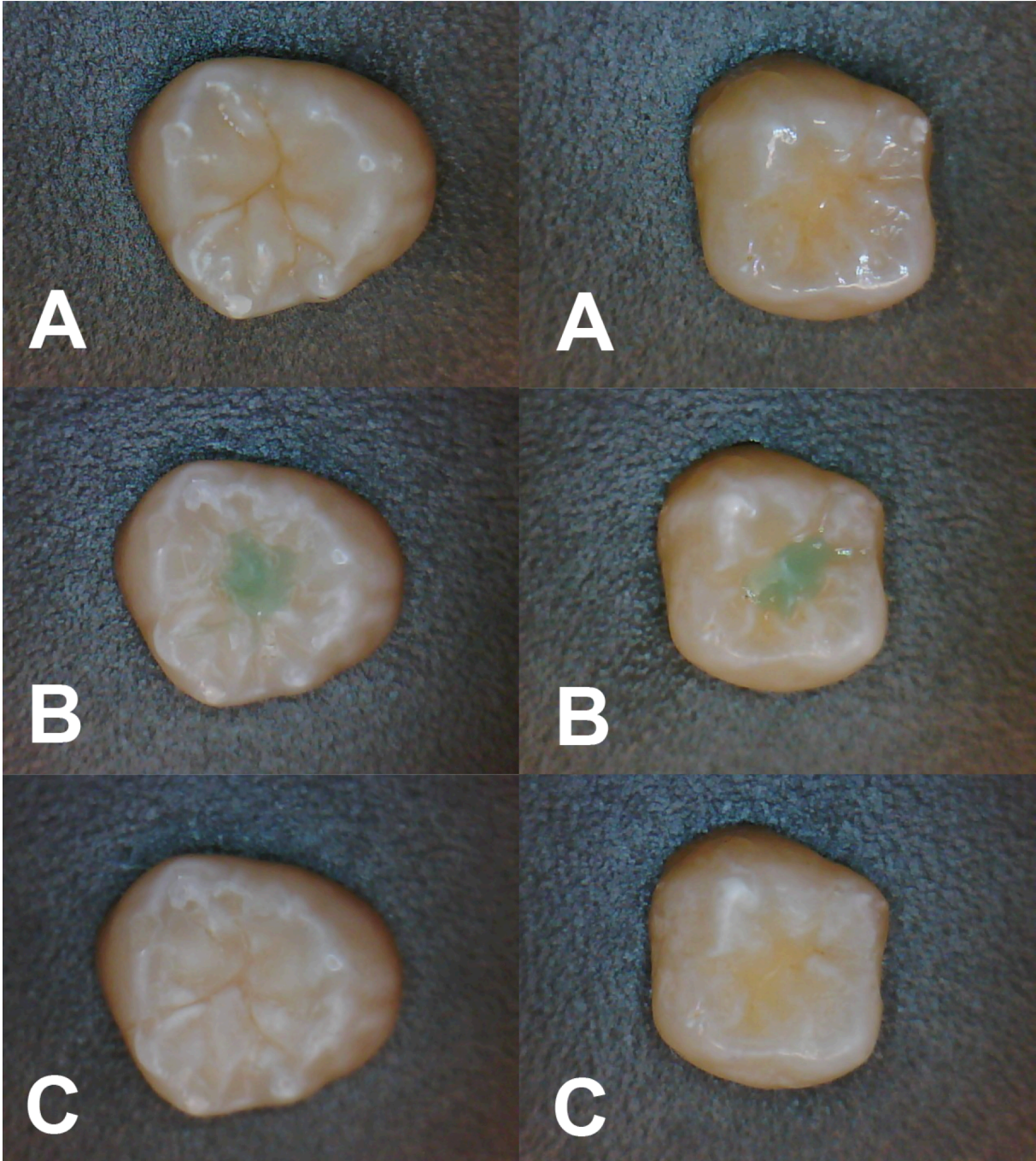


Figure 2.8: Images of two different samples taken (A) before placement of composite; (B) after placement of Grengloo™ composite; and (C) after selective removal of the composite by the laser.

2.7 REFERENCES

- Adrain, R. S., & Watson, J. (1984). Laser Microspectral Analysis - a Review of Principles and Applications. *Journal of Physics D-Applied Physics*, 17(10), 1915-&.
- Alexander, R., & Fried, D. (2001). Selective Removal of Orthodontic Composite using 355-nm Q-switched Laser Pulses, *Lasers in Surgery and Medicine*, 30 240-245 (2002). *Lasers in Surg. Med.*, 30, 240-245.
- Alexander, R., Xie, J., & Fried, D. (2002). Selective removal of residual composite from dental enamel surfaces using the third harmonic of a Q-switched Nd:YAG laser. *Lasers in Surgery and Medicine*, 30(3), 240-245.
- Almeida, H. C., Vedovello Filho, M., Vedovello, S. A. S., Young, A. A. A., & Ramirez-Ya. (2009). ER: YAG laser for composite removal after bracket debonding: a qualitative SEM analysis. *Int J Orthod Milwaukee*, 20(1), 9-13.
- Can, A. M., Darling, C. L., Ho, C., & Fried, D. (2008). Non-destructive assessment of inhibition of demineralization in dental enamel irradiated by a $\lambda=9.3$ -microm CO₂ laser at ablative irradiation intensities with PS-OCT. *Lasers in Surgery and Medicine*, 40(5), 342-349. doi:10.1002/lsm.20633
- Cheng, J. Y., Fan, K., & Fried, D. (2006). *Use of a compact fiber optic spectrometer for spectral feedback during the laser ablation of dental hard tissues and restorative materials*. Paper presented at the Lasers in Dentistry XII.
- Chrisey, D. B., & Hubler, G. K. (Eds.). (1994). *Pulsed Laser Deposition of Thin Films*. New York: John Wiley & Sons.
- Dumore, T., & Fried, D. (2000). Selective ablation of orthodontic composite by using sub-microsecond IR laser pulses with optical feedback. *Lasers in Surgery and Medicine*, 27(2), 103-110.
- Duplain, G., Boulay, R., & Belanger, P. A. (1987). Complex index of refraction of dental enamel at CO₂ wavelengths. *Appl. Optics*, 26, 4447-4451.
- Eberhard, J., Eisenbeiss, A. K., Braun, A., Hedderich, J., & Jepsen, S. (2005). Evaluation of selective caries removal by a fluorescence feedback-controlled Er:YAG laser in vitro. *Caries Res*, 39(6), 496-504.

Fan, K., Bell, P., & Fried, D. (2006). The Rapid and Conservative Ablation and Modification of Enamel, Dentin and Alveolar Bone using a High Repetition Rate TEA CO₂ Laser Operating at $\lambda=9.3\ \mu\text{m}$. *J. Biomed. Opt.*, 11(6), 064008-064011.

Fan, K., & Fried, D. (2006). *A High Repetition Rate TEA CO₂ Laser Operating at $\lambda=9.3\text{-}\mu\text{m}$ for the Rapid and Conservative Ablation and Modification of Dental Hard Tissues*. Paper presented at the Lasers in Dentistry XII.

Fan, K., & Fried, D. (2007). *Scanning ablation of root caries with acoustic feedback control*. Paper presented at the Lasers in Dentistry XIII, San Jose, CA, USA.

Featherstone, J. D., Barrett-Vespone, N. A., Fried, D., Kantorowitz, Z., & Seka, W. (1998). CO₂ laser inhibitor of artificial caries-like lesion progression in dental enamel. *Journal of dental research*, 77(6), 1397-1403.

Fried, D., Featherstone, J. D., Le, C. Q., & Fan, K. (2006). Dissolution studies of bovine dental enamel surfaces modified by high-speed scanning ablation with a $\lambda = 9.3\text{-}\mu\text{m}$ TEA CO₂ laser. *Lasers in Surgery and Medicine*, 38(9), 837-845. doi:10.1002/lsm.20385

Fried, D., Murray, M. W., Featherstone, J. D. B., Akrivou, M., Dickenson, K. M., & Duhn, C. (2001). Dental hard tissue modification and removal using sealed TEA lasers operating at $\lambda=9.6\ \mu\text{m}$. *J. Biomedical Opt.*, 6(2), 231-238.

Fried, D., Xie, J., Shafi, S., Featherstone, J. D. B., Breunig, T., & Lee, C. Q. (2002). Early detection of dental caries and lesion progression with polarization sensitive optical coherence tomography. *J. Biomed. Optics*, 7(4), 618-627.

Hibst, R., & Keller, U. (1989). Experimental studies of the application of the Er:YAG laser on dental hard substances: I. Measurement of the ablation rate. *Lasers Surg. Med.*, 9, 338-344.

Hibst, R., & Keller, U. (1991). *Removal of dental filling materials by Er:YAG laser radiation*. Paper presented at the Lasers in Orthopedic, Dental, and Veterinary Medicine.

Kim, B. M., Feit, M. D., Rubenchik, A. M., Mammini, B. M., & Da, S. L. B. (1998). Optical feedback signal for ultrashort laser pulse ablation of tissue. *Elsevier. Applied Surface Science*, 127-129, 857-862.

Lizarelli, R. d. F. Z., Moriyama, L. T., & Bagnato, V. S. (2003). Ablation of composite resins using Er:YAG laser—comparison with enamel and dentin. *Lasers in Surgery and Medicine*, 33(2), 132-139. doi:10.1002/lsm.10196

Louie, T. M., Jones, R. S., Le, C. Q., & Fried, D. (2004). *Selective removal of composite restorative materials using Q-switched 355-nm laser pulses*. Paper presented at the Lasers in Dentistry X, San Jose.

Louie, T. M., Jones, R. S., Sarma, A. V., & Fried, D. (2005). Selective removal of composite sealants with near-ultraviolet laser pulses of nanosecond duration. *Journal of Biomedical Optics*, 10(1), 14001. doi:10.1117/1.1854676

McCormack, S. M., Fried, D., Featherstone, J. D., Glena, R. E., & Seka, W. (1995). Scanning electron microscope observations of CO₂ laser effects on dental enamel. *Journal of dental research*, 74(10), 1702-1708.

Nelson, J. S., Yow, L., Liaw, L. H., Macleay, L., & Zavar, R. B. (1988). Ablation of bone and methacrylate by a prototype Er:YAG laser. *Lasers Surg Med*, 8(5), 494-500.

Niemz, M. H. (1994). Investigation and spectral analysis of the plasma-induced ablation mechanism of dental hydroxyapatite. *Appl. Phys. B*, 58, 273-281.

Oraevsky, A. A., Jacques, S. L., Pettit, G. H., Tittel, F. K., & Henry, P. D. (1993). XeCl laser ablation of atherosclerotic Aorta: Luminescence spectroscopy of ablation products. *Lasers Surg. Med.*, 13, 168-178.

Ready, J. F. (1971). *Effect of High Power Laser Radiation*. New York: Academic Press.

Rechmann, P., & Hennig, T. (1994). *Caries selective ablation: first histological examinations*. Paper presented at the Laser Surgery: Advanced Characterization, Therapeutics, and Systems IV, Los Angeles, CA, USA.

Rechmann, P., Hennig, T., von den Hoff, U., & Kaufmann, R. (1993). *Caries-selective ablation: wavelength 377 nm versus 2.9 μm*. Paper presented at the Lasers in Orthopedic, Dental, and Veterinary Medicine II, Los Angeles, CA, USA.

Sherman, D. B., Ruben, M. P., & Goldman, H. M. (1965). The Application Of Laser For The Spectrochemical Analysis Of Calcified Tissues. *Ann N Y Acad Sci*, 122, 767-772.

Smith, S. C., Walsh, L. J., & Taverne, A. A. (1999). Removal of orthodontic bonding resin residues by CO₂ laser radiation: surface effects. *J Clin Laser Med Surg*, 17(1), 13-18.

Striganov, A. R., & Sventitskii, N. S. (1968). *Tables of spectral lines of neutral and ionized atoms*. NY: Plenum.

Suri, A. (2005). (MS), University of San Francisco, CA.

Tao, Y. C., & Fried, D. (2009). Near-infrared image-guided laser ablation of dental decay. *Journal of Biomedical Optics*, 14(5), 054045. doi:10.1117/1.3253390

Thompson, R. E., & Way, D. C. (1981). Enamel loss due to prophylaxis and multiple bonding/debonding of orthodontic attachments. *Am. J. Orthodontics*, 79, 282-295.

Wheeler, C. R., Fried, D., Featherstone, J. D., Watanabe, L. G., & Le, C. Q. (2003). Irradiation of dental enamel with Q-switched lambda = 355-nm laser pulses: surface morphology, fluoride adsorption, and adhesion to composite resin. *Lasers in Surgery and Medicine*, 32(4), 310-317. doi:10.1002/lsm.10162

Wheeler, C. R., Fried, D., Featherstone, J. D. B., & Watanabe, L. G. (2003). Irradiation of dental enamel with Q-switched lambda=355-nm laser pulses: Surface morphology, fluoride adsorption, and adhesion to composite resin. *Lasers Surg Med*, 32, 310-317.

Zach, L., & Cohen, G. (1965). Pulp response to externally applied heat. *Oral. Surg. Oral. Med. Oral. Pathol.*, 19, 515-530.

Zuerlein, M., Fried, D., Featherstone, J., & Seka, W. (1999). Optical properties of dental enamel at 9 - 11 μm derived from time-resolved radiometry. *Special Topics IEEE J Quant. Elect.*, 5((4)), 1083-1089.

CHAPTER III
ANALYSIS OF ENAMEL SURFACE DAMAGE AFTER SELECTIVE LASER
ABLATION OF COMPOSITE FROM TOOTH SURFACES

3.1 SUMMARY

Resin-based composites are used for many applications in dentistry. They are difficult to remove without damage to the underlying enamel since they adhere strongly and are color matched to the tooth. The objective of this chapter is to determine if an automated laser scanning system using spectral feedback could selectively remove residual orthodontic composite from tooth surfaces with minimal damage to the underlying enamel.

A CO₂ laser operating at a wavelength of 9.3 μm with a pulse duration of 10-15 μs and a pulse repetition rate of ~200 Hz was used to selectively remove composite from the buccal surfaces of extracted teeth. A spectral feedback system utilizing a miniature spectrometer was used to control the laser scanning system. Pulpal temperature measurements were performed during composite removal to determine if there was excessive heat accumulation. Conventional and digital microscopes were used to assess the amount of enamel lost during removal.

The amount of enamel lost averaged between 20 and 25 μm for irradiation intensities from 3.8 to 4.2 J/cm², respectively. An average maximum temperature rise of 1.9 ± 1.5°C was recorded, with no teeth approaching the critical value of 5.5°C. The average time for composite removal from an area of 5 mm² was 19.3 ± 4.1 sec, fast enough for clinical feasibility.

Residual composite can be rapidly removed from tooth surfaces using a CO₂ laser with spectral feedback, with minimal temperature rise within the pulp and with minimal loss of sound enamel.

3.2 INTRODUCTION

Dental composites and glass ionomers are used as restorative materials for filling cavities and filling, shaping and covering teeth for esthetic purposes, and as adhesives. Dentists spend more time replacing existing restorations that fail due to microleakage and secondary caries than they do placing new restorations (Bernardo et al., 2007; Gordan et al., 2009). Tooth-colored restorations are difficult to differentiate from the surrounding tooth structure and adhere strongly to the underlying enamel and dentin making them challenging to remove without damaging tooth structure. Hence, the clinician frequently removes excessive amounts of healthy tooth structure to ensure complete removal of the composite (Hong & Lew, 1995; R G Oliver, 1988). Therefore, a system that can rapidly and selectively remove composite from tooth surfaces while minimizing the inadvertent removal of healthy tooth structure would be a significant improvement over current methods.

Composite-based resins are used to attach orthodontic brackets to tooth surfaces and it is difficult to remove the residual composite left on the tooth surface after bracket debonding. A wide variety of modalities have been recommended for the removal of residual composite, including high-speed and low-speed handpiece attachments, for example tungsten carbide burs, polishing discs and points, and rubber cups and polishers (Gwinnett & Gorelick, 1977; Hong & Lew, 1995; R. G. Oliver & Griffiths, 1992; Ryf et al., 2012). Iatrogenic sequelae associated with the use of high-speed and low-speed handpieces include variable enamel scratches and loss, incomplete removal of composite and excessive heat accumulation. Studies of the removal of residual composite with carbide burs are highly variable and a mean loss in excess of 50 μm has

been reported (Al Shamsi, Cunningham, Lamey, & Lynch, 2007; Fitzpatrick & Way, 1977; Tufekci, Merrill, Pintado, Beyer, & Brantley, 2004). Moreover, excessive heat accumulation during removal with the handpiece can occur (Uysal, Eldeniz, Usumez, & Usumez, 2005).

One approach to debonding esthetic ceramic brackets is to use laser energy to thermally degrade the adhesive resin with the bracket still in place (Azzeh & Feldon, 2003). However, such an approach may excessively heat up the entire tooth and residual composite may still remain on tooth surfaces. Another laser-based approach is to selectively ablate residual composite from tooth surfaces. Previous studies have shown that high ablation selectivity can be achieved using laser pulses at $\lambda = 355$ nm of nanosecond duration (Alexander et al., 2002; T. M. Louie et al., 2005; Wheeler, Fried, Featherstone, Watanabe, et al., 2003). However, the frequency-tripled Nd:YAG laser is poorly suited for the removal of sound and demineralized dental hard tissues and utilizes UV radiation. It is safer and more economical to utilize a laser that can be used for multiple applications. Carbon dioxide (CO₂) lasers, which have been used extensively for decades for soft tissue surgery, have also been advocated for use in caries removal and caries prevention due to their high absorption by carbonated apatite in dental enamel and have recently received clearance of the Food and Drug Administration for use on hard tissues. Enamel absorption is 5-6 times higher at 9.3 and 9.6 μm than the more commonly used 10.6 μm wavelength which allows more efficient heating and ablation of dental hard tissues (MJ Zuerlein et al., 1999). Therefore a pulsed CO₂ laser operating at 9.3 μm is well suited for caries removal. Moreover, the underlying enamel will be modified to a more acid resistant phase after composite

removal (Can et al., 2008; J. D. Featherstone et al., 1998; J. D. B. Featherstone, Fried, & Bitten, 1997; J. D. B. Featherstone & Nelson, 1987; D. Fried et al., 2006a; D. Fried et al., 2001).

The pulsed CO₂ laser can also be used to ablate composite selectively if spectral feedback is employed (Chan et al., 2011). During laser ablation, a luminous emission plume is produced that is unique to each tissue or material. The luminous plume generated during hard tissue ablation by the CO₂ laser consists of electronically excited atoms, ions and molecules ejected from the site of the ablated materials as described in Section 2.3.3 and previous literature (Chan et al., 2011; Cheng et al., 2006; T. Dumore & D. Fried, 2000). Individual peaks can be identified with wavelength tables of elemental spectra (Niemz, 1994). Therefore, it is possible to differentiate enamel and composite spectra by their distinct component peaks. Dumore and Fried (T. Dumore & D. Fried, 2000) showed that the plume emission spectrum acquired during the laser ablation of dental enamel possesses distinct calcium emission lines that are strong between 580 and 650 nm, giving the plume a distinct red appearance. This region is lacking in composite resin and its fillers, and can thus be used to differentiate enamel from composite.

This chapter demonstrates that composite can be selectively removed from tooth buccal and occlusal surfaces at clinically relevant rates using a CO₂ laser operating at 9.3 μm with high pulse repetition rates with minimal heat deposition (Chan et al., 2011). The selective removal of composite from the smooth buccal surfaces is more challenging than removing composite from other tooth surfaces since it is particularly important to minimize enamel loss from these highly visible tooth surfaces for esthetic reasons. The

objective of this study was to analyze the enamel surface damage produced during the removal of residual orthodontic composite from tooth buccal surfaces.

3.3 MATERIALS AND METHODS

3.3.1 Tooth Samples

Twenty-six premolars and molars were collected from patients in the San Francisco Bay Area and sterilized with gamma radiation. Eleven teeth with the roots intact were used for the measurements of heat accumulation and the time required for removal as described in Section 3.3.5 (Group #1). The roots were removed from the remaining 15 teeth and the crowns were sectioned into buccal and lingual halves and these 30 tooth halves were divided into Groups #2 and #3 that were used for the measurements of enamel loss and volume of composite/enamel removed as described in Section 3.3.6.

Orthodontic brackets were bonded to the buccal or lingual surfaces of twenty of these tooth halves (Group #2) with Grengloo™ (Ormco, Orange, CA, USA) composite. Ortho Solo™ (Ormco, Orange, CA, USA) adhesive, and 37% phosphoric acid etchant according to the manufacturer's instructions. Grengloo™ composite changes color and appears green below body temperature. This helps to identify any residual composite missed by the laser. It also has similar composition to other composites. The brackets were mechanically debonded leaving the residual composite.

For the remaining 10 tooth halves (Group #3), tooth surfaces were ground flat using an 800-grit polishing wheel and a thick layer of composite was applied to the flat surfaces; orthodontic brackets were no bonded to the surfaces.

3.3.2 Laser System

The CO₂ laser used in this study was an IMPACT[®] 2500 (GSI Lumonics, Rugby, UK) operating at a wavelength of 9.3 μm. The laser was custom-modified to produce a Gaussian output beam (single spatial mode) and a pulse duration of between 10 and 15 μs. The laser was operated at a pulse repetition rate of ~220 Hz, with a spot size of ~750 μm and a 150 μm overlap between laser spots for the experiments described in Sections 3.3.5 and 3.3.6. The tooth was cooled with a low volume/low pressure air-actuated fluid spray delivery system that provided a pulsed uniform mist at a rate of 0.5 ml/min at room temperature. The water spray was pulsed with a frequency of 0.5 Hz for a delivery rate of 10 ml/s over an area of 5 cm². The laser irradiation intensities are indicated in the text as the fluence for single incident laser pulses (not accumulated over multiple pulses) was varied using CaF₂ attenuators of various thicknesses, ranging from 1 to 20 mm.

3.3.3 Computer-controlled Laser Scanning System with Spectral Feedback

Computer-controlled XY galvanometers 6200HM series with MicroMax Series 671 (Cambridge Technology, Inc., Bedford, MA, USA) were used to scan the laser beam over sample surfaces. A laser spot size of 750 μm was used with a spot-to-spot separation of 150 μm.

The plume produced from laser irradiation of each spot was captured using a USB2000+ fiber optic spectrometer (Ocean Optics, Dunedin, FL, USA) incorporating a 2048-element CCD detector that was used in conjunction with a 1 mm bare silica-fiber to acquire spectra as previously described in Section 2.3.3 and past studies (Chan et al., 2011). Distinct calcium emission lines only present in enamel were used to

differentiate between the ablation of enamel and composite. Both composite and enamel spectra contain the strong sodium D-emission line near 580 nm. The composite spectrum is similar to the emission spectrum of ablated glass and quartz (Cheng et al., 2006). Dental hard tissues have a very strong emission line centered at 605 nm. The ratio and intensities of the 580 and 605 nm peaks were used to differentiate between composite and enamel.

A flow chart describing the algorithm used to remove the composite is shown in **Figure 3.1** and it is described in greater detail in Section 2.3.7 and Chan et al. (Chan et al., 2011). The laser beam was scanned from point to point over a matrix defining a specific area. The plume emission ratio from each irradiated spot was subsequently used to determine if that spot was enamel or composite and a new matrix was generated defining the area of composite to be removed in the following scan. This process was repeated until the entire composite was removed. A final “clean-up” scan was carried out along the margin of composite, as determined from analysis of the plume emission acquired from the initial scan, to remove residual composite at the perimeter.

3.3.4 Composite Ablation Rate Measurements

The ablation rate for Grengloo™ composite was measured and compared with previous measurement of enamel, **Chapter II: Figure 2.4** (Chan et al., 2011), at varying irradiation intensities in order to select the optimal incident laser fluence for removal. Disks, 1-2 mm thick of cured Grengloo™ (Ormco, Orange, CA) composite were prepared using a diamond saw (Isomet 5000; Buehler, Lake Bluff, IL). The incident fluence was varied from 0 to 20 J/cm² and the laser spot size was maintained at 450 μm. The laser beam was scanned in a rectangular pattern over an area roughly 3.6 x

1.5 mm with each laser spot separated by 150 μm . There were three scans for each of the 15 irradiation intensities investigated. Optical coherence tomography (OCT) was used to measure the mean depth per scan, described in [Section 2.3.4](#) (Chan et al., 2011). The same procedure was used previously to determine the rate of ablation of a more conventional Z250 composite (3M, Minneapolis, MN) and dental enamel.

3.3.5 Measurements of Heat Accumulation and the Time Required for Removal

Eleven extracted human premolars and molars with the roots intact were used for thermocouple measurements (Group #1). The roots were left on each tooth and a small hole was drilled into tooth mesial or distal surfaces at the level of the cement-enamel junction using a high-speed dental handpiece with a carbide bur (Model 1169L; Miltex, York, PA). Microthermocouples (K type, 36 G; Omega Engineering Inc., Stamford, CT) were inserted into the pulp chamber of each tooth. The laser ablation setup is shown in **Figure 3.2** which indicates the relative position of the thermocouple within the tooth and the composite on the tooth buccal surface. A high thermal conductivity silicone paste (OMEGATHERM[®] 201, Omega Engineering Inc., Stamford, CT) was used to ensure good thermal contact with the tooth. Digital periapical films were taken to verify the position of the thermocouple. Computer-controlled galvanometers scanned the laser beam to remove all residual orthodontic composite from the tooth surface in a 5 x 5 mm² matrix. A thermocouple controller (Model SR630; Stanford Research Systems, Sunnyvale, CA) was used to record the thermal data. The teeth were irradiated using a fluence of 3.8 J/cm², and a water spray at room temperature was used. A temperature rise of >5.5°C was considered the threshold for risk of pulpal inflammation (Zach & Cohen, 1965). The time taken to ablate all residual composite on the tooth surface was

recorded, as well as the temperature change from the initial temperature to the maximum temperature recorded before and after the removal process. Similar temporal profiles to those observed during composite removal from tooth occlusal surfaces were recorded (Chan et al., 2011), namely the temperature initially dropped a few degrees due to the cooling effect of the water spray and subsequently rose a few degrees as heat accumulated in the tooth when removal was completed.

3.3.6 Measurements of Enamel Loss and Volume of Composite/Enamel Removed (Groups #2 and #3)

The twenty samples (tooth halves) of Group #2 were further subdivided into two groups of 10 and irradiated at either 3.8 J/cm² (Group #2a) or 4.2 J/cm² (Group #2b). Two irradiation intensities were used to assess how sensitive the enamel loss is to slight variations in the incident fluence. Half of the residual composite was removed in a rectangular matrix of about 2.5 x 5 mm² with the laser removal program leaving half of the residual composite intact.

After composite removal by the laser, the enamel surfaces of Group #2 were analyzed with a Leitz Secolux microscope (Leica, Solms, Germany) with a magnification of 50 – 1000x. Damage to the enamel surface appeared as a roughening of enamel. The greatest enamel loss appears to have occurred at the center of each crater left by individual laser pulses. Enamel loss was assessed by measuring the vertical deviation near the center of each overlapping crater by scanning the image plane of a conventional microscope. A digital micrometer was seated on the microscope platform to measure the change in platform height as the microscope was manually focused on

the surface and at the base of the deeper craters. Five of the deeper crater areas were measured per sample, and the mean \pm standard deviation (SD) is reported.

The 20 samples of Group #2 were also visually evaluated by two observers without magnification. Teeth were categorized into four groups based on the degree of texture on the enamel surface (roughening) after laser ablation of all 20 samples (1-minimal, 2-slight, 3-moderate, 4-severe). Six of the twenty teeth were further polished after laser irradiation. Three were polished with Renew Finishing System Points #383 (Reliance Orthodontic Products Inc., Itasca, IL) on a high-speed handpiece and three were polished with prophy cups and prophy paste on a slow-speed handpiece. The teeth were then evaluated under the microscope and photographed.

The 10 samples (tooth halves) of Group #3 with composite placed on the flat surfaces were irradiated with a fluence of 4.0 J/cm^2 . All the composite was removed by scanning a 4 mm^2 area with the laser removal program. Surfaces were evaluated using the VHX-1000 optical microscopy/3D surface profilometry system (Keyence, Itasca, IL). Two lenses were used, the VH-Z25 with a magnification from 25 to 175x and the VH-Z100R with a magnification of 100 – 1000x. 3D images of the samples were acquired before and after ablation at 1000x and 175x magnification. Images at different focus positions are rapidly acquired by scanning the z-axis stage and algorithms are used to generate a depth composition image (fully focused images) with all points of the image in focus or a 3D image can be generated. The Keyence 3D shape measurement software, VHX-H3M, was used to correct the tilt of the sample and measure the variation in depth over the enamel in the post-ablated composite area. This software provided 2D profiles of the surface variation which were used to calculate the mean vertical deviation in the

surface and the surface roughness. The mean vertical deviation was calculated by measuring the mean depths of five craters. The Keyence software was also used to calculate the root mean squared (RMS) roughness of the irradiated enamel surface.

Since the Keyence microscope acquires 3D images, it is possible to determine the volume of composite removed by subtracting the 3D images taken before and after removal of the composite. Each image was acquired at 175x magnification and contained 1437x1965 pixels, ie., $\sim 1.5 \times 2 \text{ mm}^2$. The non-irradiated enamel edges on the flat ground surfaces were used as a reference for each 3D image.

3.3.7 Statistical Analysis

All statistical analysis was carried out using Prism or InStat software (Graphpad Software, La Jolla, CA). A *t*-test was used to compare the mean vertical deviation of the craters on the laser irradiated surfaces at the two different irradiation intensities, Groups #2a and #2b, to determine if they were significantly different ($p < 0.05$). Linear regression was used to compare the measured vertical deviation values to the subjective visual scores (1 – 4) for Group #2. The Pearson correlation coefficient was calculated and a *t*-test was used to determine if the slope was significantly different from zero ($p < 0.05$).

3.4 RESULTS

3.4.1 Composite Ablation Rate Measurements

The measured relationship between ablation rate and fluence is shown in **Figure 3.3**, and is very similar to Z250 composite in **Chapter II: Figure 2.4** (Chan et al., 2011). The composite ablation rate increased progressively with increasing fluence, whereas the enamel ablation rate peaked at about 20 $\mu\text{m}/\text{scan}$ above approximately 8 J/cm^2 . The

ideal fluence appears to be around 4 J/cm², where the rate of composite removal is twice that of enamel while the enamel loss is reduced to a depth of <10 µm. The use of irradiation intensities (fluence) exceeding 4-5 J/cm² will result in the removal of greater amounts of enamel which may be more selective but the greater damage to enamel is unacceptable on tooth buccal surfaces.

3.4.2 Measurements of Heat Accumulation for Removal (Group #1)

The maximum temperature excursions at the position of the pulp chamber wall opposite the enamel surfaces irradiated by the laser were measured using microthermocouples. An average maximum temperature rise of 1.9 ± 1.5°C (n = 11) was recorded, with none of the measurements approaching the critical value of 5.5°C. The mean time to remove all of the residual composite from the 5 mm² area was 19.3 ± 4.1 sec (n = 11).

3.4.3 Measurements of Enamel Loss and Volume of Composite/Enamel Removed (Groups #2 and #3)

Figure 3.4 shows teeth from Groups #2a and #2b before and after composite removal. Only half of the composite area under the bracket was irradiated by the laser leaving half the composite untouched. Five of the most severely affected areas on each tooth surface were examined using the Leitz microscope at a magnification of 200x. At a fluence of 3.8 J/cm² (Group #2a) the maximum vertical deviation averaged 22.7 ± 5.3 µm. The maximum vertical deviation that was measured ranged from 6 to 49 µm. At 4.2 J/cm² (Group #2b), the maximum vertical deviation averaged 25.3 ± 5.0 µm and the maximum ranged from 11 to 50 µm. There was no significant difference between the maximum vertical deviations for the two groups (*t*-test, *p* > 0.05).

The visual appearance of all samples in Group #2 were subjectively ranked after composite removal (1-minimal, 2-slight, 3-moderate, 4-severe) as previously described. A plot of the measured vertical deviation values vs. the subjective visual scores (1-4) shows that they were correlated; Pearson R = 0.51 ($p < 0.05$). Polishing with the Renew Finishing System #383 (Reliance Orthodontic Products Inc., Itasca, IL) removed some of the surface texture but gave a highly glossed surface. The irradiated area was not visible after additional polishing, and microscopic evaluation with the Leitz microscope indicated that the mean vertical surface deviation decreased to $17.4 \pm 6.6 \mu\text{m}$, from $24.8 \pm 6.9 \mu\text{m}$ immediately following laser irradiation for those samples. The use of prophy paste attached to a prophy cup lightly smoothed the surface texture while making the visual evaluation of the tooth surface more favorable. However, the surface roughness was altered less with the prophy paste than with the Renew Polishing points. The mean vertical surface deviation decreased to $19.1 \pm 3.2 \mu\text{m}$ from $21.1 \pm 2.1 \mu\text{m}$ for the samples polished with the prophy paste.

The Group #3 samples with the composite applied to ground flat surfaces (no brackets) were irradiated at a fluence of 4.0 J/cm^2 . These samples were imaged using the VHX-1000 microscopy/3D surface profilometry system. Both 3D and depth composition images are presented in **Figures 3.5-3.7**. **Figures 3.5 and 3.6** show the depth composition and 3D images at 175x magnification of two of the samples before and after composite removal with RMS surface roughness values of approximately 13 and $20 \mu\text{m}$. Each image represents a $1.5 \times 2 \text{ mm}^2$ area of the tooth surface. The depth composition image is best suited for showing the surface texture and uniformity while the 3D image best shows that the composite is uniformly removed leaving a flat surface.

Figure 3.7 shows higher resolution depth composition and 3D images taken in the area where the composite has been removed.

Digital profilometric measurements were also carried out for the Group #3 samples to determine the mean vertical deviation and the roughness (RMS). The RMS was $23 \pm 7.7 \mu\text{m}$ and the mean vertical deviation was $21.4 \pm 6.3 \mu\text{m}$ which is consistent with our values measured using the Leitz microscope for the Group #2 samples. The mean volume of composite that was removed by the laser in the $1.5 \times 2 \text{ mm}^2$ window was $0.23 \pm 0.1 \text{ mm}^3$.

3.5 DISCUSSION

The amount of enamel lost during the selective removal of residual orthodontic composite using a CO_2 laser with spectral feedback appears to be less than for conventional means for removal using dental low-speed and high-speed handpieces. Most debonding techniques result in some loss of enamel. The degree of enamel loss varies widely in the literature (Brown & Way, 1978b). The thickness of enamel is usually about $1500 - 2000 \mu\text{m}$, and the loss of $60 \mu\text{m}$ is not thought to be detrimental to the tooth (Thompson & Way, 1981). However, the surface fluoride layer gradient is very steep, with the highest concentration at the surface and a rapid decline in the first $20 \mu\text{m}$ of enamel (Brown & Way, 1978b). Therefore, it is desirable to preserve as much of the fluoride-rich surface layer of enamel as possible. In this chapter, the surface roughness and mean vertical deviation (enamel loss) varied from 15 to $30 \mu\text{m}$ for irradiation intensities of $3.8 - 4.2 \text{ J/cm}^2$. The irradiated enamel surface showed a morphology characteristic of surface melting with wavelike or wormlike structures, as previously described by Zuerlein et al. (Zuerlein, Fried, & Featherstone, 1999), such surfaces

manifest increased resistance to acid dissolution (Can et al., 2008; J. D. Featherstone et al., 1998; J. D. B. Featherstone et al., 1997; J. D. B. Featherstone & Nelson, 1987; D. Fried et al., 2006a; D. Fried et al., 2001). It is important to point out, that it is likely that much of that roughness is caused by the repeated melting and recrystallization of the enamel during multiple laser pulses and it is possible that very little enamel was actually vaporized and lost during the procedure. It is highly likely that most of the fluoride rich outer layer of enamel is preserved. The enamel surface texture in laser irradiated areas closely resembles the structures of melted and re-crystallized enamel observed previously (M. J. Zuerlein et al., 1999).

The time required for the CO₂ laser to remove the residual composite remaining after bracket debonding was < 20 sec which is less than conventional methods. Ryf et al. (Ryf et al., 2012) reported a total composite removal time of 65.9 ± 14.0 sec with two steps and up to 183.5 ± 14.1 sec per tooth for four-step procedures. This time was similar to what we reported for the removal of composite from tooth occlusal surfaces in **Chapter 2.4** (Chan et al., 2011). The temperature rise was also similar to the rise produced during the irradiation of the occlusal surfaces even though the thermocouples pulp chamber is closer to the tooth surface in **Chapter 2.4** (Chan et al., 2011). The temperature rise was well below the safe level of 5.5°C determined by Zach and Cohen (Zach & Cohen, 1965).

The digital microscope proved to be extremely valuable for analyzing tooth surfaces before and after laser irradiation. This is the first time this new technology has been used to examine laser-treated tooth surfaces and the depth composition and 3D images

can be used to determine the amount of composite removed from the tooth surface in addition to the surface roughness induced by laser irradiation.

Residual orthodontic composite can be selectively removed from the tooth surface using a rapidly scanned CO₂ laser with spectral feedback, with a minimal temperature rise within the pulp and acceptable damage to the underlying enamel surface.

3.6 FIGURES AND FIGURE LEGENDS

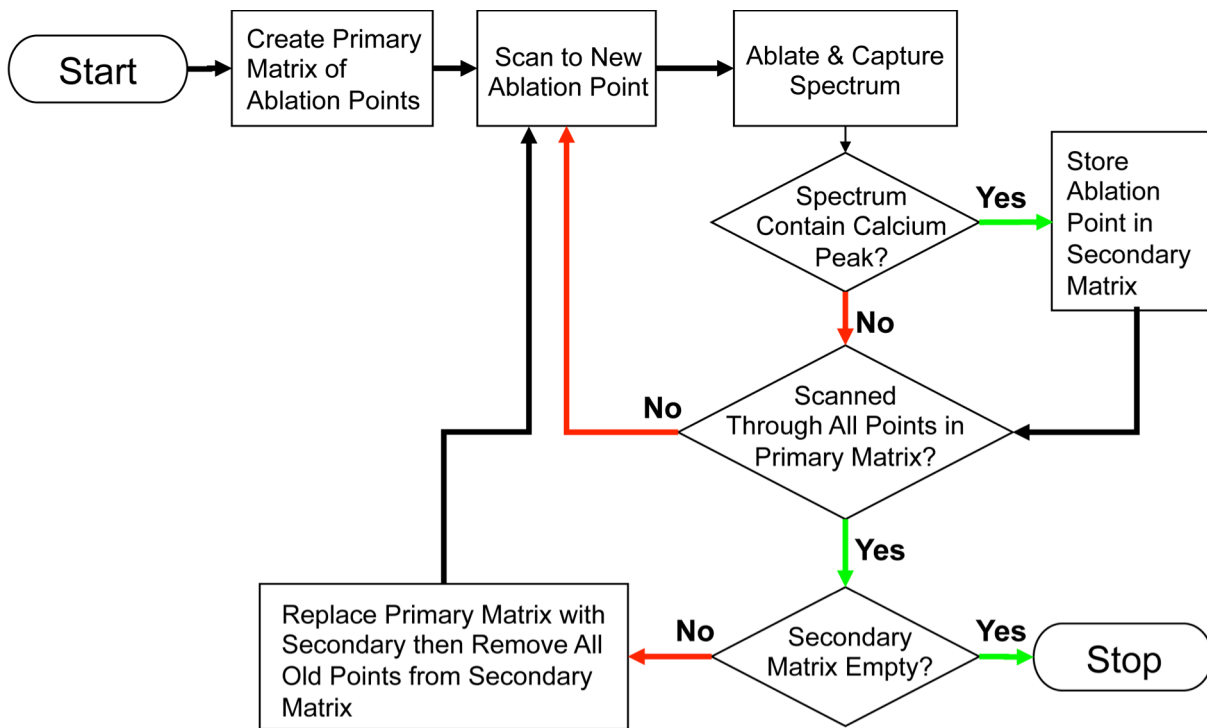


Figure 3.1: Flowchart describing the steps involved in selective ablation.

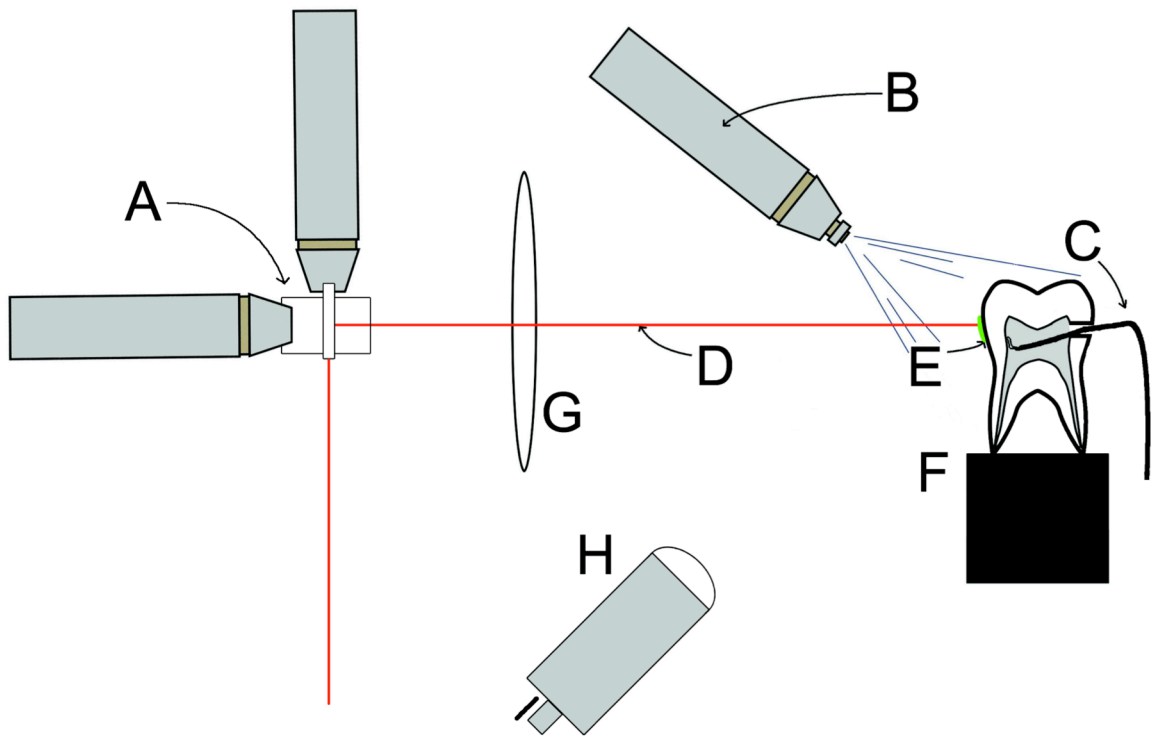


Figure 3.2: The experimental setup for selective ablation is shown above. (A) XY galvanometers; (B) water spray; (C) microthermocouple; (D) CO₂ laser beam; (E) composite on tooth buccal surface; (F) mounted tooth; (G) ZnSe f-theta scanning lens; and (H) imaging optics for spectrometer.

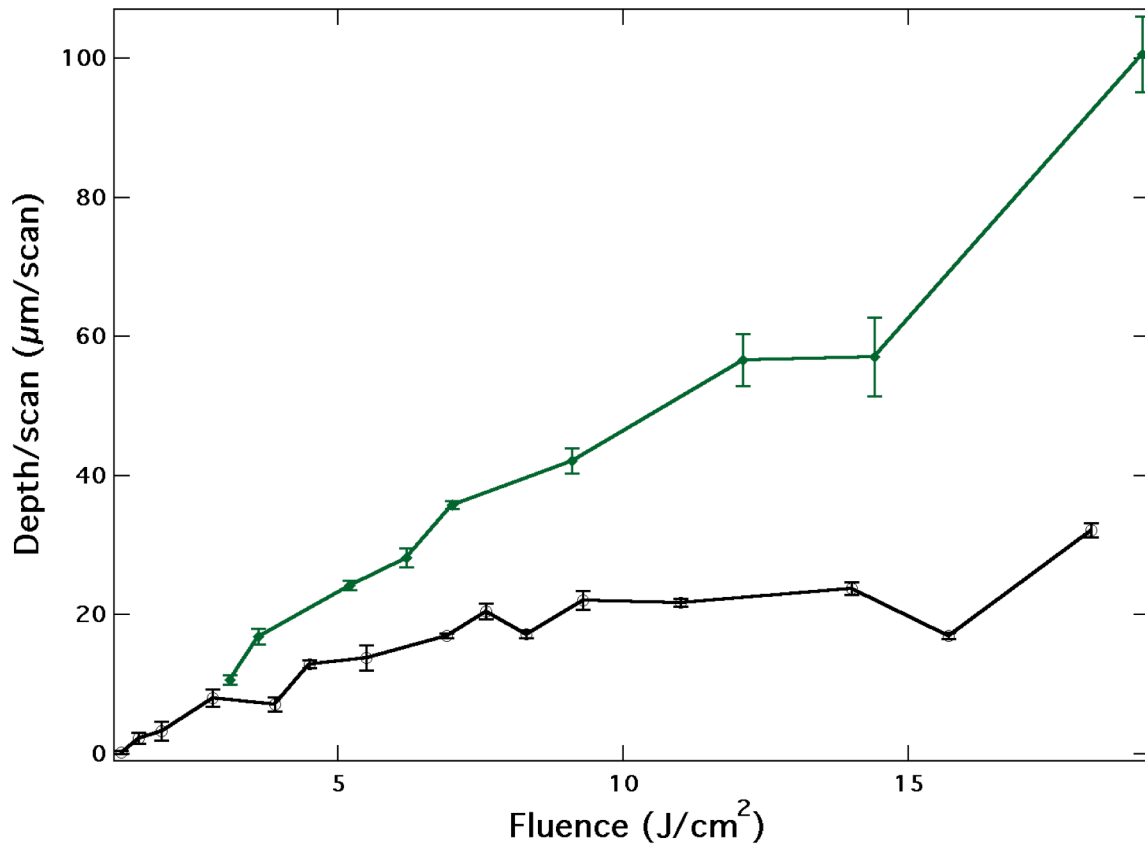


Figure 3.3: Mean depth \pm s.d. (n=3) for each scanned area for Grengloo™ composite (solid diamonds) and enamel (open circles) as a function of laser fluence. The enamel data is from **Chapter II**.

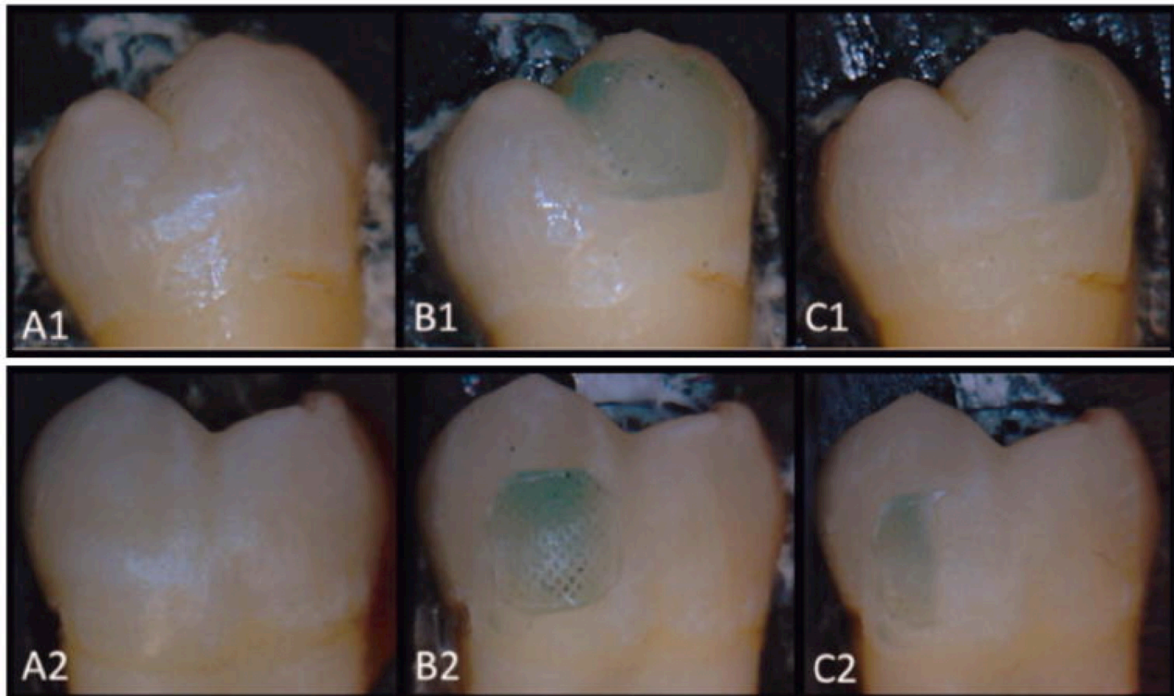


Figure 3.4: Sequential visual images of two samples (A1 – C1 and A2 – C2) during selective composite ablation. (A1 & A2) Buccal surface prior to application of Grengloo™ composite; (B1 & B2) Grengloo™ composite on buccal surfaces before selective removal; and (C1 & C2) after selective ablation at a fluence of 3.8 J/cm² (Tooth #1 – Group #2a) and 4.2 J/cm² (Tooth #2 – Group #2b).

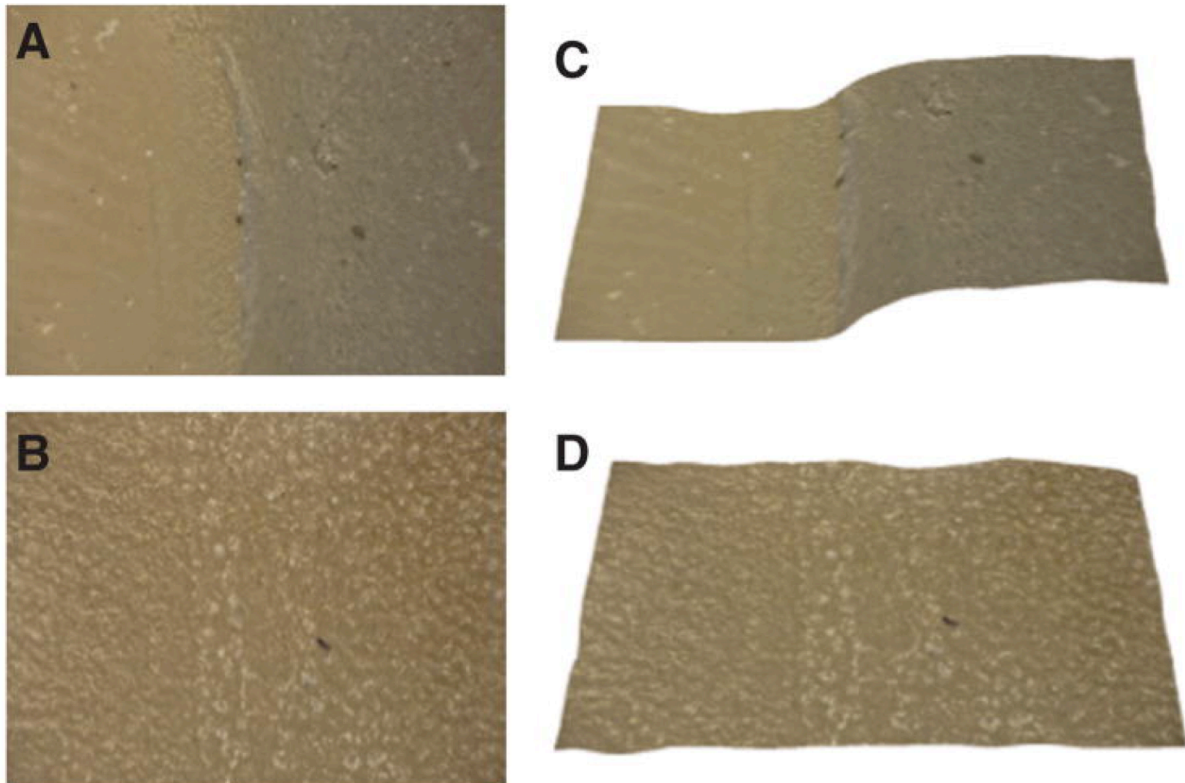


Figure 3.5: Digital microscopy tooth surface images of one sample from Group #3 before and after composite removal acquired with the VHX-1000 digital microscope at 175x magnification. Images (A) and (C) respectively show the depth composition and 3D image of the region of interest before removal of the composite. Images (B) and (D) are the corresponding images after irradiation by the laser. The surface roughness (RMS) is 12.5 μm for the enamel underlying the composite.

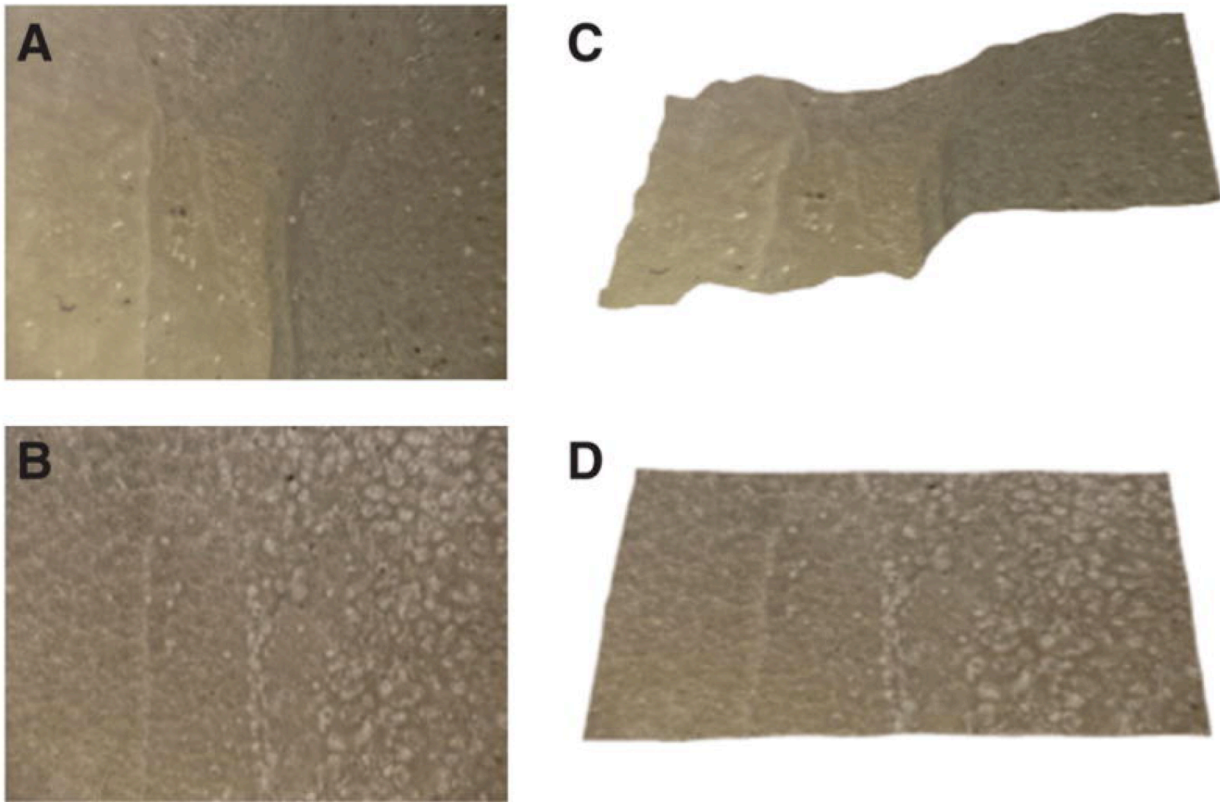


Figure 3.6: Digital microscopy tooth surface images of one sample from Group #3 before and after composite removal acquired with the VHX-1000 digital microscope at 175x magnification. Images (A) and (C) respectively show the depth composition and 3D image of the region of interest before removal of the composite. Images (B) and (D) are the corresponding images after irradiation by the laser. The surface roughness (RMS) is 19.6 μm for the enamel underlying the composite.

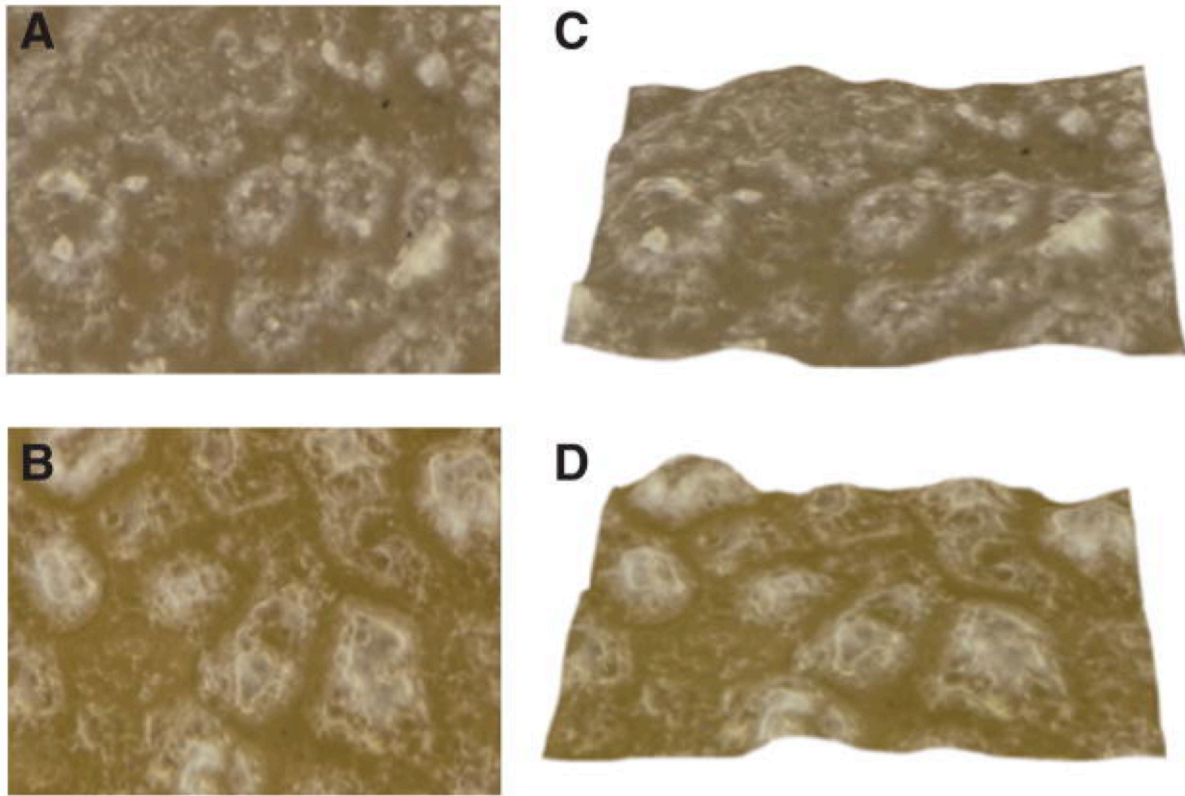


Figure 3.7: (A and B) 2D digital depth composition and (C and D) 3D images of the underlying enamel surface after laser irradiation at 1000x magnification for two samples selected from Group #3. The top – left and –right (A and C, respectively) are the same sample from **Figure 3.5** and bottom – left and –right (B and D, respectively) are the same samples from **Figure 3.6**.

3.7 REFERENCES

Al Shamsi, A. H., Cunningham, J. L., Lamey, P. J., & Lynch, E. (2007). Three-dimensional measurement of residual adhesive and enamel loss on teeth after debonding of orthodontic brackets: an in-vitro study. *American journal of orthodontics and dentofacial orthopedics*, 131(3), 301-309. doi:10.1016/j.ajodo.2006.01.026

Alexander, R., Xie, J., & Fried, D. (2002). Selective removal of residual composite from dental enamel surfaces using the third harmonic of a Q-switched Nd:YAG laser. *Lasers in Surgery and Medicine*, 30(3), 240-245.

Azzeh, E., & Feldon, P. J. (2003). Laser debonding of ceramic brackets: a comprehensive review. *American journal of orthodontics and dentofacial orthopedics : official publication of the American Association of Orthodontists, its constituent societies, and the American Board of Orthodontics*, 123(1), 79-83. doi:10.1067/mod.2003.2

Bernardo, M., Luis, H., Martin, M. D., Leroux, B. G., Rue, T., Leitao, J., & DeRouen, T. A. (2007). Survival and reasons for failure of amalgam versus composite posterior restorations placed in a randomized clinical trial. *Journal of the American Dental Association*, 138(6), 775-783.

Brown, C. R., & Way, D. C. (1978). Enamel loss during orthodontic bonding and subsequent loss during removal of filled and unfilled adhesives. *Am J Orthod*, 74(6), 663-671.

Can, A. M., Darling, C. L., Ho, C., & Fried, D. (2008). Non-destructive assessment of inhibition of demineralization in dental enamel irradiated by a lambda=9.3-microm CO2 laser at ablative irradiation intensities with PS-OCT. *Lasers in Surgery and Medicine*, 40(5), 342-349. doi:10.1002/lsm.20633

Chan, K. H., Hirasuna, K., & Fried, D. (2011). Rapid and Selective Removal of Composite from Tooth Surfaces with a 9.3- μ m CO2 Laser using Spectral Feedback. *Lasers in Surgery and Medicine*, 43(8), 824-832.

Cheng, J. Y., Fan, K., & Fried, D. (2006). *Use of a compact fiber optic spectrometer for spectral feedback during the laser ablation of dental hard tissues and restorative materials*. Paper presented at the Lasers in Dentistry XII.

Dumore, T., & Fried, D. (2000). Selective ablation of orthodontic composite by using sub-microsecond IR laser pulses with optical feedback. *Lasers in Surgery and Medicine*, 27(2), 103-110.

Featherstone, J. D., Barrett-Vespone, N. A., Fried, D., Kantorowitz, Z., & Seka, W. (1998). CO₂ laser inhibitor of artificial caries-like lesion progression in dental enamel. *Journal of dental research*, 77(6), 1397-1403.

Featherstone, J. D. B., Fried, D., & Bitten, E. R. (1997). *Mechanism of laser induced solubility reduction of dental enamel*. Paper presented at the Lasers in Dentistry III, San Jose, CA.

Featherstone, J. D. B., & Nelson, D. G. A. (1987). Laser effects on dental hard tissue. *Adv. Dent. Res.*, 1(1), 21-26.

Fitzpatrick, D. A., & Way, D. C. (1977). The effects of wear, acid etching, and bond removal on human enamel. *American journal of orthodontics* 1, 72(6), 671-681.

Fried, D., Featherstone, J. D., Le, C. Q., & Fan, K. (2006). Dissolution studies of bovine dental enamel surfaces modified by high-speed scanning ablation with a lambda = 9.3-microm TEA CO₂ laser. *Lasers in Surgery and Medicine*, 38(9), 837-845. doi:10.1002/lsm.20385

Fried, D., Ragadio, J., Akrivou, M., Featherstone, J. D., Murray, M. W., & Dickenson, K. M. (2001). Dental hard tissue modification and removal using sealed transverse excited atmospheric-pressure lasers operating at lambda=9.6 and 10.6 microm. *Journal of Biomedical Optics*, 6(2), 231-238. doi:10.1117/1.1344192

Gordan, V. V., Garvan, C. W., Richman, J. S., Fellows, J. L., Rindal, D. B., Qvist, V., . . . Gilbert, G. H. (2009). How dentists diagnose and treat defective restorations: evidence from the dental practice-based research network. *Operative dentistry*, 34(6), 664-673.

Gwinnett, A., & Gorelick, L. (1977). Gwinnett AJ, Gorelick L. Microscopic evaluation of enamel after debonding: clinical application. *Am J Orthod* 1977;71(6):651-65. *Am J Orthod*, 71(6), 651-665.

Hong, Y. H., & Lew, K. K. (1995). Quantitative and qualitative assessment of enamel surface following five composite removal methods after bracket debonding. *Eur J Orthod*, 17(2), 121-128.

Louie, T. M., Jones, R. S., Sarma, A. V., & Fried, D. (2005). Selective removal of composite sealants with near-ultraviolet laser pulses of nanosecond duration. *Journal of Biomedical Optics*, 10(1), 14001. doi:10.1117/1.1854676

Niemz, M. H. (1994). Investigation and spectral analysis of the plasma-induced ablation mechanism of dental hydroxyapatite. *Appl. Phys. B*, 58, 273-281.

Oliver, R. G. (1988). The effect of different methods of bracket removal on the amount of residual adhesive. *Amer J Orthod Dentofacial Orthop*, 93(3), 196-200.

Oliver, R. G., & Griffiths, J. (1992). Different techniques of residual composite removal following debonding--time taken and surface enamel appearance. *British journal of orthodontics*, 19(2), 131-137.

Ryf, S., Flury, S., Palaniappan, S., Lussi, A., Meerbeek, B. v., & Zimmerli, B. (2012). Enamel loss and adhesive remnants following bracket removal and various clean-up procedures in vitro. *Eur J Orthod*, 34(1), 25-32.

Thompson, R. E., & Way, D. C. (1981). Enamel loss due to prophylaxis and multiple bonding/debonding of orthodontic attachments. *Am. J. Orthodontics*, 79, 282-295.

Tufekci, E., Merrill, T., Pintado, M., Beyer, J., & Brantley, W. (2004). Enamel loss associated with orthodontic adhesive removal on teeth with white spot lesions: an in vitro study. *American journal of orthodontics and dentofacial orthopedics*, 125(6), 733-739.

Uysal, T., Eldeniz, A. U., Usumez, S., & Usumez, A. (2005). Thermal changes in the pulp chamber during different adhesive clean-up procedures. *The Angle orthodontist*, 75(2), 220-225. doi:10.1043/0003-3219(2005)075<0216:TCITPC>2.0.CO;2

Wheeler, C. R., Fried, D., Featherstone, J. D., Watanabe, L. G., & Le, C. Q. (2003). Irradiation of dental enamel with Q-switched lambda = 355-nm laser pulses: surface morphology, fluoride adsorption, and adhesion to composite resin. *Lasers in Surgery and Medicine*, 32(4), 310-317. doi:10.1002/lsm.10162

Zach, L., & Cohen, G. (1965). Pulp response to externally applied heat. *Oral. Surg. Oral. Med. Oral. Pathol.*, 19, 515-530.

Zuerlein, M., Fried, D., Featherstone, J., & Seka, W. (1999). Optical properties of dental enamel at 9 - 11 μm derived from time-resolved radiometry. *Special Topics IEEE J Quant. Elect.*, 5((4)), 1083-1089.

Zuerlein, M. J., Fried, D., & Featherstone, J. D. (1999). Modeling the modification depth of carbon dioxide laser-treated dental enamel. *Lasers in Surgery and Medicine*, 25(4), 335-347.

CHAPTER IV
DEVELOPING AND ASSESSING AN INTEGRATED SPECTRAL GUIDED LASER
SYSTEM FOR AUTOMATED COMPOSITE REMOVAL

4.1 SUMMARY

The purpose of this chapter is to assemble a laser system for the selective removal of dental composite from tooth surfaces, that is feasible for clinical use incorporating a spectral feedback system, a scanning system, articulating arm and a clinical handpiece, and evaluate the performance of that system on extracted teeth.

Ten extracted teeth were collected and small fillings were placed on the occlusal surface of each tooth. A clinical system featuring a CO₂ laser operating at 50 Hz and spectral optical feedback was used to remove the composite. Removal was confirmed using a cross polarized optical coherence tomography system (CP-OCT) designed for clinical use.

The system was capable of rapidly removing composite from small preparations on tooth occlusal surfaces with a mean loss of enamel of less than 20 μm.

This chapter demonstrates that a spectral feedback can be successfully employed in an automated system for composite removal by incorporating dual photodiodes and a galvanometer controlled CO₂ laser. Additionally, the use of registered OCT images presents as a viable method for volumetric benchmarking. Overall, this study represents the first implementation of spectral feedback into a clinical handpiece and serves as a benchmark for future clinical studies.

4.2 INTRODUCTION

Within dentistry, composite is a popular material of choice for clinicians due to its versatility. It is often color matched and physically bonded to the surrounding tooth structure making it ideal for the esthetic replacement of missing tooth structure and bonding dental appliances. A primary caveat with using dental composite is that the

placement procedure for composite is highly technique sensitive and is often incorrectly done, increasing the likelihood of secondary dental caries and need for a replacement filling (I. Mjor, Moorehead, & Dahl, 2000; I. A. Mjor, Dahl, & Moorhead, 2000). When replacing and removing unwanted composite, clinicians often have a difficult time visually differentiating composite from healthy enamel, usually resulting in the excessive removal of healthy tooth structure to ensure complete removal of the composite (Hong & Lew, 1995; R G Oliver, 1988). Therefore, a system that allows a dentist to rapidly remove composite while minimizing the damage to the underlying healthy tooth structure would provide a significant improvement over current methods.

Lasers have been used in dentistry for several treatment modalities including soft/hard dental tissue removal and caries inhibition (D. Fried et al., 2001; Miserendino & Pick, 1995; Nguyen et al., 2011; H. A. Wigdor et al., 1995; M. Zuerlein, D. Fried, J. D. B. Featherstone, & W. Seka, 1999). Studies have shown that CO₂ lasers operating at 9.3 and 9.6 μm wavelengths can be used to efficiently remove enamel and dentin (Frentzen et al., 2003; D. Fried et al., 2001; Mullejans, Eyrich, Raab, & Frentzen, 2002; Nguyen et al., 2011; M. Zuerlein et al., 1999) with minimal impact on the health of the pulp (Goodis, Featherstone, & Fried, 2002; Nair, Baltensperger, Luder, & Eyrich, 2005; H. Wigdor, Walsh, & Mostofi, 2000). A clinical study employing the same carbon dioxide laser used for this study demonstrated no pulpal effects for a pulse repetition rate of 50 Hz and an incident fluence of 20 J/cm² (Staninec et al., 2009). Similar to other CO₂ lasers, this laser has been shown to exhibit an inherent selectivity for composite by ablating more composite material per pulse compared to healthy enamel as shown in **Chapter III: Figure 3.3** (Alexander et al., 2002; Chan et al., 2011; T. Dumore & D.

Fried, 2000; T. M. Louie et al., 2005; Wheeler, Fried, Featherstone, Watanabe, et al., 2003). Additionally, the localized ablated particles created from each laser pulse become electronically excited from the laser energy thereby generating a localized luminous plume. The plume contains the emission spectra of the ablation site's elemental constituents and can therefore be used to identify and differentiate materials (Adrain & Watson, 1984; J. Ready, 2012). Spectral analysis of the plume has revealed that the distinctive high intensity calcium emission line at 605 nm found in dental hard tissues can be used to differentiate tissues rich in hydroxyapatite (i.e., dentin and enamel) from composite (see **Figure 4.1**) (Chan et al., 2011; Cheng et al., 2006; T. Dumore & D. Fried, 2000). Since the calcium emission line is primarily used for spectral differentiation, it is hypothesized that similar results can be achieved faster and cheaper by substituting the spectrometer with a pair of filtered photodiodes.

We have previously demonstrated that spectral feedback can be used to remove dental composite on an optical bench setup using a spectrometer for optical feedback. This study formed an initial proof of concept for an automated removal of composite at clinically relevant rates using a CO₂ laser operating at 9.3 μm with high pulse repetition rates and also showed that high speed removal can be achieved with minimal heat deposition, described in greater detail in Sections 2.4 and 3.4.2 (Chan et al., 2011; Chan, Hirasuna, & Fried, 2014).

This chapter pursues the next logical step by developing a spectral feedback clinical handpiece system for selective removal that is feasible for use within patients. This is achieved by incorporating an articulating arm and galvanometer into a clinical delivery system. In addition to constructing a handpiece capable of operating within the oral

cavity, the clinical system will be benchmarked to determine its efficacy for selective composite removal by using volumetric analysis techniques on 3D images captured with a high-speed optical coherence tomography (OCT) system that is suitable for clinical use.

Within the context of this study, we will test the feasibility of this clinical system through the following objectives: (i) Explore the use of photodiodes for spectral feedback of plume emission for enamel/composite identification; (ii) fabricate a clinical handpiece setup small enough for clinical feasibility; and (iii) test the efficacy of the handpiece with volumetric analyses. This will serve as the preliminary test to ensure proper composite selectivity and removal prior to moving forward into the clinic.

4.3 MATERIALS AND METHODS

4.3.1 Tooth Samples

Mandibular premolars (n = 10) were collected from patients in the San Francisco Bay Area, CA, and sterilized with gamma radiation as described in previous literature (White, Goodis, Marshall, & Marshall, 1990) and stored in a 1% thymol solution. A small pit filling prep was placed entirely within enamel with a True Speed Elite handpiece from Darby Dental (Jericho, NY) and 2 mm round bur. Grelgloo™ composite fromOrmco (Orange, CA) was placed to restore the tooth to its original contour. Following composite placement, the sample was laser treated using the experimental clinical handpiece. At each stage (original tooth, cut tooth, tooth with composite and tooth with composite removed), the sample was scanned with a cross-polarization optical coherence tomography (CP-OCT) system for volumetric analysis.

4.3.2 Clinical Laser Scanning System for Composite Removal

The clinical system consists of the following components: CO₂ laser, articulating arm, and experimental handpiece (shown in **Figures 4.2 and 4.3**) including galvanometer, lens, handpiece head, fiber optic, photodiodes, and air/water-spray. The laser used was an industrial marking laser, Impact 2500 from GSI Lumonics (Rugby, UK) operating at a wavelength of 9.3 μm. A previous study within our group has confirmed the safety of using this laser within our operating parameters (Staninec et al., 2009). The laser was custom modified to produce a Gaussian output beam (single spatial mode) with a pulse duration of between 10 and 15 microseconds. This laser is capable of high pulse repetition rates up to 500 Hz, however the rate was limited to 50 Hz. The laser energy output was monitored using a power meter EPM 1000 from Coherent-Molelectron (Santa Clara, CA) and Joulemeter ED-200 from Gentec (Quebec, Canada). An articulating arm from MLS (Novi, MI) was used to couple the laser beam to the scanning handpiece. Computer-controlled XY galvanometers 6200 HM series with MicroMax Series 671 from Cambridge Technology, Inc, (Bedford, MA) were used to scan the laser beam over sample surfaces. An f-theta scanning lens with a focal length of 90 mm from II-VI (Saxonburg, PA) was used to focus the beam onto the tooth surfaces. A razor blade was scanned across the beam to determine the diameter ($1/e^2$) of the laser beam. The laser spot size and energy employed was 433 μm and 12.8 mJ, respectively (fluence = 8.6 J/cm²).

The clinical handpiece head was custom designed in Fusion 360 from Autodesk (San Rafael, CA) and machined out of aluminum using a personal CNC machine from Tormach (PCNC-440; Waunakee, WI). Copper mirrors were polished using a Pro

Grinder Polisher from Buehler (EcoMet 250; Lake Bluff, IL) and placed at the end of the clinical head. A bifurcated fiber optic from Banner Engineering (BA23S; Minneapolis, MN) was used to collect and feed the plume emission into two photodiodes from Thorlabs (PDA100a; Newton, NJ), one of which contained a 600 nm FWHM 40 nm filter from Thorlabs (FB600-400; Newton, NJ) and the other unfiltered. The signal from the unfiltered photodiode was amplified with a 30 dB gain while a gain of 70 dB was used for the photodiode with the 600 nm filter. A custom fabricated low volume/low pressure air-actuated fluid spray delivery system was used to continuously deliver a 0.5 ml/min water spray over the tooth surface during the laser treatment. A program written in LabVIEW from National Instruments (Austin, TX) was used to control the air/water-spray, scan the laser over the tooth and ensure complete removal of the composite as shown in **Figure 4.4**.

4.3.3 Cross Polarization Optical Coherence Tomography (CP-OCT) System

The swept source CP-OCT system used for this study has been previously described by Fried et al. (D. Fried, Staninec, Darling, Kang, & Chan, 2012). The system is produced by Santec (IVS-3000-CP; Komaki, Aichi, Japan) and uses their own swept source laser (HSL-200-30; Komaki, Aichi, Japan) operating with a 30 kHz sweep rate. This system is capable of acquiring images *in vivo* and it has been used for clinical imaging studies (Chan et al., 2016; Nee et al., 2014). The Mach-Zehnder interferometer is integrated into the handpiece which also contains the microelectromechanical (MEMS) scanning mirror and the imaging optics. The handpiece is shown in **Figures 4.2 and 4.3**, the body is 7 x 17 cm² with an imaging tip that is 4 cm long and 1.5 cm across. This system operates at a wavelength of 1321 nm with a bandwidth of 111 nm with a measured resolution in air

of 11.4 μm (3 dB). The lateral resolution is 80 μm ($1/e^2$) with a transverse imaging window of 6 x 6 mm^2 and a measured imaging depth of 7 mm in air. The extinction ratio was measured to be 32 dB. Resulting images had a voxel size of 32.5 x 24.7 x 8.3 μm^3 . Postprocessing of captured OCT images was done using a program written in MATLAB from Mathworks (Natick, MA) utilizing a median filter and a rotating kernel transformation (RKT) filter (Rogowska & Brezinski, 2002).

4.3.4 Volumetric Analysis

Volumetric analysis was carried out using Avizo from FEI (Hillsboro, OR). Correlation based rigid body registration was used to align OCT scans of the tooth in the “cut” and “composite removed” based on the consistent regions of the occlusal surface (e.g., unaltered cusps and grooves of the tooth) using registration techniques described in previous literature (Jang, 2015). In short, regions of the tooth that were altered by the experiment were excluded from the image registration while consistent regions (e.g., grooves and tooth cusps) were used to align the surfaces. Each aligned image was then segmented for its respective surface to determine the volumetric space of the tooth. From these images, leftover composite (V_{LC}) and excess enamel removed (V_{EER}) was calculated. A voxel which was present in the “composite removed” volume but not present in the “cut” volume was defined as V_{LC} . Additionally, a voxel which was present in the “cut” volume but not in the “composite removed” volume was defined as V_{EER} . Volume spaces were then morphologically opened to compensate for slight image registration alignment errors.

4.4 RESULTS

4.4.1 Plume Emission Analysis

Figure 4.5 shows images of representative plumes generated from a single laser pulse on enamel (**Figure 4.5a**) and composite (**Figure 4.5b**). Plot of the photodiode response of enamel is shown in **Figure 4.5c** and composite in **Figure 4.5d**. Overall, the intensity of the plume from enamel is greater than the emission plume from composite. This was due to higher content of calcium within the enamel. However, the plume for composite ablation was physically larger and lasted longer than the enamel plume (**Figures 4.5a and 4.5b**).

4.4.2 Volumetric Measurements

OCT scans of a representative specimen can be seen in **Figures 6a-c**. A combined aligned image using correlative rigid body registration is shown in **Figure 6d**. Visual representations of extracted surfaces and volumetric measurements from the OCT scans are shown in **Figure 6e**. Across the ten samples, the mean \pm SD volume of leftover composite (V_{LC}) is $0.011 \pm 0.008 \text{ mm}^3$ and excess enamel removed (V_{EER}) is $0.032 \pm 0.029 \text{ mm}^3$. The calculated prep volume was roughly $\sim 0.6 \text{ mm}^3$ yielding a 2D area of 1.77 mm^2 , therefore the mean depth of enamel lost is roughly $\sim 18 \mu\text{m}$.

4.4.3 Clinical Handpiece Results

The run time for the composite removal program for a 1 mm^3 filling was approximately 30-40 seconds. Representative images of the original, prepped, composite placed and composite removed states are shown in **Figure 5.7**. A video of the laser program operating on a tooth sample can be found in [http://onlinelibrary.wiley.com/journal/10.1002/\(ISSN\)1096-9101/homepage/lsm-22668-](http://onlinelibrary.wiley.com/journal/10.1002/(ISSN)1096-9101/homepage/lsm-22668-)

[video.htm](#). Composite was apparently removed without major deviations to the original shape of the tooth preparation.

4.5 DISCUSSION

Within the growing challenge to improve the standards of minimally invasive dentistry, better shade matched dental composites are being developed each year, which signifies an advancement in esthetic dentistry but also leads to increased difficulty for removal. As more composite fillings and adhesives are being placed in patients, there exists an inherent need to efficiently remove composite while reducing the damage to adjacent tooth structure.

This chapter demonstrates that composite can be selectively removed from tooth surfaces using a computer-controlled CO₂ laser scanning system with integrated spectral feedback at clinically relevant rates. This also achieved several milestones needed to proceed to the clinic. Namely, we have successfully integrated the selective ablation system into a handpiece feasible for clinical use, developed a fast and inexpensive spectral feedback system utilizing two photodiodes and demonstrated that CP-OCT can be used *in vivo* for nondestructively assessing the selectivity of removal via volumetric analysis of composite and healthy tissue removal using rigid body image registration.

Several considerations went into the design of the laser removal system optimized for clinical use. An articulating arm and galvanometers were incorporated into the system to stabilize the position of the handpiece while the laser is scanned over the occlusal surface of the tooth (**Figures 4.2 and 4.3**). This combined approach allows for the system to achieve clinically acceptable speeds. The pulse repetition rate of 50 Hz was

chosen to match the corresponding pulpal safety study in previous literature (Staninec et al., 2009), but can be increased to even higher repetition rates based on the previous research, namely Section 3.4.2. At a fluence of 8.6 J/cm^2 , a depth of $60 \text{ }\mu\text{m}$ of composite removed per pulse in contrast to $20 \text{ }\mu\text{m}$ of enamel removed per pulse as shown in **Chapter III: Figure 3.3**. This fluence not only maximizes the ablation rate but also the selectivity of composite removal. In addition, this fluence operated was capable of generating the smallest possible plume, while producing a reliable optical signal for this system. The water flow rate was also adjusted to improve the spectral discrimination. Insufficient water can cause an inefficient composite ablation, namely carbonization, while too much water can attenuate the laser plume emission.

In previous chapters, a spectrometer was used for interrogating the laser plume, however this chapter demonstrates that a pair of photodiodes is sufficient in discriminating composite and sound tissue and this increases the overall clinical feasibility of the system by decreasing the total cost, increasing the signal throughput and allowing higher removal rates. Spectrometers are not only many times more expensive than individual photodiodes, they are also less sensitive and require more light for proper spectral analysis. It should be noted that, while a single photodiode setup would further increase the sensitivity of composite discrimination, it was determined that a normalized ratio produced from two photodiodes conferred higher performance. The composite plume emission at 600 nm has a longer lifetime than that of enamel (**Figure 4.5**). This is likely due to increased thermal radiation from the ejected material and the ablation rate for composite is much higher than enamel as noted in **Chapter III: Figure 3.3**. This phenomenon may be useful for calculating the total

amount of material ablated, however it was not implemented in our differentiation algorithm since other variables, namely signal attenuation brought upon by the water spray can significantly decrease this effect.

This chapter also demonstrates the use of a clinical CP-OCT for high resolution volumetric quantification. Previous studies have relied on μ XCT (Magne, 2007) or visible probe scanning (van Waes, Matter, & Krejci, 1997) for 3D measurements, however these techniques are not feasible for patient studies. Clinical cone beam CT systems can capture volumetric data within the patient but the voxel sizes (about 150-200 μm) are too large for the scale of this study. Conversely, the clinical CP-OCT system used has a higher resolution ($32.5 \times 24.7 \times 8.3 \mu\text{m}^3$) and can rapidly scan the surface of the tooth within a short amount of time (~4 seconds).

A crucial stage in the volumetric quantification was image registration, since minor misalignment between registered images may result in volumetric inaccuracies. However, the topology of the occlusal surface of the tooth provided many features which increased our confidence in the image registration results. Once image registration was completed, the process of extracting the volumetric difference is straightforward.

Overall, the clinical system performed as designed and removed the composite filling within a short period (~30 seconds). The procedure time can be further decreased by increasing the pulse repetition rate of the laser, however precautions must be taken to prevent peripheral thermal damage and excessive heating of the dental pulp. A possible workaround would include a revised alternating scanning pattern that would decrease localized heating at a specific ablation site. Following the scanning procedure, a small 3

x 3 mm² box representing the laser scanning window was visible on the occlusal surface of the enamel (**Figure 4.6**) which does not affect the esthetics of the tooth. From a volumetric perspective, excess enamel removed (0.03 mm³) is considered comparable to the average amount of enamel lost in an individual per year (0.04 mm³) (Pintado, Anderson, DeLong, & Douglas, 1997). From a depth perspective, previous studies have measured the annual enamel loss on the occlusal surface from mastication to be from 30 µm to 50 µm (Brown & Way, 1978a; Lambrechts, Braem, Vuylsteke-Wauters, & Vanherle, 1989), and therefore we consider the mean enamel loss from our study (18 µm) to be insignificant. The system was also able to remove the majority of composite leaving behind a minor amount of material that was not visually apparent. It is understood that a major limitation of this system is that the handpiece can only ablate material within its direct line of sight and is unable to remove composite hidden behind undercuts. Therefore, it is hypothesized that the leftover composite was either due to a small undercut or a minor image registration error.

In conclusion, this demonstrates an *in vitro* benchmark for testing the clinical handpiece prior to its use in a clinical study. The results demonstrate that spectral feedback methods can be implemented to selectively remove composite with minimal damage to healthy tooth structure and represents a potential advantage over the current standard of care. The next planned stage for this project is a clinical study in which we will design and fabricate a custom bite block for the handpiece for additional stability within the patient's mouth.

4.6 FIGURES AND FIGURE LEGENDS

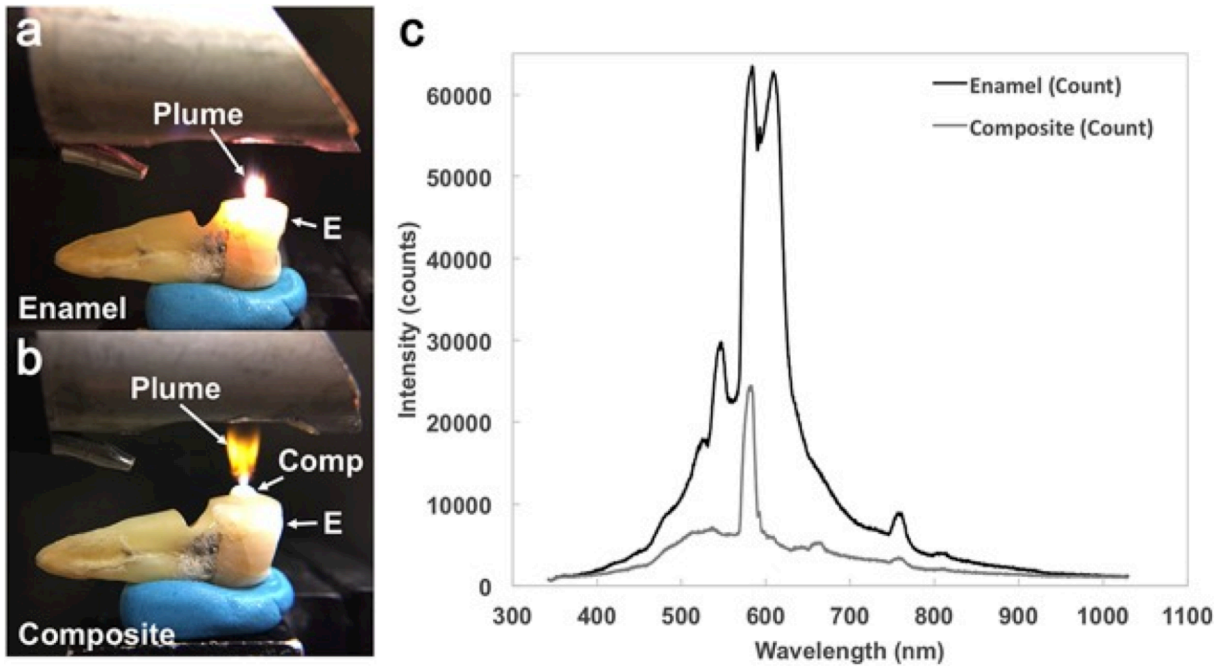


Figure 4.1: Differences in plume emission color for (a) enamel and (b) composite can be seen visually. (C) Collected spectral data for composite and enamel were plotted to highlight the differences in general intensity as well as the strong calcium emission peak (605 nm) in enamel which is not present in composite.

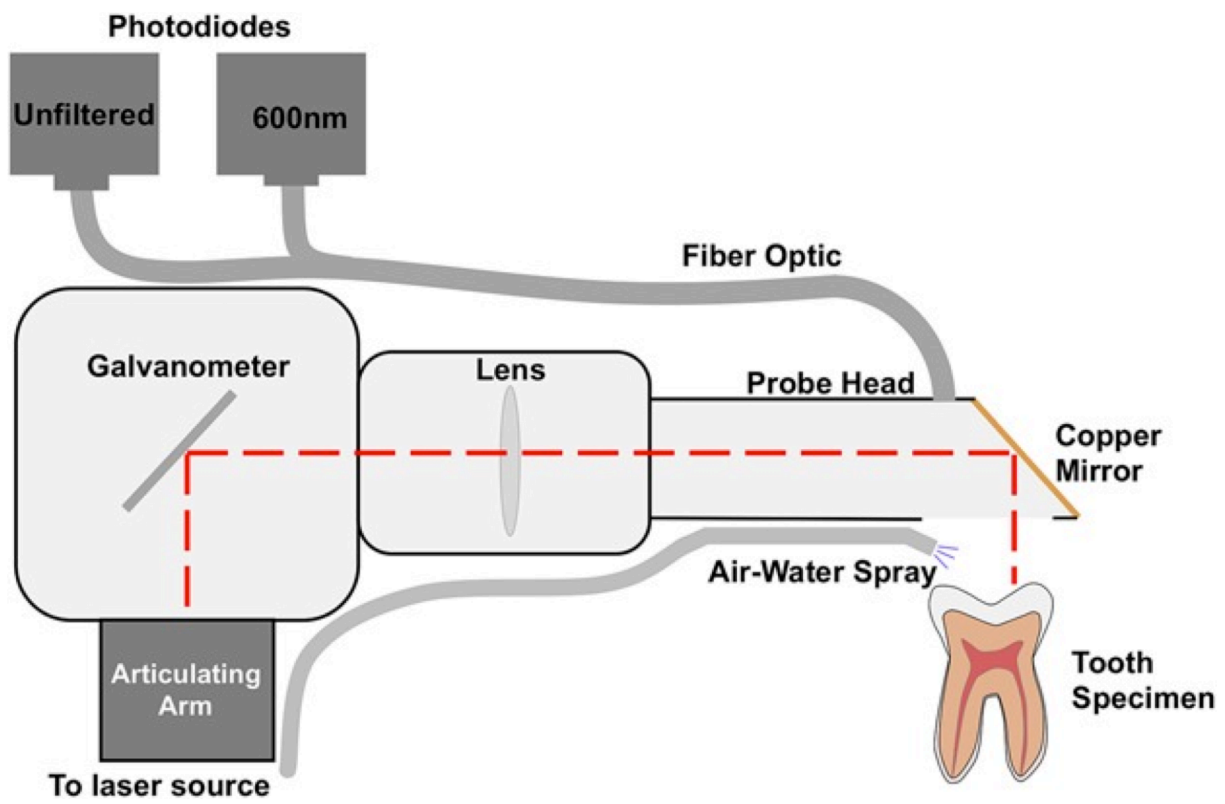


Figure 4.2: Schematic diagram of clinical laser handpiece.

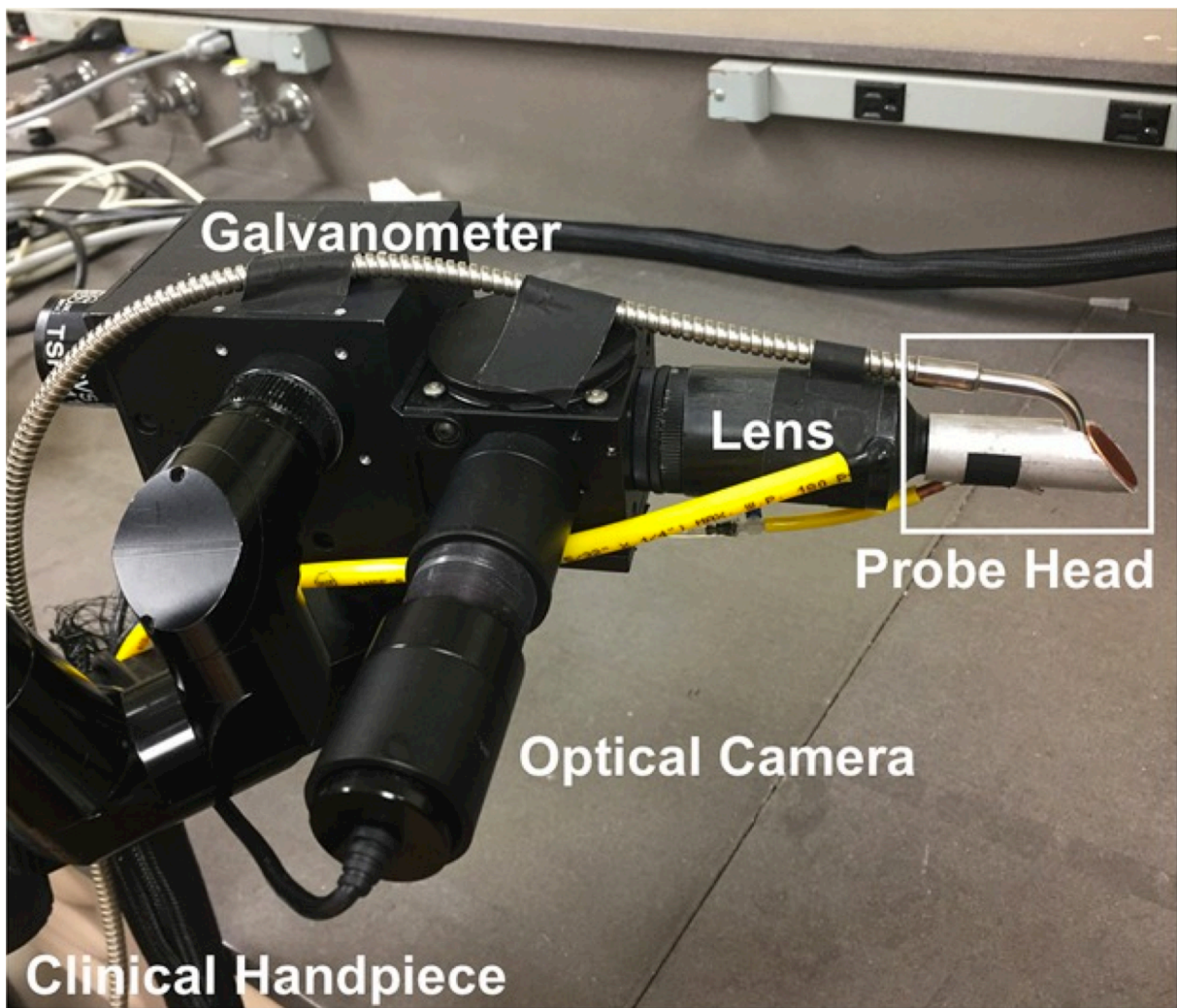


Figure 4.3: Images of clinical handpiece and clinical probe head, which is designed to fit within the patient's mouth.

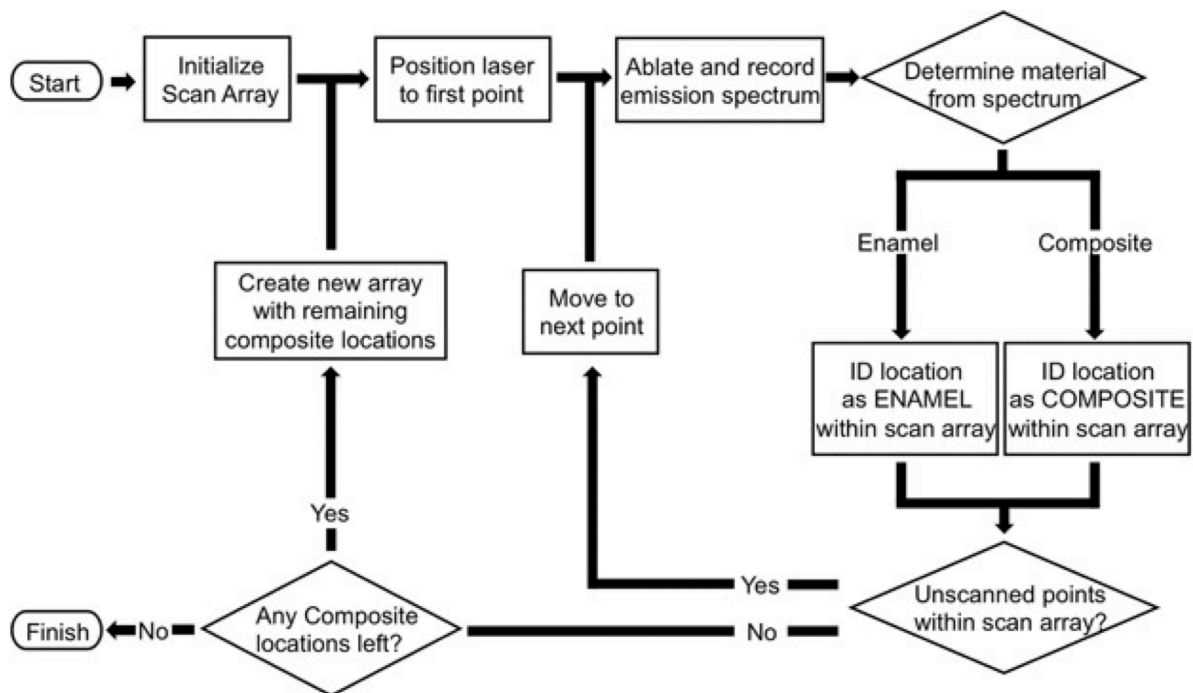


Figure 4.4: Flowchart outlining coding logical steps for selective composite ablation.

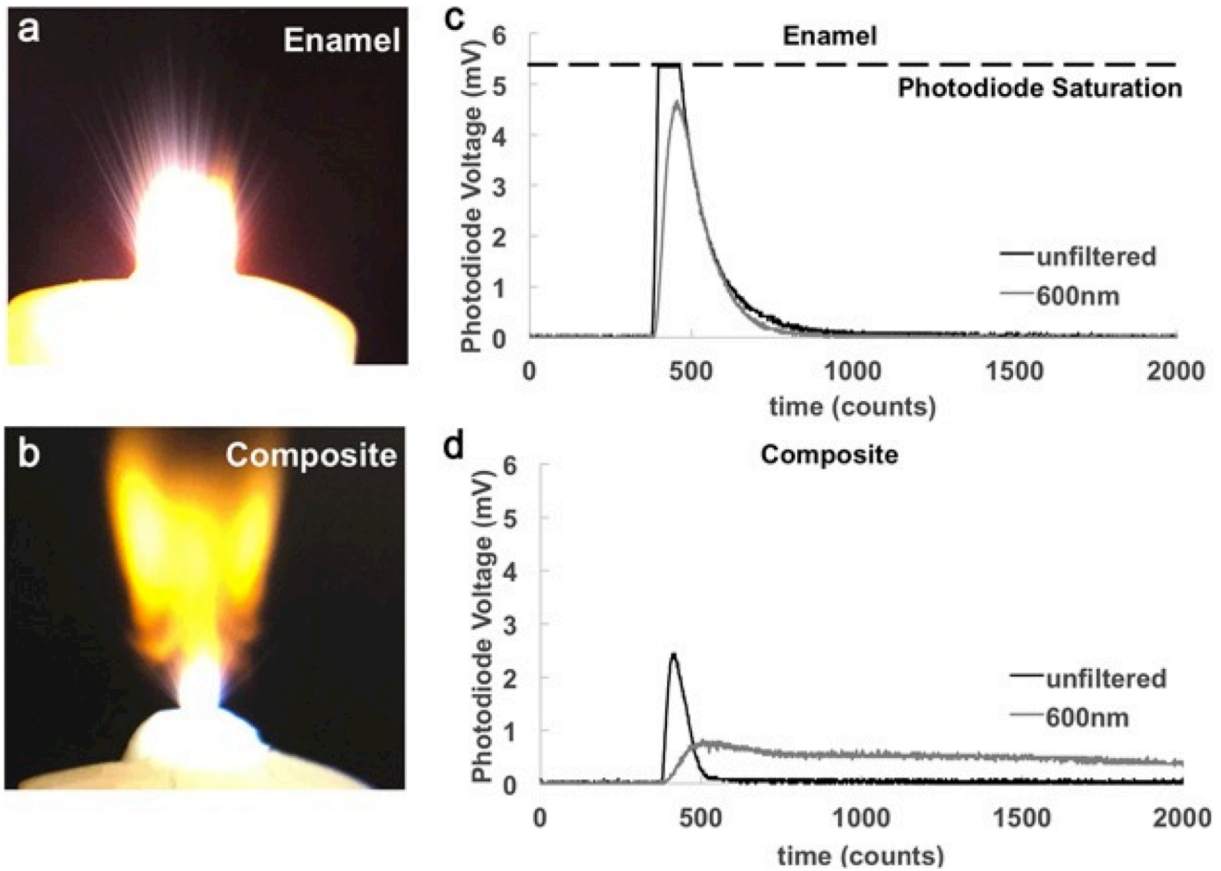


Figure 4.5: Luminous plumes generated from ablation of (a) enamel and (b) composite. Spectral emission readouts in dual photodiodes (unfiltered and 600 nm BP filter) over time are shown for (c) enamel and (d) composite showing a peak voltage ratio change between the two materials.

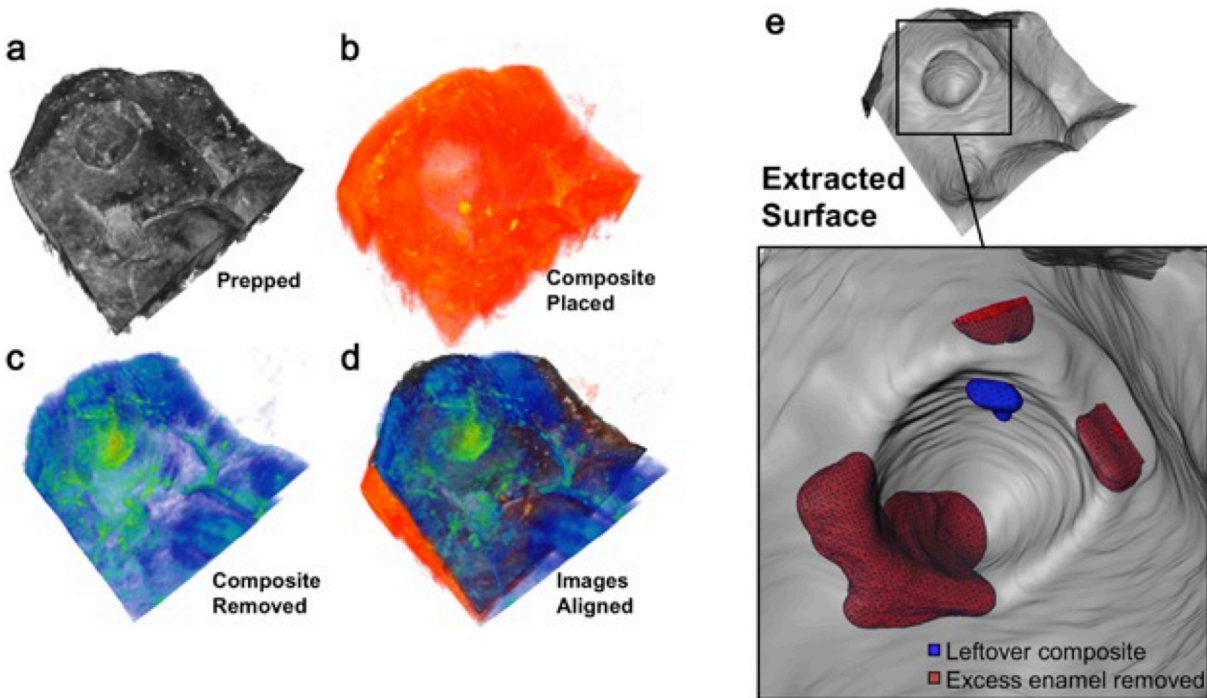


Figure 4.6: (a – d) Optical coherence tomography (OCT) scans of tooth occlusal surfaces. Scans were aligned within the same 3D space to generate volumetric measurements. (e) Tooth surfaces extracted from aligned images were used to calculate the leftover composite [volume leftover composite = volume composite removed – volume prepped] and excess enamel removed [volume enamel removed = volume prepped – volume composite removed].

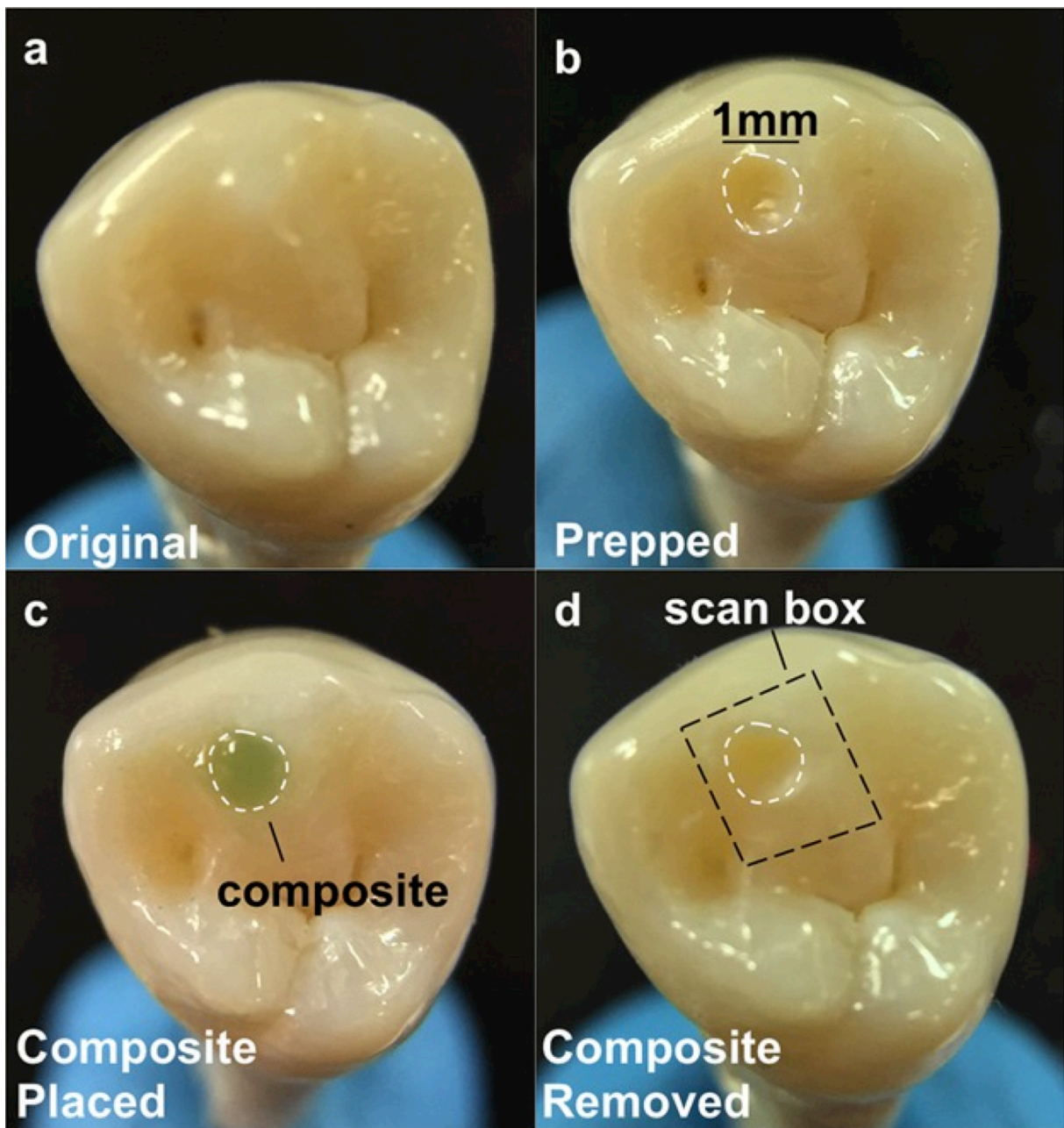


Figure 4.7: Images of (a) original tooth; (b) prepared tooth; (c) tooth with contour restored with Grelgloo™ composite; (d) tooth with composite removed via selective ablation.

4.7 REFERENCES

- Adrain, R. S., & Watson, J. (1984). Laser Microspectral Analysis - a Review of Principles and Applications. *Journal of Physics D-Applied Physics*, 17(10), 1915-&.
- Alexander, R., Xie, J., & Fried, D. (2002). Selective removal of residual composite from dental enamel surfaces using the third harmonic of a Q-switched Nd:YAG laser. *Lasers in Surgery and Medicine*, 30(3), 240-245.
- Brown, C. R., & Way, D. C. (1978). Enamel loss during orthodontic bonding and subsequent loss during removal of filled and unfilled adhesives. *Am J Orthod*, 74(6), 663-671.
- Chan, K. H., Hirasuna, K., & Fried, D. (2011). Rapid and Selective Removal of Composite from Tooth Surfaces with a 9.3- μ m CO₂ Laser using Spectral Feedback. *Lasers in Surgery and Medicine*, 43(8), 824-832.
- Chan, K. H., Hirasuna, K., & Fried, D. (2014). Analysis of enamel surface damage after selective laser ablation of composite from tooth surfaces. *Photonics Lasers Med*, 3(1), 37-45. doi:10.1515/plm-2013-0052
- Chan, K. H., Tom, H., Lee, R. C., Kang, H., Simon, J. C., Staninec, M., . . . Fried, D. (2016). Clinical Monitoring of Smooth Surface Enamel Lesions Using CP-OCT During Nonsurgical Intervention. *Lasers Surg Med*, 48(10), 915-923. doi:10.1002/lsm.22500
- Cheng, J. Y., Fan, K., & Fried, D. (2006). *Use of a compact fiber optic spectrometer for spectral feedback during the laser ablation of dental hard tissues and restorative materials*. Paper presented at the Lasers in Dentistry XII.
- Dumore, T., & Fried, D. (2000). Selective ablation of orthodontic composite by using sub-microsecond IR laser pulses with optical feedback. *Lasers in Surgery and Medicine*, 27(2), 103-110.
- Frentzen, M., Gotz, W., Ivanenko, M., Afilal, S., Werner, M., & Hering, P. (2003). Osteotomy with 80-microsecond CO₂ laser pulses - histological results. *Lasers Med Sci*, 18(2), 119-124.
- Fried, D., Ragadio, J., Akrivou, M., Featherstone, J. D., Murray, M. W., & Dickenson, K. M. (2001). Dental hard tissue modification and removal using sealed transverse excited

atmospheric-pressure lasers operating at $\lambda=9.6$ and 10.6 microm. *Journal of Biomedical Optics*, 6(2), 231-238. doi:10.1117/1.1344192

Fried, D., Staninec, M., Darling, C., Kang, H., & Chan, K. (2012). Monitoring tooth demineralization using a cross polarization optical coherence tomographic system with an integrated MEMS scanner. *Proc SPIE Int Soc Opt Eng*, 8208, 82080i. doi:10.1117/12.914599

Goodis, H., Featherstone, J., & Fried, D. (2002). *Pulpal Safety of a New 9.6 μm TEA CO₂ Laser used for Caries Prevention*. Paper presented at the Lasers in Dentistry VIII, San Jose.

Hong, Y. H., & Lew, K. K. (1995). Quantitative and qualitative assessment of enamel surface following five composite removal methods after bracket debonding. *Eur J Orthod*, 17(2), 121-128.

Jang, A. T. (2015). *A multiscale approach to link organ-level biomechanics with tissue-level mechanobiology of a bone-periodontal ligament-tooth fibrous joint*. (PhD), University of California, San Francisco, San Francisco, CA.

Lambrechts, P., Braem, M., Vuylsteke-Wauters, M., & Vanherle, G. (1989). Quantitative in vivo wear of human enamel. *J Dent Res*, 68(12), 1752-1754. doi:10.1177/00220345890680120601

Louie, T. M., Jones, R. S., Sarma, A. V., & Fried, D. (2005). Selective removal of composite sealants with near-ultraviolet laser pulses of nanosecond duration. *Journal of Biomedical Optics*, 10(1), 14001. doi:10.1117/1.1854676

Magne, P. (2007). Efficient 3D finite element analysis of dental restorative procedures using micro-CT data. *Dent Mater*, 23(5), 539-548. doi:10.1016/j.dental.2006.03.013

Miserendino, L. J., & Pick, R. M. (1995). *Lasers in Dentistry*. Chicago: Quintessence.

Mjor, I., Moorehead, J., & Dahl, J. (2000). Reasons for replacement of restorations in permanent teeth in general dental practice. *Int Dent J*, 50, 361-366.

Mjor, I. A., Dahl, J. E., & Moorhead, J. E. (2000). Age of restorations at replacement in permanent teeth in general dental practice. *Acta Odontol Scand*, 58(3), 97-101.

Mullejans, R., Eyrich, G., Raab, W. H., & Frentzen, M. (2002). Cavity preparation using a superpulsed 9.6-microm CO₂ laser--a histological investigation. *Lasers Surg Med*, 30(5), 331-336.

Nair, P. N. R., Baltensperger, E. M., Luder, E. H. U., & Eyrich, G. K. H. (2005). Observations on pulpal response to carbon dioxide laser drilling of dentine in healthy human third molars *Lasers Medical Sciences*, 19(240-247).

Nee, A., Chan, K., Kang, H., Staninec, M., Darling, C. L., & Fried, D. (2014). Longitudinal monitoring of demineralization peripheral to orthodontic brackets using cross polarization optical coherence tomography. *J Dent*, 42(5), 547-555. doi:10.1016/j.jdent.2014.02.011

Nguyen, D., Chang, K., Hedayatollahnajafi, S., Staninec, M., Chan, K., Lee, R., & Fried, D. (2011). High-speed scanning ablation of dental hard tissues with a $\lambda=9.3 \mu\text{m}$ CO₂ laser: adhesion, mechanical strength, heat accumulation, and peripheral thermal damage. *J Biomed. Opt.*, 16(7), 071410:071411-071418. doi:10.1117/1.3603996

Oliver, R. G. (1988). The effect of different methods of bracket removal on the amount of residual adhesive. *Amer J Orthod Dentofacial Orthop*, 93(3), 196-200.

Pintado, M. R., Anderson, G. C., DeLong, R., & Douglas, W. H. (1997). Variation in tooth wear in young adults over a two-year period. *J Prosthet Dent*, 77(3), 313-320.

Ready, J. (2012). *Effects of high-power laser radiation*. New York, USA: Academic Press, Inc.

Rogowska, J., & Brezinski, M. E. (2002). Image processing techniques for noise removal, enhancement and segmentation of cartilage OCT images. *Phys Med Biol*, 47(4), 641-655.

Staninec, M., Darling, C. L., Goodis, H. E., Pierre, D., Cox, D. P., Fan, K., . . . Fried, D. (2009). Pulpal effects of enamel ablation with a microsecond pulsed $\lambda = 9.3\text{-microm}$ CO₂ laser. *Lasers in Surgery and Medicine*, 41(4), 256-263. doi:10.1002/lsm.20748

van Waes, H., Matter, T., & Krejci, I. (1997). Three-dimensional measurement of enamel loss caused by bonding and debonding of orthodontic brackets. *Am J Orthod Dentofacial Orthop*, 112(6), 666-669.

Wheeler, C. R., Fried, D., Featherstone, J. D., Watanabe, L. G., & Le, C. Q. (2003). Irradiation of dental enamel with Q-switched $\lambda = 355\text{-nm}$ laser pulses: surface morphology,

fluoride adsorption, and adhesion to composite resin. *Lasers in Surgery and Medicine*, 32(4), 310-317. doi:10.1002/lsm.10162

White, J. M., Goodis, H. E., Marshall, S. J., & Marshall, G. W. (1990). Sterilization of teeth by gamma radiation. *Trans. Acad. Dent. Mater.*, 3, 141-142.

Wigdor, H., Walsh, J. T., & Mostofi, R. (2000). *The effect of the CO₂ laser (9.6 μm) on the dental pulp in humans*. Paper presented at the Lasers in Dentistry VI, San Jose.

Wigdor, H. A., Walsh, J. T., Jr., Featherstone, J. D., Visuri, S. R., Fried, D., & Waldvogel, J. L. (1995). Lasers in dentistry. *Lasers Surg Med*, 16(2), 103-133.

Zuerlein, M., Fried, D., Featherstone, J. D. B., & Seka, W. (1999). Absorption coefficients of dental enamel at CO₂ Wavelengths. *Special Topics J. Quantum Electronics*, 5(4), 1083-1089.

CHAPTER V

2D VISUALIZATION AND DETECTION OF DENTAL LESION SEVERITY

5.1 SUMMARY

Several studies have demonstrated the potential of cross-polarization optical coherence tomography (CP-OCT) to quantify the severity of early caries lesions (tooth decay) on tooth surfaces. The purpose of this study is to show that 2D images of the lesion depth and the integrated reflectivity can be used to accurately represent the severity of early lesions. Simulated early lesions of varying severity were produced on tooth samples using simulated lesion models. Methods were developed to convert 3D CP-OCT images of the samples to 2D images of the lesion depth and lesion integrated reflectivity. Calculated lesion depths from OCT were compared with lesion depths measured from histological sections examined using polarized light microscopy. The 2D images of the lesion depth and integrated reflectivity are well suited for visualization of early demineralization.

5.2 INTRODUCTION

New methods are needed for the nondestructive measurement of tooth demineralization and remineralization to monitor the progression of incipient caries lesions (tooth decay) for effective nonsurgical intervention and to evaluate the performance of anticaries treatments such as chemical treatments or laser irradiation. A nondestructive, quantitative method of monitoring demineralization and remineralization *in vivo* with high sensitivity would be invaluable for use in short-term clinical trials for various anticaries agents such as fluoride dentrifices and antimicrobials, particularly in high risk areas of the tooth such as the pits and fissures of the occlusal surfaces. Optical coherence tomography (OCT) is uniquely capable of this task since it provides a measure of the reflectivity from each layer of the lesion and is able to resolve the formation of

remineralized zones of increased mineral density and reduced light scattering. OCT is not only valuable as a nondestructive tool for the assessment of anticaries agents *in vivo* but is also valuable for *in vitro* studies as well since it does not require thin sectioning and it can be carried out rapidly. Several studies both *in vitro* and *in vivo* have shown that cross polarization is advantageous for quantifying the severity of demineralization on tooth surfaces (Baumgartner et al., 2000; Dicht et al., 1999; Everett et al., 1999; Feldchtein et al., 1998; D. Fried et al., 2002; Jones et al., 2006; Kang et al., 2010; M. H. Le et al., 2010). OCT typically produces vast volumes of data and methods are needed for analysis that are amenable to automation.

In the cross-polarization image, the reflectivity from lesion areas can be directly integrated to represent the severity of demineralization. Methods have also been applied using conventional OCT systems but the strong surface reflection from the tooth surface greatly interferes, making direct integration of the reflectivity from the lesion problematic.

Amaechi et al. (Amaechi, Higham, Podoleanu, Rodgers, & Jackson, 2001) demonstrated that the loss of penetration depth in conventional OCT images correlated well with the mineral loss measured with microradiography for shallow artificial lesions on smooth surfaces. Although this approach provided good results for shallow lesions on flat surfaces, there are several issues with using the loss of light penetration as a measure of lesion severity. In order to utilize loss of OCT signal intensity one must arbitrary intensity loss. This is feasible for smooth surfaces with uniform artificial lesions of known depth, but is not possible for highly convoluted surfaces, irregular lesion geometry or for lesions with significant structural characteristic of natural lesions.

Moreover, OCT provides measurements of the reflectivity from each layer in the tissue. Since the reflectivity increases markedly with increases in light scattering, the lesion is most likely to cause an increase in signal rather than a loss in signal especially for natural lesions and one cannot assume that the underlying enamel is sound.

Other groups have looked at fitting the profile of the a-scans in OCT images to represent the extent of demineralization or to calculate attenuation coefficients (Mandurah et al., 2013; Mujat, van der Veen, Ruben, ten Bosch, & Dogariu, 2003; Popescu, Sowa, Hewko, & Choo-Smith, 2008). Unfortunately, natural and simulated caries lesions typically do not have a uniform composition. Cross-sectional profiles of caries lesions, both natural and simulated, show that lesions are not uniform and typically have a surface zone of higher mineral content above the lesion body (Fejerskov & Kidd, 2003). The evolution of the OCT signal intensity with increasing depth or a-scan shape is complex and is dependent on the lesion geometry as well as the characteristics/performance of the OCT system. Lesions have been observed to both completely block or attenuate penetration of the signal or cause an apparent increase of penetration. In fact, this can lead to contradictory interpretations of photon propagation in the lesion Popescu et al. (Popescu et al., 2008) concluded that increasing demineralization in the lesion actually decreased the total scattering in the lesion because the rate of decline of the a-scan intensity decreased in natural smooth surface lesions compared to sound enamel. The authors attributed this phenomenon to the different scattering behavior of pores in the lesion but this interpretation is not supported by any modeling or experimental measurements and it contradicts previous angularly resolved light scattering measurements in sound and demineralized enamel in

the near-IR which shows a 2-3 fold increase in light scattering with demineralization (Darling et al., 2006). It is also interesting to point out that two methods discussed above are completely contradictory approaches to monitoring lesion severity. In the first approach of Amaechi et al. (Amaechi et al., 2001), increased attenuation of the a-scan indicates increasing lesion severity while in the second approach (Popescu et al., 2008) decreased attenuation of the a-scan indicates increasing lesion severity. The opposing interpretations of a-scan profiles, or the rate of a-scan decline, clearly suggest that the a-scan profile is unreliable as an indicator of lesion severity.

Since areas of demineralization appear with increased reflectivity in the OCT images, the most obvious approach is to directly measure the reflectivity from the lesion area and use that as a measure of lesion severity. However, the high refractive indices of dental hard tissues, produces a strong surface reflection at the tooth surface. Utilizing high-resolution OCT systems with axial depth resolution of less than 10 μm , does not prevent the strong surface reflection from dominating the reflectivity at greater depths from the surface. The axial resolution is defined as the point at which the peak intensity of the Gaussian shaped coherence function drops by 3 dB in intensity. However, the strong surface reflection may be 30-40 dB higher than the reflectivity originating from deeper layers in the lesion, which can prevent the resolution of any information from those layers because the intensity of the tail of the Gaussian peak can exceed and mask the signal from those layers. In the cross-polarization image, the reflection from the tooth surface is reduced by 20-30 dB so that the specular reflectance at the surface does not interfere as significantly with the underlying layers. Moreover, the reflectivity

from sound enamel is suppressed near the tooth surface and there is a higher contrast between sound and demineralized enamel in the cross polarization image.

One can also attempt to reduce the reflection from the tooth surface by deliberately imaging the sample at an angle, or by producing an artificial displacement by covering the surface with a thick layer of water or a high refractive index liquid with a refractive index similar to enamel. Imaging the sample at an angle is a simple and effective method of reducing the specular reflection of the surface, however, it is only effective for flat samples. Applying a liquid to the surface is more problematic since it is difficult to control the thickness of the layer and beading of the liquid causes distortion of the optical path length, distorting the image of the lesion. Moreover, the addition of a liquid profoundly influences the scattering behavior of the lesion, since light scattering is caused by the pores produced by loss of mineral. If the lesion is imbibed with a fluid of the same refractive index, it becomes transparent because the scattering resulting from the porosity of the lesion is lost without the refractive index mismatch between the mineral and the air/water boundary in the pore. The magnitude of scattering/reflectivity is also dependent on the hydration of the lesion and it is well known that blowing air onto a shallow lesion (white spot lesion) increases contrast for better visibility.

Several studies have demonstrated that the lesion severity can be represented by the integrated reflectivity with depth in the cross-polarization optical coherence tomography (CP-OCT) image. The integrated reflectivity, ΔR (reflectivity [intensity units $\times \mu\text{m}$]), is a measurement analogous to integrated mineral loss, ΔZ (volume % $\times \mu\text{m}$), **Figure 5.3** (Jones et al., 2006; P Ngaotheppitak et al., 2005). ΔZ is used in microradiography which is the gold standard for measuring mineral loss, it is the integrated mineral loss over the

lesion depth, volume percent mineral x microns (de Josselin de Jong, van der Linden, Borsboom, & ten Bosch, 1988). Microradiography requires destruction of the samples and cannot be used *in vivo*.

In addition, PS-OCT was successfully employed for monitoring demineralization *in vivo* (T. Louie et al., 2010). Small areas of demineralization were produced on tooth buccal surfaces by placing orthodontic bands to accumulate plaque. In addition, small incisions were cut in the grooves of the occlusal surfaces to trap plaque in those areas to produce occlusal demineralization. Tooth surfaces were scanned *in vivo* using PS-OCT before band/incision placement and following a one month check-up. Teeth were extracted, serial sectioned and analyzed using polarized light microscopy (PLM) and transverse microradiography (TMR) for comparison with the PS-OCT images. Lesions were formed after one month and there was a significant increase in the integrated reflectivity with depth (ΔR) calculated from the cross-polarization optical coherence tomography (CP-OCT) images in lesion areas on both buccal and occlusal surfaces along with a corresponding increase in the integrated mineral loss (ΔZ) measured with TMR (gold standard). This demonstrated that CP-OCT can be used *in vivo* to monitor demineralization on tooth surfaces; even in the convoluted topography of the occlusal surfaces. The wetting of tooth surfaces by saliva appeared to improve the performance of PS-OCT by reducing the surface reflectivity.

The measurement of lesion depth poses a challenge in OCT, because boundaries have to be defined for quantifying the lesion depth. This is challenging because of the high dynamic range of the reflectivity. For example, as described earlier, for a system having an axial resolution in enamel of 10 μm , the intensity from a reference mirror will fall off

by 3 dB after 10 μm . If the lesion has a reflectivity that is 10-20 dB greater than the reflectivity of the underlying sound enamel, then the depth at which the reflectivity falls off to the level of the sound enamel will exceed that considerably. This problem also applies to defining the beginning of the lesion at the sample surface as well. One cannot simply choose the value at which the peak intensity falls off by 3 dB because the reflectivity varies throughout the breadth of the lesion, i.e., it is not simply a single peak. The signal fall off is very complicated because the light is exponentially attenuated while propagating through the sample and compounded exponentially attenuated upon exiting the sample. Lesions typically appear deeper in OCT images than they actually are and algorithms are needed to select the appropriate boundary cutoff points. Cutoff intensity values such as the depth at which there is a $1/e^2$ decrease in intensity can be chosen which appears to work somewhat effectively on enamel (Can et al., 2008) but can overestimate the lesion depth. Another promising method is to use edge detection algorithms to find the lesion edges and set the $1/e^2$ cutoff based on those edges (M. H Le, Darling, & Fried, 2009).

The large volume of data typically produced in a full 3D OCT image precludes manual methods of analysis. Moreover, the visual presentation of 3D volumetric data may be challenging. We have demonstrated that automated algorithms can be developed to calculate the lesion depth from CP-OCT images and then integrate over that depth to calculate the lesion severity (Can et al., 2008; M. H Le et al., 2009). The purpose of this chapter is to demonstrate efficient and accurate segmentation techniques for visualizing 3D CP-OCT images as 2D images of lesion depth and integrated reflectivity for better representing lesion severity on both smooth and convoluted tooth surfaces. Moreover,

such images are convenient for comparison with other 2D imaging methods such as fluorescence, and visible and near-IR reflectance imaging.

5.3 MATERIALS AND METHODS

5.3.1 Samples and Lesion Preparation

Ten enamel blocks (~2 x 10 mm) were prepared from extracted bovine incisors acquired from a slaughterhouse and mounted on delrin blocks. Each enamel sample was partitioned into six regions or windows (two sound and four demineralization areas) by etching 140 µm wide incisions spaced 1.4 mm apart across each of the enamel blocks using a laser. Incisions were etched using a CO₂ laser (Impact 2500, GSI Lumonics Rugby, UK) operating at a wavelength of 9.3 µm, pulse duration of 15 µs and a pulse repetition rate of 5 Hz. A water spray was used and the incident fluence was 170 J/cm² with a spot size of 150 µm. The high fluence was used to demarcate the laser-irradiated area. A thin layer of acid resistant varnish, red nail polish, Revlon (New York, NY) was applied to protect the sound enamel control area on each end of the block. Samples were exposed to a pH cycling model in which they were placed in a demineralization solution for 6 hrs followed by a remineralization solution for 17 hrs each day (D. Fried et al., 2002). This model better simulates the natural process of lesion generation that takes place in the oral environment. The demineralization solution was composed of a 40 ml aliquot of 2.0 mmol/L calcium, 2.0 mmol/L phosphate and 0.075 mol/L acetate at pH 4.7. The remineralization solution was composed of a 40 ml aliquot of 1.5 mmol/L calcium, 0.9 mmol/L phosphate, 150 mmol/L potassium chloride, and 20 mmol/L cacodylate at pH 7.0. pH cycling was repeated for intervals of 3, 6, 9, 12 day periods for each window.

Human teeth with non-carious occlusal surfaces were collected with the approval of the Committee on Human Research (CHR) and sterilized with gamma radiation. Tooth occlusal surfaces were air abraded with 50 µm glass beads for twenty seconds to remove all the stain and debris from the fissures and remove the outermost fluoride rich layers of enamel, in order to facilitate the demineralization of those surfaces. Next, teeth were mounted in black orthodontic acrylic blocks. Samples were stored in a moist environment of 0.1% thymol to maintain tissue hydration and prevent bacterial growth. Incisions 50 µm deep were cut using the CO₂ laser described above to produce 4 x 4 mm windows on the occlusal surface of each tooth. The laser incisions also inhibit decay in the laser area due to thermal modification of the enamel and are therefore very effective in providing a separation between the sound and demineralized areas. The channels cut by the laser also serve as reference points for optical coherence tomography and for serial sectioning and are sufficiently narrow that they do not interfere with calculations of the image contrast. The enamel surrounding the 4 x 4 mm windows created by the laser was covered with red fingernail polish (Revlon, New York, NY). The varnish was removed using acetone after the lesions were generated. We chose not to use a clear varnish as was done in an earlier study (Wu & Fried, 2009) because it was difficult to ensure complete coverage over the irregular tooth surfaces. Artificial lesions were created within the 4 x 4 mm windows by immersing each tooth into a 50 ml aliquot of a Ca/PO₄/acetate solution containing 2.0 mmol/L calcium, 2.0 mmol/L phosphate, and 0.075 mol/L acetate maintained at pH 4.5 and a temperature of 37°C for either 24 or 48 hours. This well proven model produces subsurface lesions approximately 50-150 µm deep with intact surfaces (J. D. B. Featherstone, Glena,

Shariati, & Shields, 1990; Jones et al., 2006; Jones & Fried, 2006; Kang et al., 2010; M. H. Le et al., 2010). In **Figure 5.1**, a depth composition 2D image and a 3D image taken with a Keyence VHX-1000 digital microscope (Keyence America, Elmwood peak, NJ) are shown for a sample after 24 hrs of demineralization. This new type of microscope allows acquisition of either high depth of field images similar to scanning electron microscopy or 3D images of the surface tomography that are well suited for imaging tooth occlusal surfaces.

5.3.2 Polarization Sensitive Optical Coherence Tomography (PS-OCT) System

An all-fiber-based optical coherence domain reflectometry (OCDR) system was used with polarization maintaining (PM) optical fiber, high-speed piezoelectric fiber-stretchers and two balanced InGaAs receivers that was designed and fabricated by Opti-phase, Inc. (Van Nuys, CA). The two-channel system was integrated with a broadband superluminescent diode (SLD) Denselight (Jessup, MD) and a high-speed XY-scanning system (ESP 300 controller and 850G-HS stages, National Instruments, Austin, TX) for *in vitro* optical tomography. This system is based on a polarization-sensitive Michelson white light interferometer. The high power (15 mW) polarized SLD source, emitted near-IR light at a center wavelength of 1317 nm with a spectral bandwidth full-width at half-maximum (FWHM) of 84 nm and it was aligned using polarization controller to deliver 15 mW into the slow axis of the PM fiber (interferometer source arm). This light was split into the reference and sample arms of the Michelson interferometer by a 50/50 PM-fiber coupler. The sample arm was coupled to an AR-coated fiber-collimator to produce a 6 mm in diameter, collimated beam. That beam was focused onto the sample surface using a 20 mm focal length AR-coated planoconvex lens. This configuration provided a

lateral resolution of approximately 20 μm and an axial resolution of 10 μm in air with a signal to noise ratio of greater than 40-50 dB. The PS-OCT system is completely controlled using Labview software (National Instruments, Austin, TX). Reflectivity values per pixel are presented as linear intensity units (IU). IU units are detector volts divided by 32 μV .

PS-OCT scans for the bovine enamel blocks were 280 x 60 x 2000 pixels with each of the 280 b-scans placed 50 μm apart for a volume of 14 mm x 3 mm x 5.74 mm in air. Scans for the occlusal surfaces were 175 pixels x 110 pixels x 2000 pixels with each of the 175 b-scans space 50 μm apart for a volume of 8.75 mm x 5.5 mm x 5.74 mm in air. Samples were stored in water and 0.1% thymol and scanned with the surface dry.

5.3.3 Image Analysis

Raw OCT data was analyzed using a custom written program in Labview (National Instruments, Austin, TX). Co-polarization and cross-polarization optical coherence tomography (CP-OCT) images were acquired for each sample, however only the cross-polarization images were processed and analyzed. For speckle noise reduction, signals not exceeding four standard deviations from the mean background noise floor were reduced to the mean background value and a Gaussian blur smoothing algorithm was applied using a 5 x 5 pixel convolution kernel (Kang et al., 2010; M. H. Le et al., 2010). The program first locates the maximum of each a-scan and differentiates the a-scan maximum as either demineralized or sound using the signal-to-noise ratio as a threshold. The depth of the lesion is next calculated by locating the upper and lower lesion boundaries by identifying the first pixels that fall under the threshold of e^{-2} of the maximum value. The distance per pixel conversion factor was obtained experimentally

by system calibration. A linear relationship was established between the OCT lesion depth and the histological depths measured using polarized light microscopy (PLM). Based on this relationship, a linear correction was applied to the lesion depth calculated from OCT:

$$\text{Corrected Data} = 1.55 - \text{OCT pixel depth} - 66.2 \text{ (eq. 5.1)}$$

Each a-scan of the CP-OCT images was reduced to single values representing the mean reflectivity per pixel, the integrated reflectivity over a fixed depth, the calculated lesion depth, and the integrated reflectivity over the calculated image depth. The mean reflectivity per pixel was calculated by dividing the sum of each a-scan in linear intensity units (IU) by the number of pixels in each a-scan. The integrated reflectivity (ΔR) was calculated by integrating the reflectivity in IU units over either a fixed depth in microns (150 μm for bovine enamel blocks and 250 μm for the 24 hr and 48 hr lesions in tooth occlusal surfaces) or the lesion depth calculated as described above.

5.4 RESULTS AND DISCUSSION

The bovine enamel samples exposed to pH cycling yielded lesions with intact surfaces, i.e. subsurface lesions. Lesion depths varied from 40 μm to 110 μm after 3, 6, 9, or 12-days of pH cycling. **Figure 5.2** shows OCT b-scans of both the parallel and perpendicular polarization states (**Figure 5.2B & C**) and the corresponding polarized light microscope image (**Figure 5.2A**) of a thin section cut from that sample. Note how there is minimal reflectivity from the sound areas in the cross-polarization image vs the co-polarization image. The lesion depth in both the PLM and CP-OCT images increases monotonically with increasing periods of pH cycling.

An accurate determination of the lesion depth is the most challenging task in analysis of the CP-OCT images. In order to determine the lesion depth in the CP-OCT image, the depth at which the signal intensity falls by $1/e^2$ from the peak value was used as an initial estimate. This choice results in an overestimate of the actual lesion depth for lesions less than 100 μm deep. **Figure 5.3** shows a plot of the lesion depths estimated from the CP-OCT images using the $1/e^2$ cutoff point vs the lesion depth measured using polarized light microscopy. Linear regression shows a strong linear correlation ($R^2 = 0.69$) between the two methods. The depth determination also relies on accurate knowledge of the refractive index and a refractive value of 1.63 was used to represent sound enamel. However, the refractive index of the demineralized enamel is lower due to the loss of mineral density and the lower refractive index of the lesion is expected to lead to an underestimation of the actual lesion depth. This error is expected to increase with increasing lesion depth. We adjusted the lesion depths determined using CP-OCT using the linear relationship between the PLM and CP-OCT lesion depths from **Figure 5.3**. Depths in microns were adjusted by multiplying by 1.55 and subtracting by 66.2 (**eq.1**). The adjusted depths and the depths measured using PLM are plotted in **Figure 5.4** for comparison. Note that the mean lesion depth for the sound window is not zero for either CP-OCT or PLM. It is difficult to differentiate edge shadowing effects resulting from surface topography in PLM images from demineralization close to the sample surface, namely the sample edge appears to be 10-20 μm thick. This problem with PLM is more pronounced for occlusal surfaces where there is a great deal of curvature (**Figures 5.8 and 5.9**). The higher mean lesion depth and corresponding high standard deviation for CP-OCT was caused by a single sample. One of the sound windows

yielded a very high lesion depth producing the high standard deviation for the sound window in **Figure 5.4**. Close examination of the OCT scans from the sample showed that there was strong reflectivity from the sound window on the upper half of the window. From the CP-OCT scans it appears that demineralization may have occurred beneath part of the protected window. Unfortunately, this could not be independently confirmed. Since only one intact PLM slice survived sectioning without fracture and that appeared “clean” with no artifact or demineralization visible on the sound windows. Without definitive histological confirmation, this sample was not rejected from the study. If that single outlier is rejected, the adjusted mean lesion depth for the remaining 9 samples assessed with CP-OCT is -1.75 ± 15 . Note that this is negative because the depth correction involves a subtraction constant.

The CP-OCT images for the ten bovine enamel blocks 280 x 60 x 2000 pixels representing a volume of 14 mm x 3 mm x 5.74 mm in air (3.59 mm in enamel) were processed as described in [Section 5.3.3](#) with the applied depth correction to generate 2D images in various formats. **Figure 5.5** shows four images of one of the bovine enamel blocks with six windows. The first image (**Figure 5.5A**) represents the mean reflectivity and this was calculated by taking the mean value of all the pixels in each of the a-scans. The limitation of this approach is that each pixel includes the a-scan signal intensities outside the lesion’s a-scan range (i.e. signals from background, sound enamel structure, dentino-enamel junction reflections, and dentin). The second image (**Figure 5.5B**) represent the reflectivity integrated over a fixed depth and this was calculated by integrating the reflectivity in each a-scan from the sample surface to a fixed depth of 150 μm . A depth of 150 μm was chosen based on the assumption that

the artificially simulated lesions should be no deeper than 150 μm from previous experiments (D. Fried et al., 2002; P. Ngaotheppitak, C. L. Darling, & D. Fried, 2005). The reflectivity of sound enamel is not zero, therefore in this approach the contribution of the pixels between the actual lesion depth and 150 μm in each a-scan inflates the integrated reflectivity value of the lesion. In the third image (**Figure 5.5C**), each pixel represents the value of the calculated lesion depth. The last image (**Figure 5.5D**) shows the integrated reflectivity over the calculated lesion depth and best represents the lesion severity in a single 2D image.

The same approach utilized to analyze the bovine enamel blocks was applied to simulated lesions produced in the 4 x 4 mm windows on the occlusal surfaces of human teeth (**Figure 5.1**). The same algorithms were applied and the same linear correction was applied to the depths calculated for the CP-OCT images which were 175 px x 110 px x 2000 px for a volume of 8.75 mm x 5.5 mm x 5.74 mm. **Figures 5.6 and 5.7** show images of the 4 x 4 mm windows on samples exposed to the demineralization solution for 24 and 48 hours, respectively. Four images are shown, including the mean reflectivity, the reflectivity integrated over a depth of 250 μm , the calculated lesion depth and the reflectivity integrated over the calculated lesion depth. These images show considerable variation in the lesion severity over the 4 x 4 mm window. It is difficult to produce uniform lesions in the occlusal surfaces due to the varying angle of the enamel prisms, high fluoride content in the outer enamel layers and the presence of prismless enamel (Fejerskov & Kidd, 2003). The demineralization viewed under visible light appear quite uniform (**Figure 5.1**) indicating that visible light reflectance measurements do not represent the varying severity of the lesions.

The 24 hr and 48 hr demineralization samples were sectioned to confirm that the lesion depths determined using our algorithm with CP-OCT compare reasonably with the depths shown by polarized light histology. **Figures 5.8 and 5.9** show PLM images from 24 hr and 48 hr samples along with b-scan CP-OCT images matched to that section. The variation in the lesion depth in the PLM images, higher near the laser incisions and shallower in the center are mirrored in the OCT images. The depth of demineralization is indicated at three points in the image. The depths indicated by PLM are consistently higher due to edge effects in the slice resulting from the steep sloping topography of the occlusal surface. The sound edges are 29 μm thick on the left side of the sample and 54 μm thick on the right side. Therefore the 30 μm difference in depth between the two methods can be easily explained by the sample curvature. There is a very deep lesion area on this sample (**Figure 5.8C, 3rd mark**). This may be a very small pre-existing lesion or an area more susceptible to demineralization.

The lesions in the 48 hr sample are proportionally deeper (**Figure 5.9**). The sound edges are 74 μm on the left side and 28 μm on the right side so the agreement is quite reasonable.

Images of the reflectivity integrated over the calculated lesion depth are well suited for monitoring the development of caries lesions *in vivo* or *in vitro*. This measure is directly comparable to the gold standard for demineralization, ΔZ , the integrated mineral loss over the lesion depth, volume percent mineral x microns and have labeled it ΔR , with units of intensity x microns. Direct measurements of ΔZ require the use of microradiography and tooth destruction making the method unsuitable for use *in vivo*, therefore the use of a surrogate nondestructive measurement such as ΔR , is extremely

valuable. A good example of the utility of this approach is provided in the following description of one of our ongoing clinical studies.

An *in vivo* study employing a CP-OCT system was used to monitor the development of demineralization peripheral to orthodontic brackets (Nee et al., 2014). Small lesions commonly appear around orthodontic brackets, particularly near the cervical margins between the base of the bracket and the gingiva since it is difficult to keep this area free of plaque. In this study, volumetric 6 mm x 6 mm x 6 mm cross polarization tomographic images were acquired of the bracket and the area surrounding it. These images were rapidly and automatically converted to images of the reflectivity integrated over the calculated lesion depth, ΔR . Using these 2D images, we were able to successfully monitor *in vivo* and quantify an increase in the severity of demineralization between the base of the bracket and the gum line over time.

Presentation of the OCT images in the calculated depth and ΔR formats is also advantageous for comparison with other optical imaging methods such as reflectance imaging and fluorescence imaging. The intensity in these images represents either the reflectivity integrated over the depth or the loss in intensity over depth. Comparison of such images with OCT images can show how the image contrast changes with both lesion severity and lesion depth.

Different approaches have been proposed over the past decade to quantify the severity of demineralization from conventional and cross-polarization OCT images. The use of the cross-polarization OCT images allows direct integration of the reflectivity from lesion areas minimizing the interference from the strong surface reflection from the tooth surface. This greatly facilitates automated analysis which is required to handle the great

wealth of data contained in OCT images. This chapter demonstrates that 2D images of the calculated lesion depth and the reflectivity integrated over the calculated lesion depth are well suited for representing the severity of demineralization. This approach is quite valuable for monitoring lesion severity both *in vivo* and *in vitro* and for comparing the inhibition of demineralization by various anti-caries agents.

5.5 FIGURES AND FIGURE LEGENDS

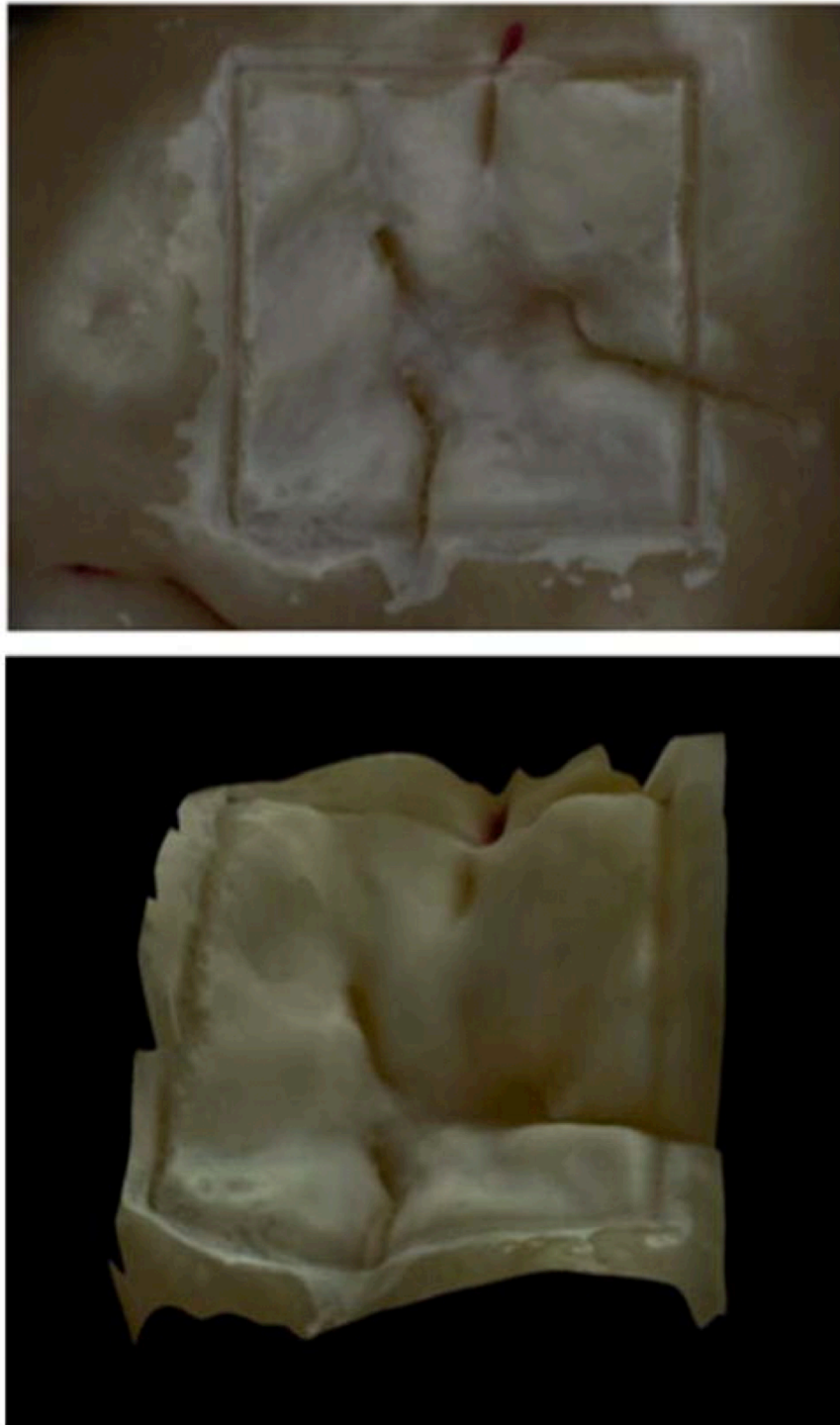


Figure 5.1: Images of one of the samples used in this study taken with the Keyence VHX-1000E digital microscope (Itasca, IL). (Top) Depth composition image of the 4 x 4 mm window on the occlusal surface of a human tooth after 24 hrs demineralization. (Bottom) 3D image of the same 4 x 4 mm window.

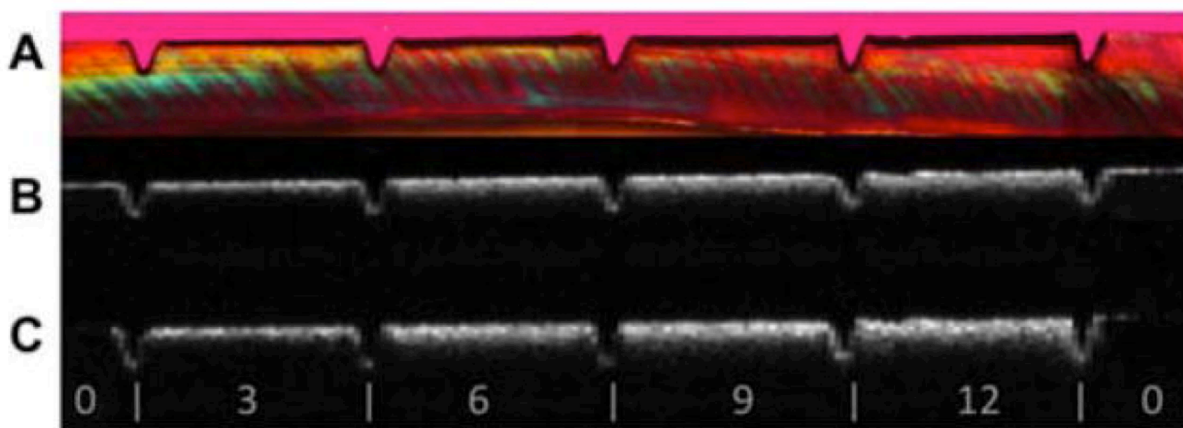


Figure 5.2: Comparison of polarization sensitive – optical coherence tomography (PS-OCT) b-scans for both linear polarizations with a histological section viewed under polarized light. (A) Polarized light microscopy (PLM) image of the thin section; (B) Co-polarization optical coherence tomography b-scan image; and (C) Cross-polarization optical coherence tomography b-scan image. The individual windows located between the laser incisions marked with the white bars are indicated for 0, 3, 6, 9, and 12 days of exposure to pH cycling.

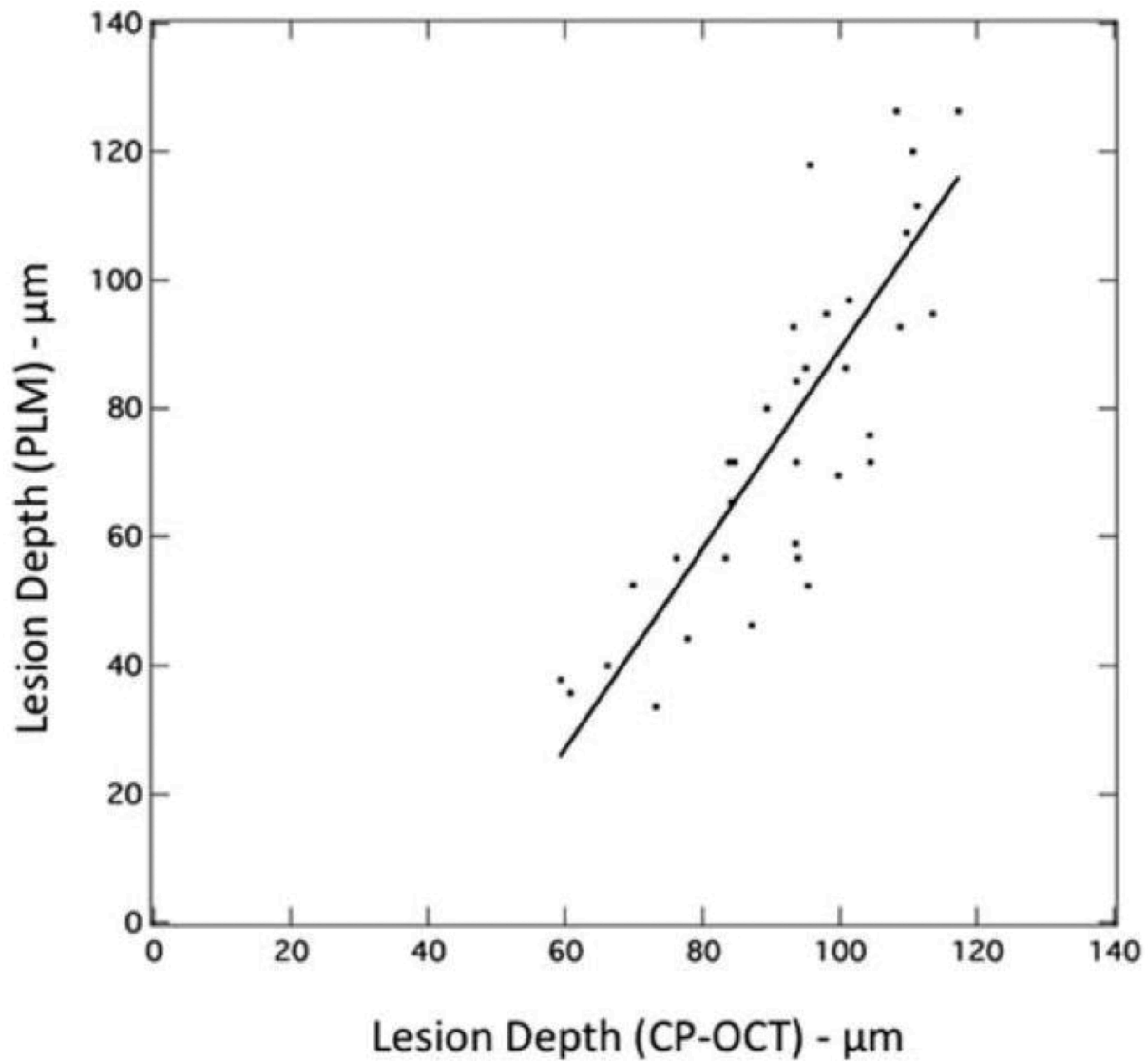


Figure 5.3: (A) Plot of lesion depth determined from the cross polarization – optical coherence tomography (CP-OCT) image with a user defined cutoff point ($1/e^2$) vs. depth determined using polarized light microscopy (PLM).

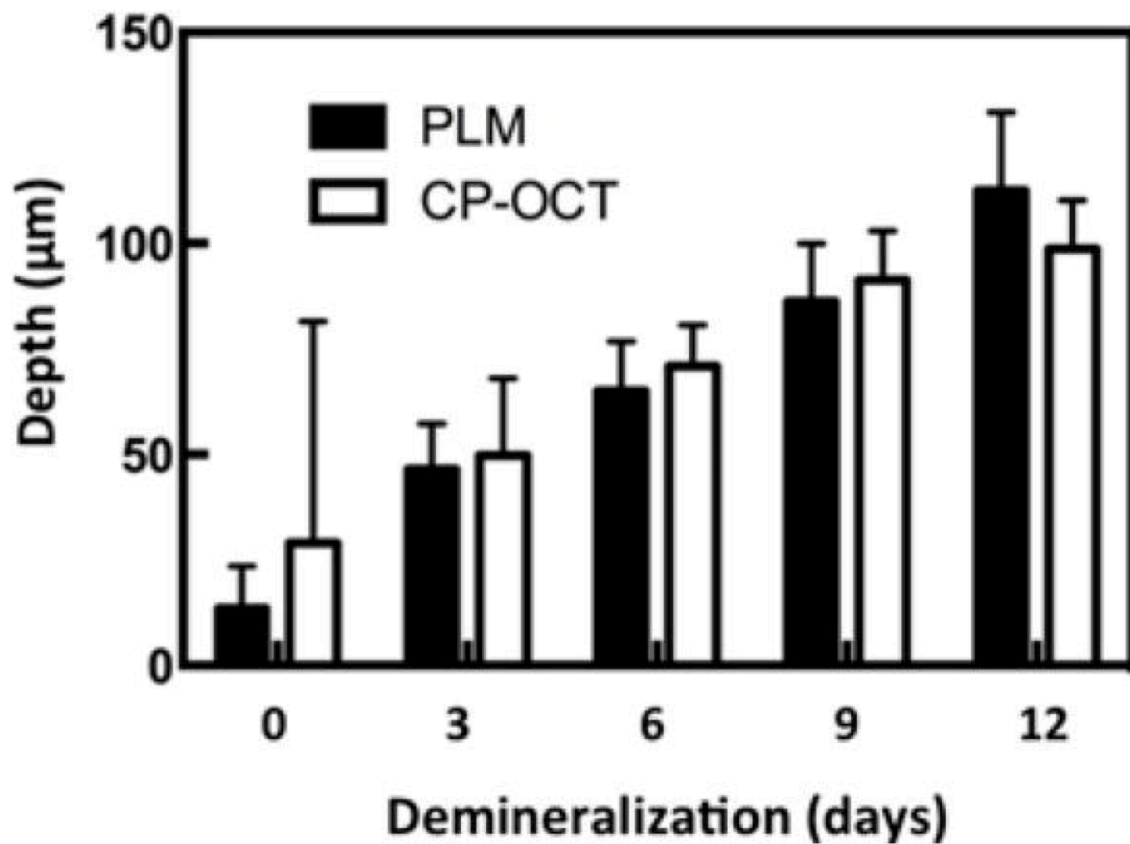


Figure 5.4: Bar graph comparing the mean \pm s.d. of the adjusted lesion depths calculated using cross polarization – optical coherence tomography (CP-OCT) and those calculated from polarized light microscopy (PLM) for the ten bovine enamel samples.

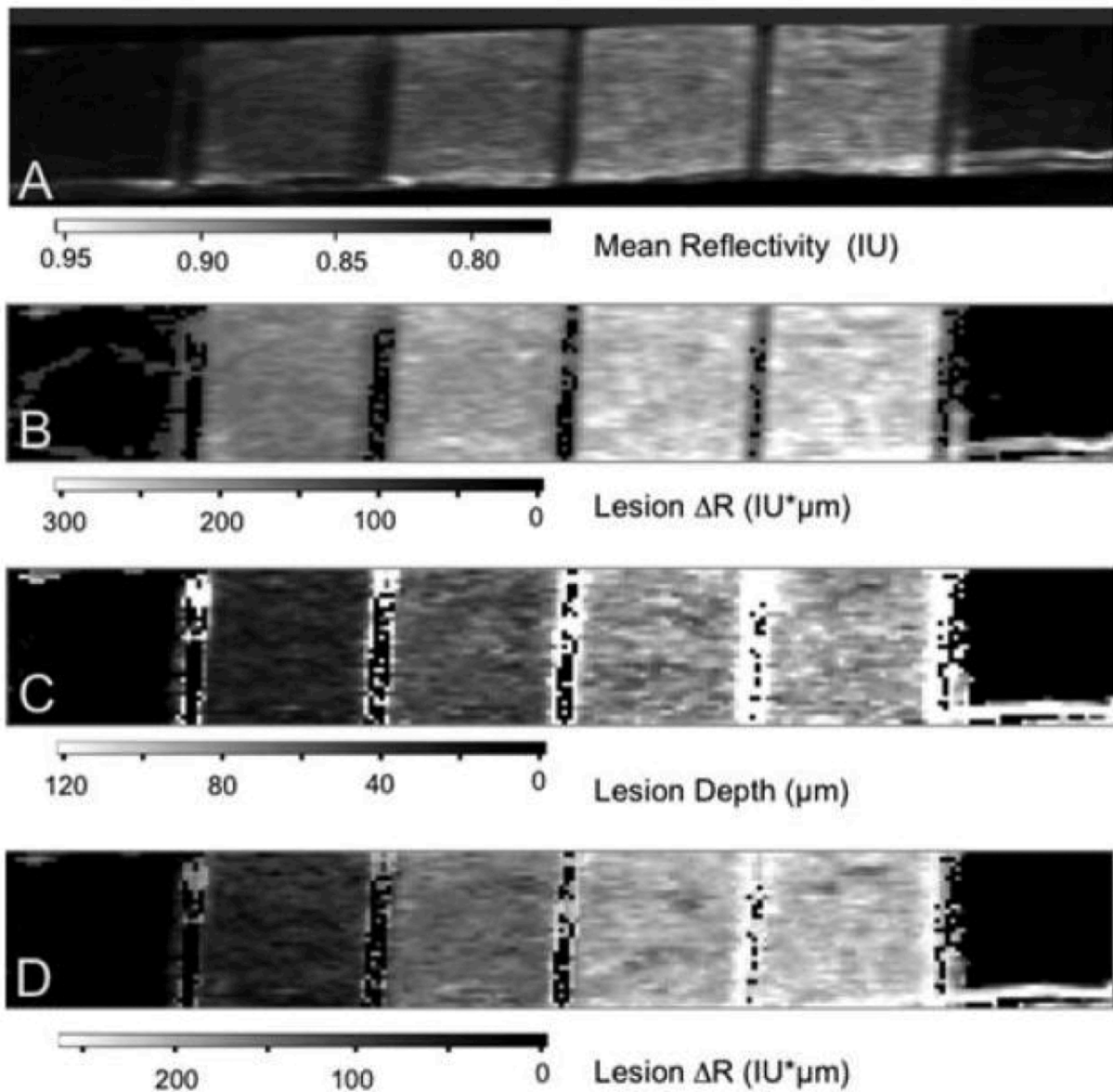


Figure 5.5: Two dimensional images of one of the bovine enamel samples are shown including: (A) the image contrast ratio; (B) the reflectivity integrated over a fixed depth of 150 μm ; (C) the calculated lesion depth; and (D) the reflectivity integrated over the calculated lesion depth. Values are shown in the grayscale bars below each image.

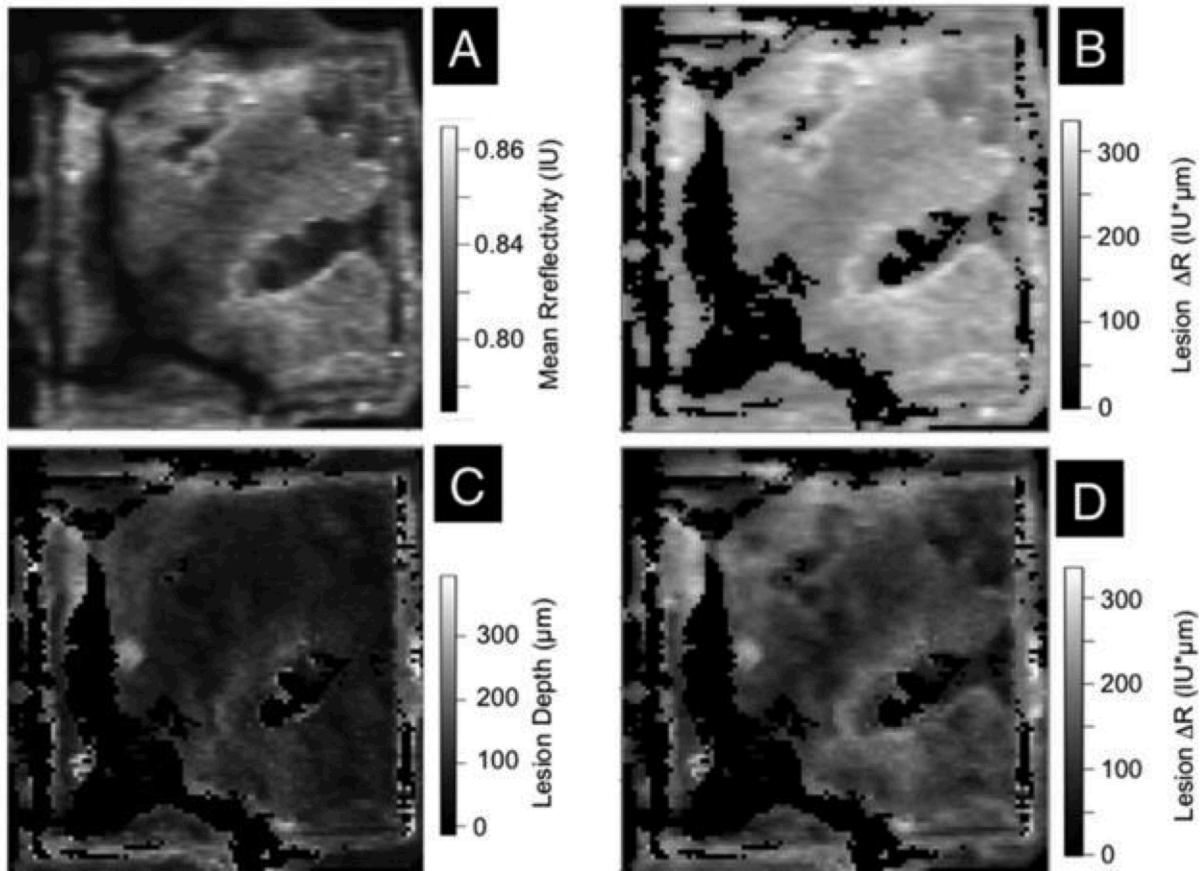


Figure 5.6: Two dimensional images of the occlusal surface of one of the teeth after 24 hrs of pH 4.5 demineralization solution are shown including: (A) the image contrast ratio; (B) the reflectivity integrated over a fixed depth of 250 μm ; (C) the calculated lesion depth; and (D) the reflectivity integrated over the calculated lesion depth. Values are shown in the grayscale bars to the right of each image.

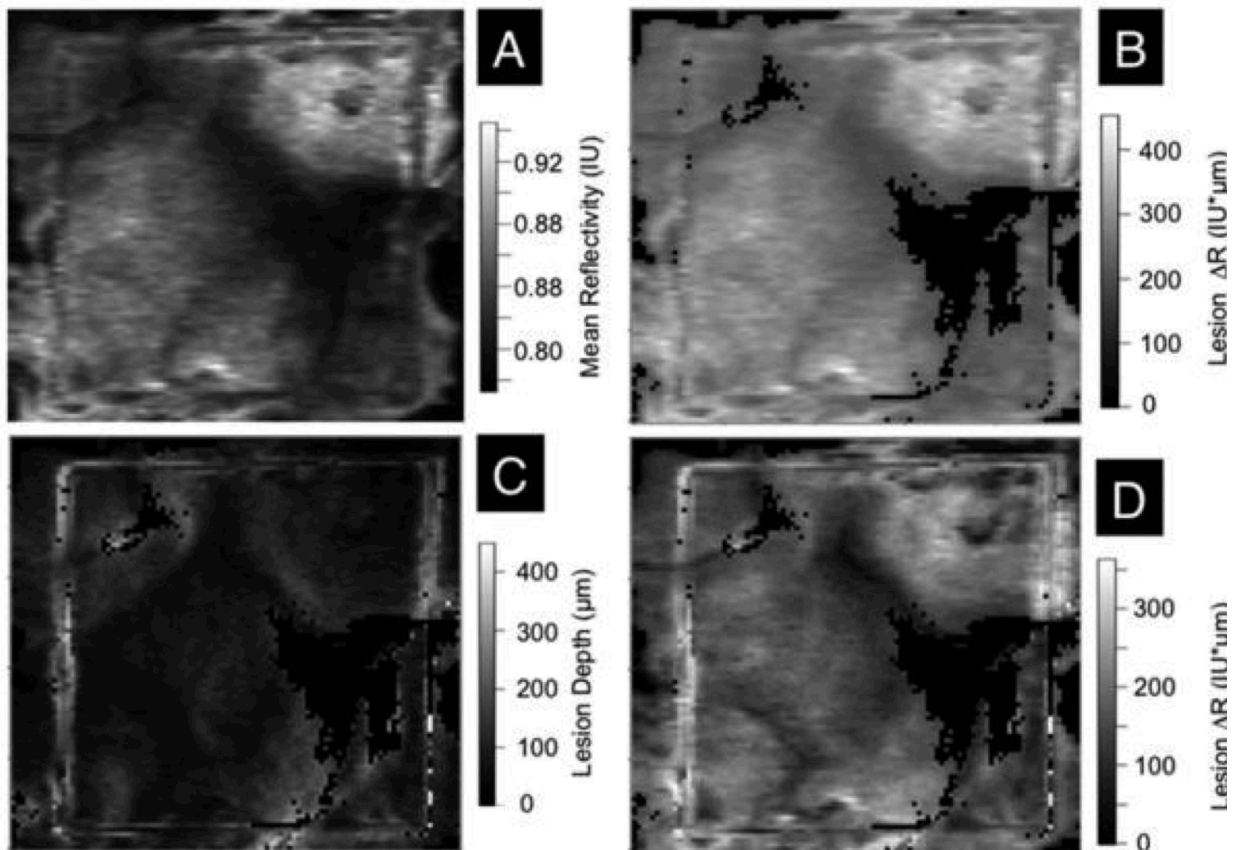


Figure 5.7: Two dimensional images of the occlusal surface of one of the teeth after 48 hrs of pH 4.5 demineralization solution are shown including: (A) the image contrast ratio; (B) the reflectivity integrated over a fixed depth of 250 μm ; (C) the calculated lesion depth; and (D) the reflectivity integrated over the calculated lesion depth. Values are shown in the grayscale bars to the right of each image.

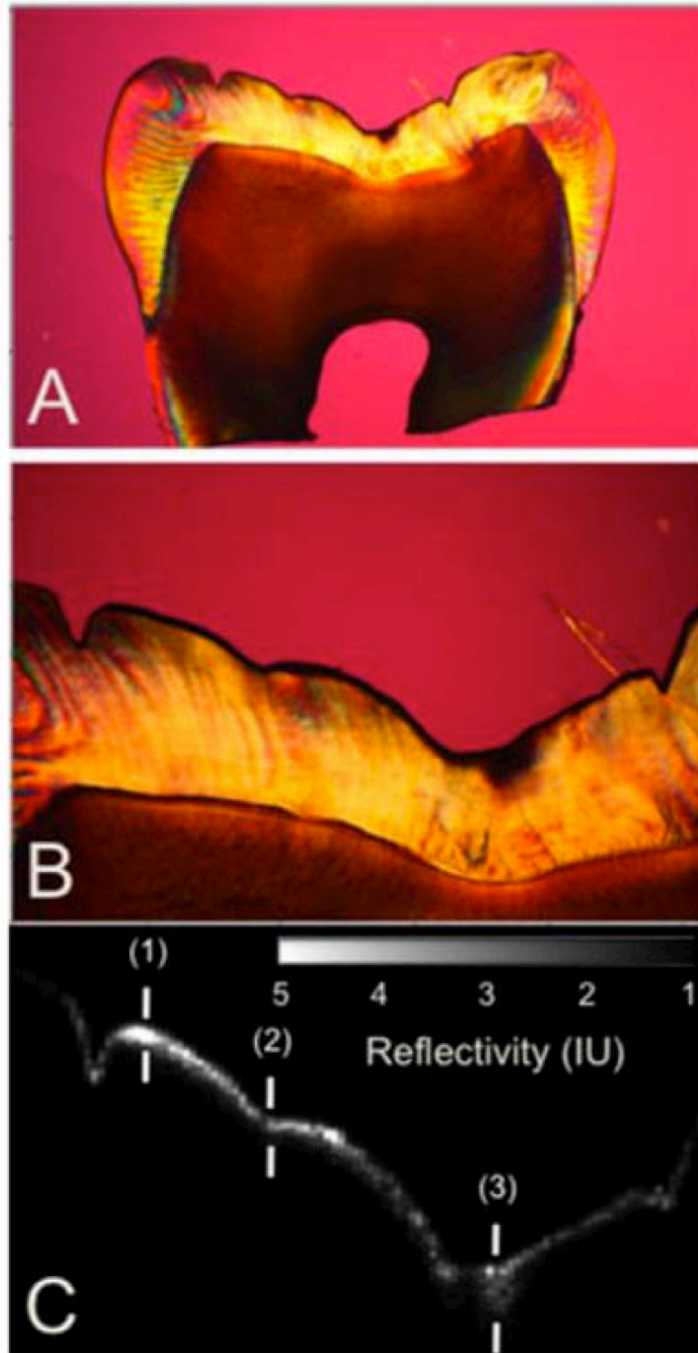


Figure 5.8: Comparison of a cross polarization – optical coherence tomography (CP-OCT) b-scan image taken across the 4 x 4 mm window on the occlusal surface of one of the 24 hrs demineralized tooth samples with a histological section viewed under polarized light. (A) Polarized light microscopy (PLM) image of the entire thing section; (B) Magnified PLM image of region of interest; (C) Matching cross polarization b-scan image of region of interest. The depths represented by the three marks (1 – 3) are (1) 50 μm with PLM and 57 μm with CP-OCT; (2) 72 μm with PLM and 52 μm with CP-OCT; (3) 283 μm with PLM and 237 μm with CP-OCT.

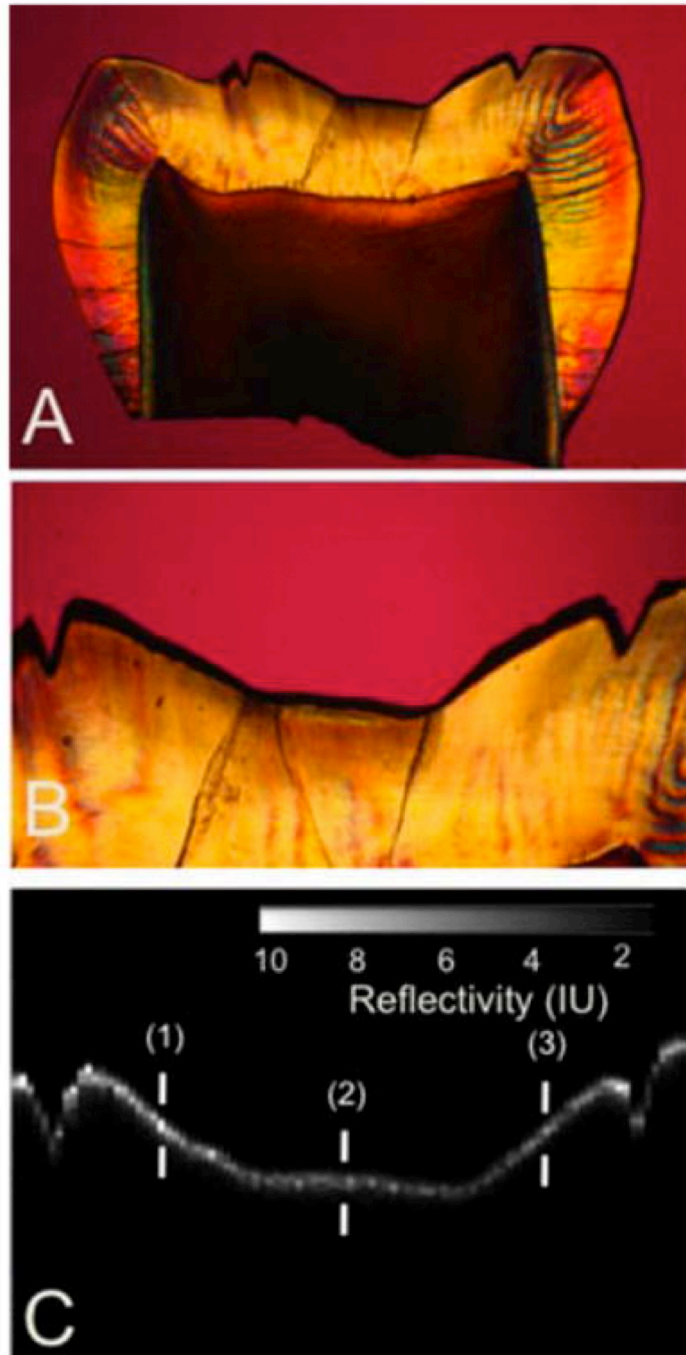


Figure 5.9: Comparison of a cross polarization – optical coherence tomography (CP-OCT) b-scan image taken across the 4 x 4 mm window on the occlusal surface of one of the 48 hrs demineralized tooth samples with a histological section viewed under polarized light. (A) Polarized light microscopy (PLM) image of the entire thing section; (B) Magnified PLM image of region of interest; (C) Matching cross polarization b-scan image of region of interest. The depths represented by the three marks (1 – 3) are (1) 108 μm with PLM and 83 μm with CP-OCT; (2) 94 μm with PLM and 77 μm with CP-OCT; (3) 153 μm with PLM and 121 μm with CP-OCT.

5.6 REFERENCES

- Amaechi, B. T., Higham, S. M., Podoleanu, A. g., Rodgers, J. A., & Jackson, D. A. (2001). Use of Optical Coherence Tomography for Assessment of Dental caries. *J Oral Rehab*, 28(12), 1092-1093.
- Baumgartner, A., Dicht, S., Hitzenberger, C. K., Sattmann, H., Robi, B., Moritz, A., . . . Fercher, A. F. (2000). Polarization-sensitive optical optical coherence tomography of dental structures. *Caries Res.*, 34, 59-69.
- Can, A. M., Darling, C. L., Ho, C., & Fried, D. (2008). Non-destructive assessment of inhibition of demineralization in dental enamel irradiated by a $\lambda=9.3$ -microm CO2 laser at ablative irradiation intensities with PS-OCT. *Lasers in Surgery and Medicine*, 40(5), 342-349. doi:10.1002/lsm.20633
- Darling, C. L., Huynh, G. D., & Fried, D. (2006). Light scattering properties of natural and artificially demineralized dental enamel at 1310 nm. *Journal of Biomedical Optics*, 11(3), 34023. doi:10.1117/1.2204603
- de Josselin de Jong, E., van der Linden, A. H. I. M., Borsboom, P. C. F., & ten Bosch, J. J. (1988). Determination of mineral changes in human dental enamel by longitudinal microradiography and scanning optical mintoring and their correlation with chemical analysis. *Caries Res.*, 22, 153-159.
- Dicht, S., Baumgartner, A., Hitzenberger, C. K., Sattmann, H., Robi, B., Moritz, A., . . . Fercher, A. F. (1999). *Polarization-sensitive optical optical coherence tomography of dental structures*. Paper presented at the Lasers in Dentistry V, San Jose.
- Everett, M. J., Colston, B. W., Sathyam, U. S., Silva, L. B. D., Fried, D., & Featherstone, J. D. B. (1999). *Non-invasive diagnosis of early caries with polarization sensitive optical coherence tomography (PS-OCT)*. Paper presented at the Lasers in Dentistry V, San Jose.
- Featherstone, J. D. B., Glena, R., Shariati, M., & Shields, C. P. (1990). Dependence of *in vitro* demineralization and remineralization of dental enamel on fluoride concentration. *J. Dent. Res.*, 69, 620-625.
- Fejerskov, O., & Kidd, E. (Eds.). (2003). *Dental Caries: The Disease and its Clinical Management*. Oxford: Blackwell.

Feldchtein, F. I., Gelikonov, G. V., Gelikonov, V. M., Iksanov, R. R., Kuranov, R. V., Sergeev, A. M., . . . Reitze, D. H. (1998). In vivo OCT imaging of hard and soft tissue of the oral cavity. *Optics Express*, 3(3), 239-251.

Fried, D., Xie, J., Shafi, S., Featherstone, J. D. B., Breunig, T., & Lee, C. Q. (2002). Early detection of dental caries and lesion progression with polarization sensitive optical coherence tomography. *J. Biomed. Optics*, 7(4), 618-627.

Jones, R. S., Darling, C. L., Featherstone, J. D., & Fried, D. (2006). Imaging artificial caries on the occlusal surfaces with polarization-sensitive optical coherence tomography. *Caries research*, 40(2), 81-89. doi:10.1159/000091052

Jones, R. S., & Fried, D. (2006). Remineralization of enamel caries can decrease optical reflectivity. *Journal of dental research*, 85(9), 804-808.

Kang, H., Jiao, J. J., Lee, C., Le, M. H., Darling, C. L., & Fried, D. (2010). Nondestructive Assessment of Early Tooth Demineralization Using Cross-Polarization Optical Coherence Tomography. *IEEE journal of selected topics in quantum electronics : a publication of the IEEE Lasers and Electro-optics Society*, 16(4), 870-876. doi:10.1109/JSTQE.2009.2033610

Le, M. H., Darling, C. L., & Fried, D. (2009). *Methods for calculating the severity of demineralization on tooth surfaces*. Paper presented at the Lasers in Dentistry VX, San Jose.

Le, M. H., Darling, C. L., & Fried, D. (2010). Automated analysis of lesion depth and integrated reflectivity in PS-OCT scans of tooth demineralization. *Lasers Surg Med*, 42(1), 62-68. doi:10.1002/lsm.20862

Louie, T., Lee, C., Hsu, D., Hirasuna, K., Manesh, S., Staninec, M., . . . Fried, D. (2010). Clinical assessment of early tooth demineralization using polarization sensitive optical coherence tomography. *Lasers in Surg. Med.*, 42, 738-745.

Mandurah, M. M., Sadr, A., Shimada, Y., Kitasako, Y., Nakashima, S., Bakhsh, T. A., . . . Sumi, Y. (2013). Monitoring remineralization of enamel subsurface lesions by optical coherence tomography. *Journal of Biomedical Optics*, 18(4), 046006. doi:10.1117/1.JBO.18.4.046006

Mujat, C., van der Veen, M. H., Ruben, J. L., ten Bosch, J. J., & Dogariu, A. (2003). Optical path-length spectroscopy of incipient caries lesions in relation to quantitative light-induced fluorescence and lesion characteristics. *Applied optics*, 42(16), 2979-2986.

Nee, A., Chan, K., Kang, H., Staninec, M., Darling, C. L., & Fried, D. (2014). Longitudinal monitoring of demineralization peripheral to orthodontic brackets using cross polarization optical coherence tomography. *J Dent*, *42*(5), 547-555. doi:10.1016/j.jdent.2014.02.011

Ngaotheppitak, P., Darling, C. L., & Fried, D. (2005). Measurement of the severity of natural smooth surface (interproximal) caries lesions with polarization sensitive optical coherence tomography. *Lasers in Surgery and Medicine*, *37*(1), 78-88. doi:10.1002/lsm.20169

Ngaotheppitak, P., Darling, C. L., & Fried, D. (2005). Polarization Optical Coherence Tomography for the Measuring the Severity of Caries Lesions. *Lasers Surg Med*, *37*(1), 78-88.

Popescu, D. P., Sowa, M. G., Hewko, M. D., & Choo-Smith, L. P. (2008). Assessment of early demineralization in teeth using the signal attenuation in optical coherence tomography images. *Journal of Biomedical Optics*, *13*(5), 054053. doi:10.1117/1.2992129

Wu, J., & Fried, D. (2009). High contrast near-infrared polarized reflectance images of demineralization on tooth buccal and occlusal surfaces at $\lambda = 1310\text{-nm}$. *Lasers in Surgery and Medicine*, *41*(3), 208-213. doi:10.1002/lsm.20746

CHAPTER VI

**MULTISPECTRAL CROSS-POLARIZATION REFLECTANCE MEASUREMENTS OF
DEMINERALIZATION ON TOOTH SURFACES**

6.1 SUMMARY

The enamel scattering coefficient decreases markedly with increasing wavelength from the visible to the near-infrared (NIR). However beyond 1300 nm the scattering coefficient is difficult to measure and it is not known whether light scattering continues to decrease significantly at longer wavelengths. It is hypothesized that water absorption is a major contributor to the contrast between sound and demineralized enamel beyond 1300 nm since deeply penetrating photons in sound enamel are likely absorbed by water. Reflectance images of demineralization on tooth surfaces were acquired at wavelengths near 1450, 1860, 1880, and 1950 nm. The magnitude of water absorption is similar at 1450 and 1880 nm but varies markedly between 1860, 1880, and 1950 nm. Multispectral comparisons of lesion contrast provide insight into the mechanism responsible for higher contrast at longer NIR wavelengths. The highest contrast was at 1950 nm; however, the markedly higher contrast at 1880 compared to 1450 nm and similar contrast between 1860 and 1880 nm suggests that the enamel scattering coefficient continues to decrease beyond 1300 nm, and that reduced light scattering in sound enamel is most responsible for the higher lesion contrast at longer NIR wavelengths. This has important implications for the choice of wavelengths for caries detection and diagnostic devices, including the performance of optical coherence tomography beyond 1300 nm.

6.2 INTRODUCTION

The detection and diagnosis of caries lesions (dental decay) is a significant problem in dentistry. Conventional methods rely on a combination of visual and tactile inspection, which are prone to subjective bias, interference from tooth staining, and may incur

iatrogenic damage, the latter through the use of a dental explorer (Fejerskov & Kidd, 2003). Radiographs have poor sensitivity in diagnosing early occlusal cavities due to overlapping features of the crown. Furthermore, studies have shown that visible- and fluorescence-based caries detection systems suffer false positives from stains (Alfano et al., 1984; Ferreira Zandona et al., 1998; Stookey, 2005; Tranaeus, Shi, Lindgren, Trollsas, & Angmar-Mansson, 2002). A recent summary of caries detection methods is presented by Zandona and Epure (Zandona & Epure, 2018). Several studies both *in vitro* and *in vivo* have demonstrated that near-infrared (NIR) reflectance imaging at longer NIR wavelengths (beyond 1300 nm) yields higher contrast between demineralization and sound tooth structure than visible reflectance and fluorescence without the interference of stains (Bühler, Ngaotheppitak, & Fried, 2005; Chung et al., 2011; W. A. Fried, Darling, Chan, & Fried, 2013; R. Jones, G. Huynh, G. Jones, & D. Fried, 2003; Simon et al., 2016; Staninec et al., 2010; Wu & Fried, 2009; Zakian et al., 2009).

The light scattering in sound enamel decreases as $1/\lambda^3$ with increasing wavelength from 400 to 1300 nm as shown in **Figure 6.1** (D. Fried et al., 1995). Enamel contains ~10% water, and water absorption increases beyond 1400 nm, also shown in **Figure 6.1**. The Rayleigh-like wavelength dependence of the light scattering suggests that the scattering is mainly due to the individual enamel crystals that are much smaller than the wavelength of visible light (D. Fried et al., 1995). Optical measurements at 1550 nm yielded a similar attenuation coefficient to that measured at 1310 nm; however, with an attenuation coefficient of only 2 to 3 cm^{-1} , it is extremely difficult to decouple the contributions of surface scattering and water absorption from the bulk scattering in the

enamel (Jones & Fried, 2002). The lesion contrast or contrast of demineralization arises due to the formation of pores in the enamel that highly scatter light. At 1300 nm, the scattering of the demineralized enamel increases by more than 2 orders of magnitude over sound enamel (Darling et al., 2006).

Water may also play an important role in contributing to the lesion contrast. The water in sound enamel (~10% by volume) and in the underlying dentin (~22% by volume) can absorb incident photons (Fejerskov & Kidd, 2003). At wavelengths beyond 1300 nm, most of the photons incident on the sound tooth penetrate through the transparent enamel to reach the highly scattering dentin. Therefore, higher water absorption likely reduces the intensity of light reflected from sound areas of the tooth.

Water can also fill the pores in the lesion markedly reducing the light scattering from the lesion. This phenomenon can be exploited to help differentiate active lesions from arrested lesions that have greatly reduced permeability (R. C. Lee, Darling, Staninec, Ragadio, & Fried, 2017; R. C. Lee, Staninec, Le, & Fried, 2016). Clinicians typically blow air over lesions for a few seconds during clinical examination to better view the lesion.

Recent studies suggest that there is reduced scattering at NIR wavelengths beyond 1600 nm for greater optical penetration in bone and soft tissues (Sordillo, Pu, Pratavieira, Budansky, & Alfano, 2014; Weber et al., 2013). Standard InGaAs detectors are not sensitive past 1700 nm. New extended range InGaAs NIR cameras allow access to wavelengths beyond 1700 nm, and initial studies show higher contrast for lesions on occlusal surfaces from 1700 to 2350 nm; however, the sensitivity is not sufficient to use narrow-band filters to sample individual wavelengths, and the use of

high intensity narrow-bandwidth diode-laser sources suffer from speckle interference (Ng, Simon, Fried, & Darling, 2018). In this chapter, teeth were scanned across the laser diode and fiber laser sources, and images were acquired using a single detector. Wavelengths of 1450, 1860, 1880, and 1950 nm were examined. The magnitude of water absorption is similar at 1450 and 1880 nm, whereas the magnitude of water absorption varies markedly between 1860, 1880, and 1950 nm. Comparisons of the contrast of early demineralization on tooth surfaces at these wavelengths allow us to estimate the contributions of reduced light scattering and water absorption at longer NIR wavelengths.

6.3 MATERIALS AND METHODS

6.3.1 Sample Preparation

Ten human teeth with non-cariou occlusal surfaces were collected and sterilized with gamma radiation. Tooth occlusal surfaces were abraded using air abrasion with 50 μm glass beads for 20 sec to remove all stain and debris from the fissures and to remove the outermost fluoride-rich layers of enamel to facilitate the demineralization of those surfaces (W. A. Fried et al., 2013). Next, teeth were mounted in black orthodontic acrylic blocks. Samples were stored in a moist environment of 0.1% thymol to maintain tissue hydration and prevent bacterial growth. The outlines of a 4 x 4 mm window (roughly ~50 μm deep) were cut on the occlusal surfaces of each tooth using an Impact 2500 CO₂ laser from GSI Lumonics (Northville, Michigan) operating at a wavelength of 9.3 μm , pulse width of 15 μs , and repetition rate of 5 Hz. These markings served as a reference point to denote the demineralized area. The enamel surrounding the 4 x 4 mm windows was covered with acid-resistant varnish. Artificial lesions were created within the 4 x 4

mm windows by immersing each tooth into a 50 mL aliquot of a Ca/PO₄/acetate solution maintained at pH of 4.5 as described in a previous study (W. A. Fried et al., 2013). Varnish was removed using acetone after the lesions were generated (**Figure 6.2a**). Using nondestructive cross-polarized optical coherence tomography (CP-OCT), we confirmed lesion presence and measured the lesion depth to be between 50 to 150 μm deep with intact surfaces (**Figure 6.2b**) (Chan et al., 2015; Jones et al., 2006; Kang et al., 2010).

6.3.2 Near-Infrared Reflectance Imaging System and Laser Sources

Linearly polarized and collimated light from the near-infrared (NIR) lasers was focused onto the tooth samples with an $f = 100$ mm lens. Computer-controlled XY motion control system, ESP-301, and UTM150 stages from Newport (Irvine, CA) were used to scan the samples for NIR reflectance image acquisition. Cross-polarized backscattered light from the tooth surface was collected with a model PDA10DT extended range InGaAs detector from Thorlabs (Newton, NJ). Laser light sources were: a 1468 nm superluminescent diode (SLD) with a bandwidth of 40 nm and a peak output of 14 mW, model 1480 from Exalos (Langhorne, PA); a tunable 1860 to 1880 nm thulium fiber laser with an output up to 2 W, model TLT-5 from IPG Photonics (Oxford, MA); and a linearly polarized 200 mW 1950-nm fiber laser, model AP-CW from AdValue Photonics (Tucson, AZ). The 1468 nm source is not a narrow bandwidth laser source, rather it is a SLD with a bandwidth of 40 nm, and water absorption varies from 28.6 cm⁻¹ at 1448 nm to 19.8 cm⁻¹ at 1488 nm with 25.6 cm⁻¹ at 1468 nm (Hale & Querry, 1973). The water absorption coefficients are 14.2, 31.1, and 113.5 cm⁻¹ at 1860, 1880, and 1949 nm, respectively (Hale & Querry, 1973).

6.3.3 NIR Reflectance Image Acquisition and Analysis

These 10 samples were imaged with the point-to-point scanning system. Samples were air-dried for ~10 sec prior to image acquisition. Each image was scanned with a highly reflective reference and normalized for comparison. The dot pitch between each scanned point was ~50 μm . The reflectance intensity was acquired and averaged over five iterations at each point.

For each sample and wavelength, the entire 4 x 4 mm window was summed and averaged to quantify the lesion intensity (I_L). A fixed 2 x 2 mm sound enamel area was selected outside the 4 x 4 mm window at each wavelength to calculate each sample/wavelength's mean sound intensity (I_S). Image contrast was calculated using:

$$\text{Image Contrast} = (I_L - I_S) / I_L \text{ (eq. 6.1)}$$

The image contrast varies from 0 to 1 with 1 being very high contrast and 0 being no contrast or lack of signal. Repeated measures analysis of variance followed by the Tukey-Kramer *post hoc* multiple comparison test was used to compare the image contrast at the four wavelengths. All quantitative analysis was done with IgorPro from Wavemetrics (Portland, OR) and Prism from GraphPad (San Diego, CA).

6.4 RESULTS

Normalized point-to-point scanning reflectance images of two samples are shown in **Figure 6.3** for 1470, 1860, 1880, and 1950 nm. Demineralization appears whiter with higher intensity than sound enamel in these images. The higher reflectivity of the sound area outside the 4 x 4 mm windows is obviously higher for the shorter wavelength 1470 nm light even though the water absorption is as high as it is at 1860 nm. Sound enamel areas also appear darker at 1950 nm than at the other three wavelengths. The images

appear similar although there are some differences in the images. Those differences are likely due to wavelength differences in the extinction of the polarizers and slight differences in the optical systems between the three laser systems. The lower extinction ratio of the polarizers and slight differences in the optical systems between the three laser systems. The lower extinction ratio of the polarizers is most obvious at 1950 nm where more specular reflection is clearly evident. The mean contrast \pm standard deviation is plotted in **Figure 6.4** for the four wavelengths. The highest mean contrast was at 1950 nm, with 0.80 ± 0.07 , and it was significantly higher ($p < 0.05$) than the other wavelengths. The contrast was similar at 1860 and 1880 nm, 0.68 ± 0.10 and 0.67 ± 0.09 , respectively, and was significantly higher ($p < 0.05$) than at 1468 nm- 0.33 ± 0.13 .

6.5 DISCUSSION

A comparison of the lesion contrast for the four wavelengths suggests that the lesion contrast continues to increase beyond 1300 nm due to the decreasing scattering coefficient of enamel. There was no significant difference in the contrast between 1860 and 1880 nm even though the magnitude of water absorption at 1880 is more than twice as high as it is at 1860 nm. The contrast was much higher at 1880 compared to 1470 nm even though the magnitude of water absorption is similar. This observation was surprising to us, and we had suspected that water absorption contributed to a greater degree to the lesion contrast. However, this result does not contradict prior studies. In a previous study, we found that the lesion contrast was similar at 1450 and 1500 to 1750 nm (Chung et al., 2011). The highest contrast was achieved at 1950 nm where the water absorption is eight times higher than at 1860 nm; however, the contrast was only

slightly higher than at 1860 nm and that small increase in contrast can also be explained by the lower light scattering in the sound enamel.

There were some problems with the study, the most significant being the interference of specular reflection at 1950 nm and the use of three different laser systems. It is possible that specular reflectance may have influenced the contrast at 1950 nm; however, even without the 1950 nm data, it is obvious that light scattering in sound enamel continues to decrease with increasing wavelength beyond 1300 nm.

The most obvious implication of this study is the impact on the choice of wavelengths for caries detection and diagnosis. It appears that the use of longer wavelengths is advantageous for increasing the contrast of demineralization on tooth surfaces. In addition, these results suggest that it is not necessary to image at wavelengths coincident with the strong water absorption bands, such as 1450 or 1940 nm. The need for narrow-bandwidth sources poses additional challenges, including the difficulty of achieving sufficient intensity or throughput with low-cost broadband sources, such as tungsten-halogen lamps. In addition, the operation of optical coherence tomography (OCT) systems at wavelengths beyond 1300 nm has been proposed to achieve higher performance for imaging hard tissues (Bühler et al., 2005; R. Jones et al., 2003). This chapter provides the first evidence that light scattering in sound enamel significantly decreases beyond 1300 nm, which may be advantageous for achieving greater imaging depths for OCT.

6.6 FIGURES AND FIGURE LEGENDS

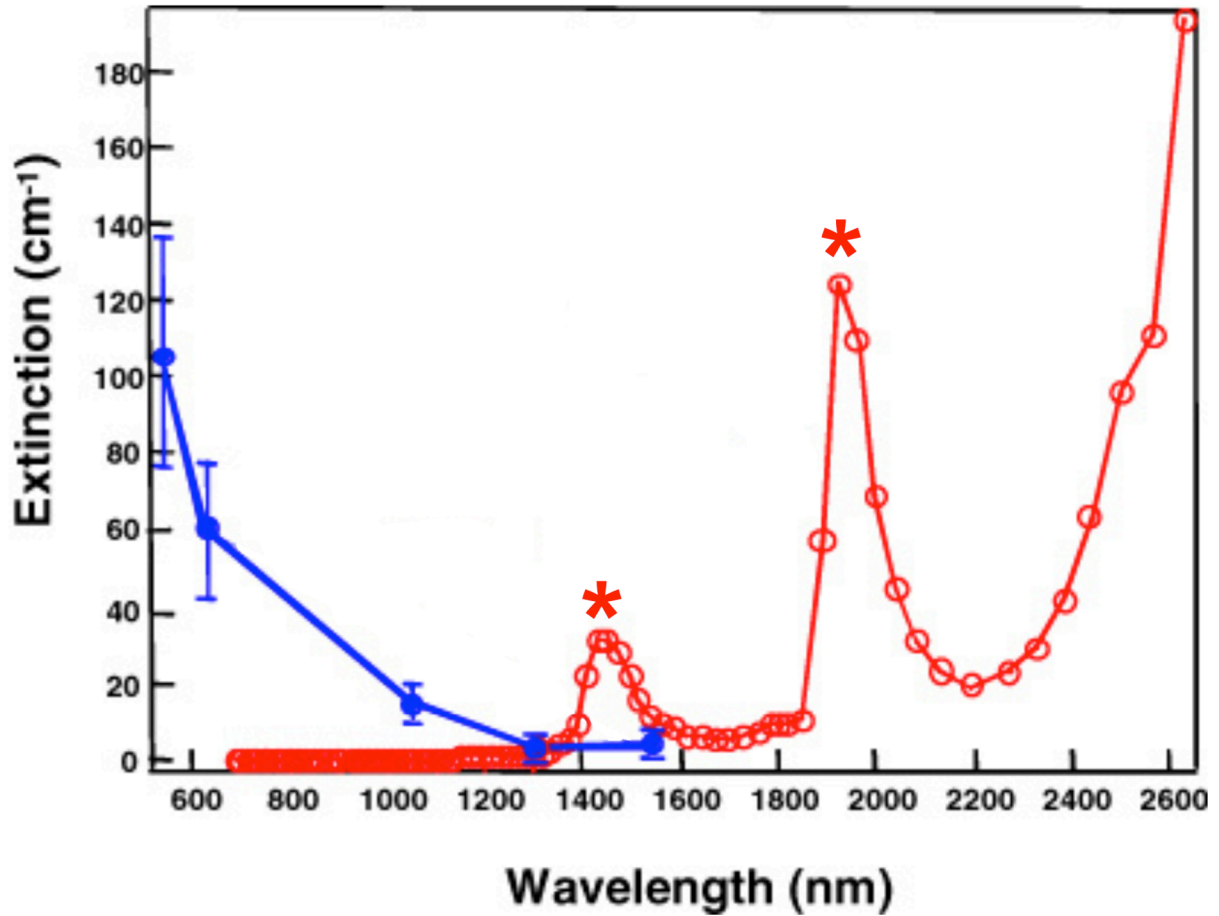


Figure 6.1: Enamel attenuation spectra (blue) and water absorption spectra (red). Notable water absorption peaks (*) are found at 1450 and 1940 nm (at 28.6 and 119 cm⁻¹, respectively). (D. Fried, Glens, Featherstone, & Seka, 1995; Hale & Query, 1973; Simon et al., 2016)

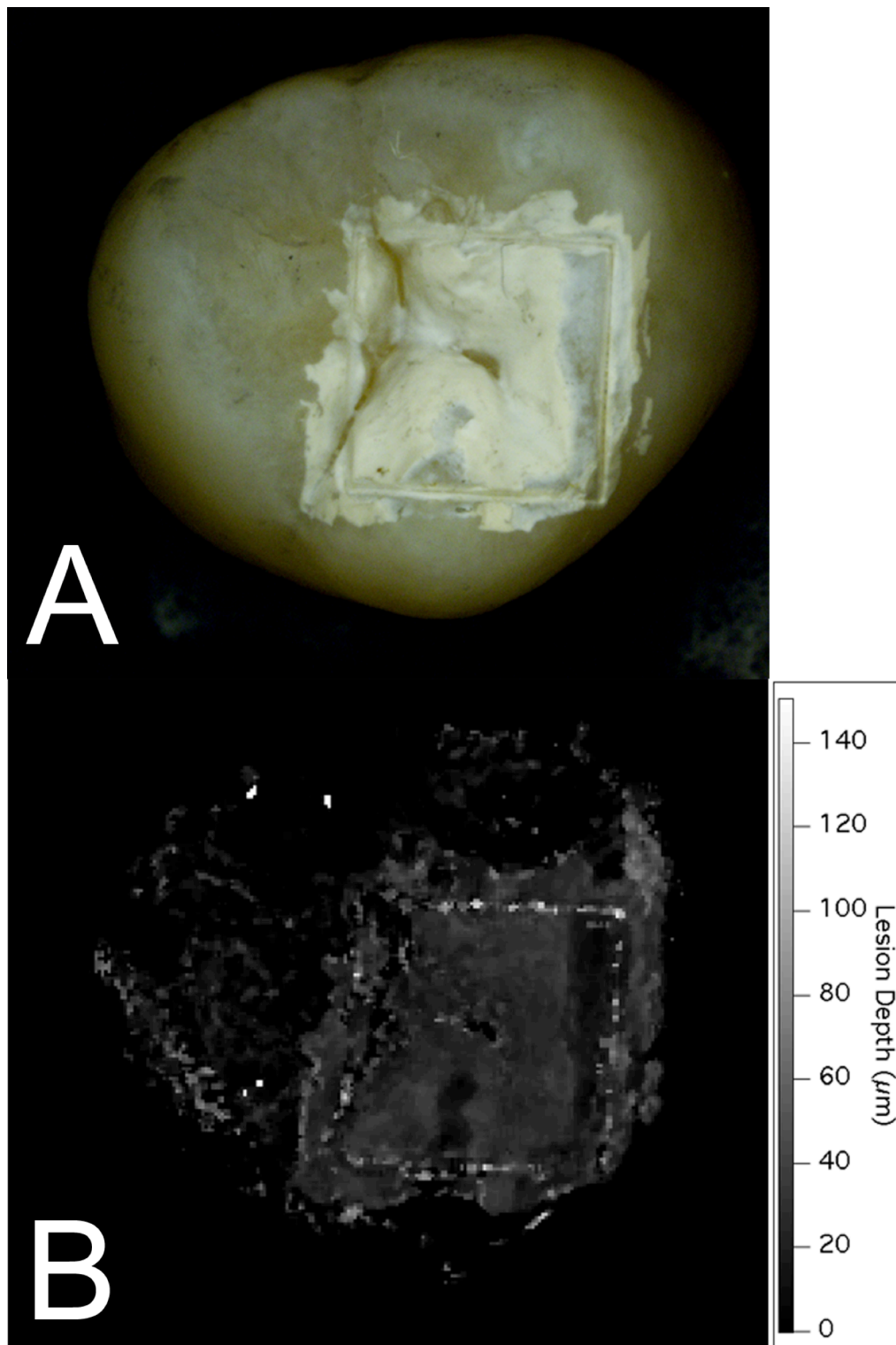


Figure 6.2: (A) Digital microscopy image of one of the tooth samples with demineralization and (B) lesion depth map generated from cross polarized – optical coherence tomography (CP-OCT) scans.

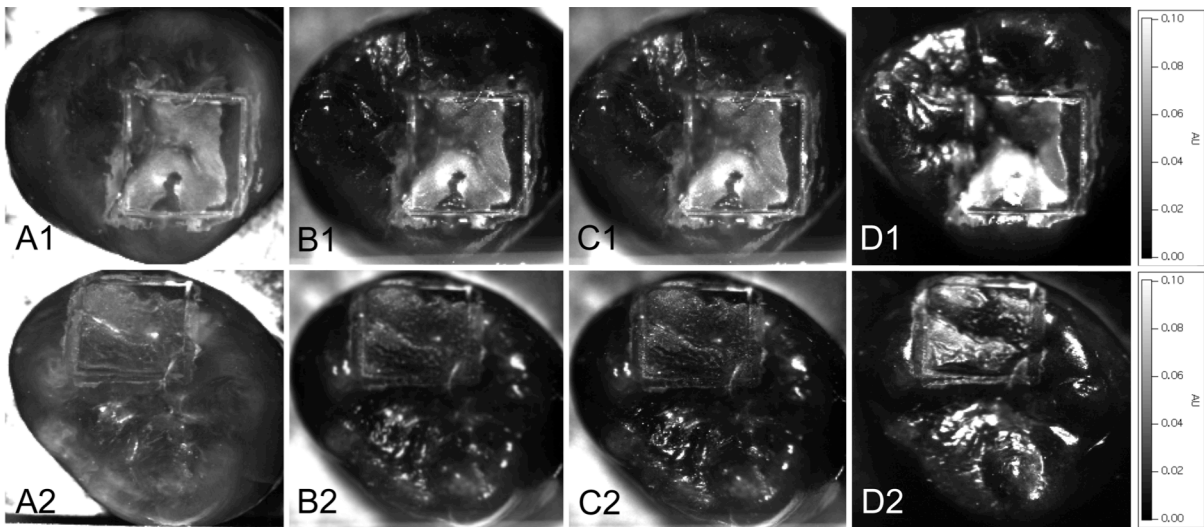


Figure 6.3: Near-infrared (NIR) reflectance images generated by the point-to-point scanner for two tooth samples at (A1 and A2) 1470 nm; (B1 and B2) 1860 nm; (C1 and C2) 1880 nm; and (D1 and D2) 1950 nm.

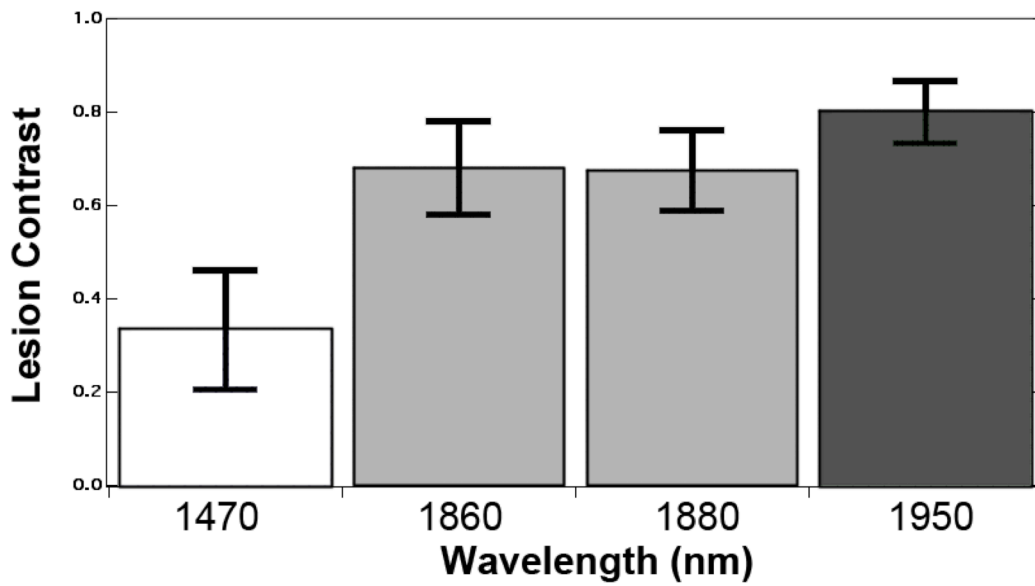


Figure 6.4: Mean lesion contrast \pm standard deviation ($n = 10$). Bars of the same color are statistically similar, $p > 0.05$.

6.7 REFERENCES

Alfano, R. R., Lam, W., Zarrabi, H. J., Alfano, M. A., Cordero, J., & Tata, D. B. (1984). Human teeth with and without caries studied by laser scattering, fluorescence and absorption spectroscopy. *IEEE J Quant Electr*, 20, 1512-1515.

Bühler, C. M., Ngaotheppitak, P., & Fried, D. (2005). Imaging of occlusal dental caries (decay) with near-IR light at 1310-nm. *Optics Express*, 13(2), 573-582.

Chan, K. H., Chan, A. C., Fried, W. A., Simon, J. C., Darling, C. L., & Fried, D. (2015). Use of 2D images of depth and integrated reflectivity to represent the severity of demineralization in cross-polarization optical coherence tomography. *Journal of biophotonics*, 8(1-2), 36-45

Chung, S., Fried, D., Staninec, M., & Darling, C. L. (2011). Multispectral near-IR reflectance and transillumination imaging of teeth. *Biomedical Optics Express*, 2(10), 2804-2814.

Darling, C. L., Huynh, G. D., & Fried, D. (2006). Light scattering properties of natural and artificially demineralized dental enamel at 1310 nm. *Journal of Biomedical Optics*, 11(3), 34023.

Fejerskov, O., & Kidd, E. (Eds.). (2003). *Dental Caries: The Disease and its Clinical Management*. Oxford: Blackwell.

Ferreira Zandona, A. G., Analoui, M., Beiswanger, B. B., Isaacs, R. L., Kafrawy, A. H., Eckert, G. J., & Stookey, G. K. (1998). An in vitro comparison between laser fluorescence and visual examination for detection of demineralization in occlusal pits and fissures. *Caries Res*, 32(3), 210-218.

Fried, D., Glens, R. E., Featherstone, J. D., & Seka, W. (1995). Nature of light scattering in dental enamel and dentin at visible and near-infrared wavelengths. *Applied optics*, 34(7), 1278-1285.

Fried, W. A., Darling, C. L., Chan, K., & Fried, D. (2013). High Contrast Reflectance Imaging of Simulated Lesions on Tooth Occlusal Surfaces at Near-IR Wavelengths. *Lasers Surg. Med*, 45, 533-541.

Hale, G. M., & Querry, M. R. (1973). Optical constants of water in the 200-nm to 200- μ m wavelength region. *Appl. Optics*, 12, 555-563.

Jones, R., Huynh, G., Jones, G., & Fried, D. (2003). Near-infrared transillumination at 1310-nm for the imaging of early dental decay. *Optics Express*, 11(18), 2259-2265.

Jones, R. S., Darling, C. L., Featherstone, J. D., & Fried, D. (2006). Imaging artificial caries on the occlusal surfaces with polarization-sensitive optical coherence tomography. *Caries research*, 40(2), 81-89.

Jones, R. S., & Fried, D. (2002). *Attenuation of 1310-nm and 1550-nm Laser Light through Sound Dental Enamel*. Paper presented at the Lasers in Dentistry VIII, San Jose.

Kang, H., Jiao, J. J., Lee, C., Le, M. H., Darling, C. L., & Fried, D. (2010). Nondestructive Assessment of Early Tooth Demineralization Using Cross-Polarization Optical Coherence Tomography. *IEEE journal of selected topics in quantum electronics : a publication of the IEEE Lasers and Electro-optics Society*, 16(4), 870-876.

Lee, R. C., Darling, C. L., Staninec, M., Ragadio, A., & Fried, D. (2017). Activity assessment of root caries lesions with thermal and near-IR imaging methods. *Journal of biophotonics*, 10(3), 433-445.

Lee, R. C., Staninec, M., Le, O., & Fried, D. (2016). Infrared Methods for Assessment of the Activity of Natural Enamel Caries Lesions. *IEEE journal of selected topics in quantum electronics : a publication of the IEEE Lasers and Electro-optics Society*, 22(3).

Ng, C., Simon, J. C., Fried, D., & Darling, C. L. (2018). SWIR reflectance imaging of demineralization on the occlusal surfaces of teeth beyond 1700-nm. *Proc. SPIE*, 10473(Lasers in Dentistry XXIV).

Simon, J. C., Lucas, S. A., Staninec, M., Tom, H., Chan, K. H., Darling, C. L., . . . Fried, D. (2016). Near-IR transillumination and reflectance imaging at 1,300 nm and 1,500-1,700 nm for in vivo caries detection. *Lasers Surg Med*, 48(9), 828-836.

Sordillo, L. A., Pu, Y., Pratavieira, S., Budansky, Y., & Alfano, R. R. (2014). Deep optical imaging of tissue using the second and third near-infrared spectral windows. *J Biomed Opt*, 19(5), 056004.

Staninec, M., Lee, C., Darling, C. L., & Fried, D. (2010). In vivo near-IR imaging of approximal dental decay at 1,310 nm. *Lasers in Surgery and Medicine*, 42(4), 292-298.

Stookey, G. K. (2005). Quantitative light fluorescence: a technology for early monitoring of the caries process. *Dent Clin North Am*, 49(4), 753-770, vi.

Tranaeus, S., Shi, X. Q., Lindgren, L. E., Trollsas, K., & Angmar-Mansson, B. (2002). In vivo repeatability and reproducibility of the quantitative light-induced fluorescence method. *Caries Res*, 36(1), 3-9.

Weber, J. R., Baribeau, F., Grenier, P., Emond, F., Dubois, S., Duchesne, F., . . . Moghadam, H. G. (2013). Towards a bimodal proximity sensor for in situ neurovascular bundle detection during dental implant surgery. *Biomed Opt Express*, 5(1), 16-30.

Wu, J., & Fried, D. (2009). High contrast near-infrared polarized reflectance images of demineralization on tooth buccal and occlusal surfaces at $\lambda = 1310\text{-nm}$. *Lasers in Surgery and Medicine*, 41(3), 208-213.

Zakian, C., Pretty, I., & Ellwood, R. (2009). Near-infrared hyperspectral imaging of teeth for dental caries detection. *Journal of Biomedical Optics*, 14(6), 064047-064047.

Zandona, A. F., & Epure, E. (2018). Evolution of caries diagnosis. *Decisions Dent*, 4(2), 43-46.

CHAPTER VII
**SELECTIVE ABLATION OF DENTAL CARIES USING COAXIAL CO₂ AND NEAR-
INFRARED LASERS**

7.1 SUMMARY

The purpose of this study was to determine the feasibility of image-guided laser ablation of demineralization from tooth occlusal surfaces using coaxial near-infrared (NIR) and CO₂ lasers. A CO₂ laser operating at a wavelength of 9.3 μm was combined with a thulium-doped fiber laser operating at 1880 nm for the selective removal of simulated occlusal caries lesions from ten tooth samples. Serial NIR reflectance images at 1880 nm were used to guide the CO₂ laser for image-guided laser ablation. Polarization-sensitive optical coherence tomography (PS-OCT) was used to assess the initial depth of the lesions before removal and assess the volume of sound and demineralized tissue removed by the CO₂ laser. PS-OCT scans indicated that roughly ~99% of the lesion was removed using image-guided laser ablation. A mean volume of 0.191 mm³ or 11.9 μm/voxel of excess enamel was removed during lesion removal. A co-aligned NIR/CO₂ laser scanning system has great potential for the highly selective removal of dental decay (demineralization).

7.2 INTRODUCTION

Despite the many advances in dentistry, dental decay remains the most common chronic disease in children (B. A. Dye et al., 2007). Greater emphasis is being placed on minimally invasive procedures to preserve healthy tooth structure (Vila Verde, Ramos, & Stoneham, 2009). A highly selective tool that removes unwanted decay, yet leaves sound enamel intact will markedly reduce the amount of healthy tissue loss that is generally associated with conventional cavity preparations. Overaggressive cavity preparations could lead to pulpitis and consequently require more invasive and expensive treatments, particularly tooth extraction or root canal treatment. Additionally,

incomplete removal of demineralized carious tissue or cariogenic bacteria in the fissure can harbor an active biofilm and lead towards risk of secondary caries (Fejerskov & Kidd, 2003; Hevinga et al., 2007; Kidd, 2004).

Lasers can be focused to very small spot sizes and are ideally suited for the removal of debris and demineralization and sterilization of the pits and fissures of the occlusal surface prior to the placement of sealants (Powell & Whisenant, 1991). CO₂ laser wavelengths at $\lambda = 9.3 - 9.6 \mu\text{m}$ coincide with the strongest molecular absorption bands in dental hard tissues due to the phosphate ion in hydroxyapatite (Duplain et al., 1987; MJ Zuerlein et al., 1999). Moreover, CO₂ lasers can render the irradiated surface more acid-resistant to prevent future decay (J. D. Featherstone et al., 1998; J. D. B. Featherstone & Nelson, 1987; Fowler & Kuroda, 1986; D. Fried, Featherstone, Le, & Fan, 2006b; Hsu, Darling, Lachica, & Fried, 2008; Kuroda & Fowler, 1984; D. G. A. Nelson, Jongebloed, & Featherstone, 1986). Lasers can be operated at high pulse repetition rates and precisely scanned at high speeds using galvanometer based scanners or micro-electromechanical systems (MEMS) (Nguyen et al., 2011).

Several imaging approaches have been investigated for guiding the removal of dental decay. Fluorescence has been proposed as a means of guiding caries removal by both laser and mechanical means (Almaz, Simon, Fried, & Darling, 2016; Eberhard, Bode, Hedderich, & Jepsen, 2008; Eberhard et al., 2005; W. A. Fried et al., 2013; Jepsen, Acil, Peschel, Kargas, & Eberhard, 2008). Increased levels of porphyrins accumulate in dentinal caries lesions due to the high porosity and that fluorescence has been employed for caries detection; the Diagnodent device uses such fluorescence. However, the fluorescence is not specifically associated with cariogenic bacteria since

they do not contain porphyrins nor is it correlated with the degree of demineralization. Moreover, the fluorescence is weak and diffuse and poorly suited for precise guidance of the laser. In addition, stains can lead to false-positive readings, which is a major problem for fluorescence imaging. However, the highly-conjugated organic molecules associated with staining do not absorb near-infrared (NIR) light beyond 1200 nm.

Previous studies have established that imaging dental decay using NIR wavelengths coincident with higher water absorption and longer wavelengths yield markedly higher contrast between carious and sound tissue (Almaz et al., 2016; Daniel Fried et al., 2005; Simon et al., 2014). Demineralized tooth surfaces are highly porous producing markedly higher light scattering compared to sound tooth surfaces. NIR light is ideally suited for image-guided laser ablation since the contrast between sound and demineralized enamel is highest at wavelengths beyond 1400 nm and there is no interference from stain (Almaz et al., 2016). Therefore, using NIR images of teeth to guide the CO₂ laser over areas of demineralization is an ideal approach for selective caries removal. In the previous chapter, it was indicated that even higher contrast of demineralization is obtainable beyond 1700 nm due to the further reduction in the light scattering in sound enamel (Chan & Fried, in press). In this chapter, NIR light at 1880 nm, which yields significantly higher contrast of demineralization than 1450 nm and was previously employed for past image-guided ablation studies, was used to guide a CO₂ laser for selective caries removal (Tom, Chan, Darling, & Fried, 2016).

Previous studies established that NIR reflectance images can be used to guide a CO₂ laser for the selective removal of caries lesions on smooth and occlusal surfaces (Tao & Fried, 2009; Tom et al., 2016). This was accomplished by re-iterating a four-phase

process until complete caries removal: taking NIR reflectance image with an InGaAs camera, segmenting demineralization, generating ablation maps or look-up tables (LUTs) of the caries lesion, and scanning the CO₂ laser over demineralized areas for removal. However, this approach had significant limitations, the setup was not integrated and it was challenging to precisely align the path of the CO₂ laser with the NIR reflectance images; furthermore, lesion segmentation was performed by manually adjusting a global threshold, which is not ideal. In this chapter, coaxial CO₂ and NIR lasers were used to acquire images of demineralization of the tooth surface and selectively remove this demineralization. In addition to greatly reducing the cost of the system since an InGaAs camera is no longer needed, the system eliminates alignment errors since the tooth does not need to be removed from the system for serial NIR imaging. Moreover, longer wavelengths ($\lambda > 1700$ nm) can be used beyond the sensitivity of conventional InGaAs cameras where higher contrast is attainable such as 1880 nm.

New lesion detection/segmentation tools were also investigated and developed to accurately identify areas of demineralization on tooth surfaces for subsequent laser ablation. In order to assess the accuracy and selectivity of lesion removal, *a priori* knowledge of the lesion volume is required for removal. Previous studies performed selective removal analysis using histological samples to verify lesion absence, however new methods for monitoring and evaluating dental caries excavation are readily available. Polarization-sensitive optical coherence tomography (PS-OCT) is capable of measuring the initial depth and volume of lesions before removal and assessing the volume of sound and demineralized tissue removed (Chan et al., 2015; Jang, Chan, &

Fried, 2017; R. C. Lee, Kang, Darling, & Fried, 2014). By nondestructively scanning the tooth before and after lesion removal, PS-OCT was used to demonstrate that a coaxial NIR/CO₂ image-guided laser ablation system is capable of selectively removing early occlusal surface demineralization with high selectivity.

7.3 MATERIALS AND METHODS

7.3.1 Sample Preparation

Ten human teeth with non-carious occlusal surfaces were collected and sterilized with gamma radiation. Tooth occlusal surfaces were abraded using air abrasion with 50 µm glass beads for 20 sec to remove all stain and debris from the fissures and remove the outermost fluoride rich layers of enamel to facilitate the demineralization of those surfaces. Next, teeth were mounted in black orthodontic acrylic blocks. Samples were stored in a moist environment of 0.1% thymol to maintain tissue hydration and prevent bacterial growth. The outlines of a 4 x 4 mm window (roughly 50 µm deep) were cut on the occlusal surfaces of each tooth using a CO₂ laser (GSI Lumonics, Impact 2500), operating at a wavelength of 9.3 µm, pulse width of 15 µs, and repetition rate of 5 Hz. These markings served as a reference point to denote the demineralized area. The enamel surrounding the 4 x 4 mm windows was covered with acid resistant varnish. Subsurface artificial lesions with intact surfaces were created within the 4 x 4 mm windows by immersing each tooth into a 50 ml aliquot of a Ca/PO₄/acetate solution containing 2.0 mmol/L calcium, 2.0 mmol/L phosphate, and 0.075 mol/L acetate maintained at a pH of 4.5 and incubated for 48 hours at 37°C (**Figure 7.1A**) (J. D. B. Featherstone et al., 1990). Non-destructive cross-polarized optical coherence

tomography (CP-OCT) was used to verify lesion presence and measure the depth of demineralization (lesion depth) that varied between 50-150 μm deep (**Figure 7.1B**).

7.3.2 Coaxial NIR/CO₂ Laser System

A diagram of the experimental setup is shown (**Figure 7.2**). An air-cooled radiofrequency excited laser prototype, Model DL-500 from Access Laser Co. (Everett, WA) operating at a wavelength of 9.3 μm was used with a pulse duration of 25 μs and a pulse repetition rate of \sim 50 Hz (max rate 500 Hz). The laser energy output was monitored using a power meter, EPM 1000, Coherent-Molelectron (Santa Clara, CA), and Joulemeter ED-200 from Gentec (Quebec, Canada). The laser beam was focused to a beam diameter of 250 μm using a $f = 100$ mm ZnSe scanning lens from II-VI Inc. (Saxonburg, PA). A razor blade was scanned across the beam to determine the diameter ($1/e^2$) of the laser beam. The incident fluence was 31 J/cm^2 , which removes \sim 30 μm of sound enamel per pulse. Computer-controlled XY galvanometers 6200HM series with MicroMax Series 671 from Cambridge Technology, Inc. (Cambridge, MA) were used to scan the CO₂ laser beam over the sample surfaces. An air-actuated fluid spray delivery system consisting of a 780S spray valve, a Valvemate 7040 controller, and a fluid reservoir from EFD, Inc. (East Providence, RI) was used to provide a uniform spray of fine water mist onto the tooth surfaces at \sim 2 mL/min.

In order to acquire reflectance images, 1880 nm NIR light from a thulium-doped fiber laser, Model TLT-5, from IPG Photonics (Oxford, MA) was focused onto the occlusal surface of the sample using the same ZnSe $f = 100$ mm scanning lens. Crossed polarizers were placed after the light source and before the detector to remove specular reflection (glare) that interferes with measurements of the lesion contrast. We had

intended to acquire the NIR images using the same XY galvanometers used to scan the CO₂ laser, however we required images of the entire tooth and the imaging area was limited by the fixed field of view of the detector. Therefore, tooth samples were scanned using mechanical stages for NIR image acquisition. Computer-controlled high-speed stage actuators, UTM150 and 850G, from Newport (Irvine, CA) were used to scan tooth surfaces across the NIR fiber laser beam with a 50 µm pixel pitch. At each scanned point, backscattered NIR light was collected and averaged over 5 times using an extended range InGaAs photodetector, PDA10DT from ThorLabs (Newton, NJ), and reconstructed into a 2D 8-bit grayscale reflectance image. Prior to imaging, tooth surfaces were air-dried for ~10-20 sec.

7.3.3 Lesion Segmentation and Removal

The flowchart (**Figure 7.3**) outlines the steps used for the selective removal of demineralization from tooth surfaces. NIR reflectance images were taken by scanning the tooth across the NIR laser beam and acquiring backscattered signal with the extended-range InGaAs photodetector. This data was rasterized into a NIR image. The lesion segmentation algorithm detects and creates a look-up table (LUT) that maps our lesion areas. LUTs were used to direct the CO₂ laser using galvanometer mirror scanners over demineralized areas. The distance between laser pulses was 50 µm, roughly 1/5 of the 250 µm laser spot diameter. Repeated NIR reflectance images and LUTs were taken and these steps were repeated until the lesion was no longer discriminated by the detection algorithm. All image analysis was carried out using Labview from National Instruments (Austin, TX).

Speckle noise is an inherent concern with narrow band laser imaging. An opening operator (3 x 3 px square structuring element) filters out speckle noise by clearing lone pixels while preserving the foreground image and its shape. A lesion segmentation program developed using Labview was used to evaluate the intensity of each pixel, which represents the acquired backscattered signal. Highly scattering demineralized surfaces confer higher signal or appear brighter in NIR reflectance images, while sound tissues appear dark. Pixel intensities were clustered automatically through an adaptive thresholding method based on Otsu's method (6 cluster groups) (Otsu, 1979). This classifies groups of pixels as either sound or demineralization by deriving the optimal pixel intensity threshold of each cluster for the least possible variance.

As the lesion is removed, differentiating the decreasing amount of lesion pixels from an increasing amount of sound tissue pixels becomes challenging. The bimodality between lesion and sound pixels of the image is lost as the lesion and its pixels are removed. This causes ambiguity in defining thresholds for classifying lesion and sound tissue groups. A lesion control or phantom of demineralized tissue pixel intensity is necessary; therefore the initial NIR reflectance image containing the simulated demineralization is appended with the newly acquired scanned image to serve as a reference. In order to append these images together, a scattering reference target was scanned along with the sample to represent the maximum signal from scattering so that sequential NIR reflectance images could be normalized and compared with each other. Healthy sound enamel structure outside the artificially generated lesion was imaged to provide a positive control of sound tissue pixel intensity. A LUT was created that demarcated lesion areas for removal by the CO₂ laser.

7.3.4 Polarization Sensitive – Optical Coherence Tomography (PS-OCT)

The initial lesion depth, the volume of tissue removed by the laser and the residual demineralization after removal were all assessed using polarization sensitive – optical coherence tomography (PS-OCT). An all-fiber-based optical coherence domain reflectometry (OCDR) system (time domain) with polarization maintaining (PM) optical fiber, high-speed piezoelectric fiber-stretchers and two balanced InGaAs receivers that was designed and fabricated by Optiphase, Inc., Van Nuys, CA was used. This two-channel system was integrated with a broadband superluminescent diode (SLD) from Denselight (Jessup, MD) and a high-speed XY-scanning system containing a ESP 300 controller and 850G-HS stages from Newport (Irvine, CA) for *in vitro* PS-OCT imaging. This system is based on a polarization sensitive Michelson white light interferometer. The high power (15 mW) polarized SLD source operated at a center wavelength of 1317 nm with a spectral bandwidth full-width at half-maximum (FWHM) of 84 nm. The sample arm was coupled to a fiber-collimator to produce a 6 mm diameter, collimated beam. This beam was focused onto the sample surface using an $f = 20$ mm lens to yield a lateral resolution of approximately ~ 20 μm and an axial resolution of 10 μm in air with a signal to noise ratio greater than 40 – 50 dB. The PS-OCT system is completely controlled using Labview software. The system is described in greater detail in the following references (Bush, Davis, & Marcus, 2000; D. Fried et al., 2002). Acquired scans are compiled into *b-scan* image files (Brezinski, 2006). PS-OCT images consist of two orthogonal images, a co-polarization image with the same polarization as the incident light and a cross-polarization image with the orthogonal polarization.

7.3.5 Processing of PS-OCT Images and Analysis of Selectivity

Both the co-polarization and cross-polarization (CP) images were utilized in this study. The co-polarization image was used to assess the volume of tissue ablated. The CP-OCT image was used to assess the initial lesion depth and severity. Strong specular reflection from the tooth surface greatly interferes with the measurement of demineralization near the tooth surface. Use of the CP-OCT image reduces that interference and also increases the contrast between sound and demineralized enamel for more accurate assessment of lesion depth and severity (Chan et al., 2015; D. Fried et al., 2002).

PS-OCT *a-scans* were averaged over 5 times to reduce speckle noise. Data obtained from the PS-OCT scans were further processed using Matlab software from Mathworks (Natick, MA). A global threshold filter was applied using the mean and 4 times the standard deviation of the background, which was calculated from the top 200 pixels of the *a-scans*. A 3D anisotropic Gaussian filter based on Law et al. was used to further remove speckle noise (Law & Chung, 2009). Lee and Rhoades demonstrated that applying a 2D rotating kernel transformation (RKT) to OCT *b-scans* improved differentiation of the cartilage-bone border by suppressing noisy signals while simultaneously keeping the details of critical components (Y. K. Lee & Rhodes, 1990; Rogowska, Bryant, & Brezinski, 2003). Studies have shown that the 2D RKT filter can be applied for dental applications, namely detecting dental caries and remineralized surface zones using PS-OCT (R. C. Lee et al., 2014). However, occlusal lesions have irregular shapes and applying a 2D RKT filter on individual *b-scans* is not appropriate. When a 2D RKT filter is applied to the edge of a lesion, these lesion edge signals are

unintentionally filtered out thus underestimating the size of the lesion body. Therefore, we created a 3D rotating kernel transformation (5 x 5 x 5 px kernel) to fully utilize the 3D dataset and help signals of the lesion and occlusal surface stand out.

PS-OCT segmentation was used to extract surface and lesion volume information. Co-polarization OCT images contain the strong reflections from the tooth surface. Conversely, CP-OCT filters out specular reflection from the surface and picks up the subsurface scattering signals emanating from the lesions. A full-width half-maximum (FWHM) growing region edge detector starting at the top of every *a-scan* was used to identify the occlusal surface in CP-OCT images. Lesion detection was based on previous work by Lee et al. (R. C. Lee et al., 2014). For lesion detection, an edge locator was used on each *a-scan* in the CP-OCT images and two passes were employed to detect the two edges of the lesion: the top and base. Each pass starts from the position of the maximum peak intensity and locates the first pixel, for which the intensity value is less than $1/e^2$ multiplied by the maximum peak intensity. Lesion depth was estimated by measuring the distance between the two edges. 3D volumetric datasets were created based on the lesion and surface segmentation.

Determining the amount of tissue ablated is key for assessing the selectivity of the integrated caries ablation system. A 3D iterative closest point algorithm was used to register the occlusal surface data before and after laser treatment (**Figure 7.4**). Alignment pre- and post-ablation surface points within the 4 x 4 mm window can cause alignment problems since ablation occurred inside the windows, therefore these data points were cropped out during 3D registration. The 3D registration transformation

matrix was applied to the moving data set (post-ablation) and a linear interpolation algorithm was applied to fill in the gaps.

Volumetric PS-OCT data can be translated into *en face* 2D projection images representing the depth and severity of demineralization (Chan et al., 2015; Simon et al., 2014). This approach was used for visualizing ablation depths and lesion depths (**Figures 7.6A, B, & D**). The intensity in these 2D maps represent the depth of tissue removed and the remaining depth of demineralization with respect to its location on the occlusal surface.

Ablation volume was calculated by summation of the height differences between pre-ablation and registered post-ablation surfaces. Lesion segmentation was applied to pre- and post-ablation CP-OCT data to compute the lesion volume before and after automated removal. Comparisons made between the initial lesion and the post-ablative lesion volume and the volume of tissue ablated were used to calculate the amount of sound tissue removed and the lesion volume remaining.

7.3.6 Digital Microscopy

Tooth surfaces were examined after laser irradiation using an optical microscopy/3D surface profilometry system, the VHX-1000 from Keyence (Elmwood, NJ). The VH-Z25 lens with a magnification from 25-150x was used. Depth composition digital microscopy images (DCDM) were acquired by capturing serial images of varying depth and reconstructing a depth composition image with all points at optimum focus displayed in a 2D image. Images of the samples were acquired before and after ablation at 25x and 50x magnification.

7.4 RESULTS

Demineralized enamel was selectively removed from the 4 x 4 mm windows on the ten teeth according to the process described in the flowchart (**Figure 7.3**). Sequential point-to-point NIR reflectance images were taken during the ablation process using the NIR fiber laser and the InGaAs detector (**Figures 7.5A-D**). Demineralization appears whiter due to increased scattering and the sound tissue structure appears dark. The mean lesion to sound contrast ratio for the ten sample windows was calculated to be 0.67 ± 0.09 . Contrast varies from 0 to 1 with a maximum contrast of 1. Therefore a mean contrast of ~ 0.7 can be considered extremely high. Lesion detection was performed within the 4 x 4 mm windows using an adaptive thresholding method (outlined in [Section 7.3.3](#)). Afterwards, a look-up-table (LUT) was created and demarcated lesion areas for laser treatment (**Figures 7.5E-H**). Using the LUTs, the CO₂ laser was scanned over the identified lesion area for removal. As the lesion was removed, areas of high reflectivity within the 4 x 4 mm window diminished until the lesion was no longer detected (**Figure 7.5**).

PS-OCT scans taken before and after selective laser ablation were used to assess caries removal. A 2D ablation depth map (**Figure 7.6A**) was created by the registration and subtraction of the initial and final surfaces from the co-polarization OCT scans. Brighter pixels in these depth maps represent deeper ablation depths. For comparison, the initial 2D lesion depth map (**Figure 7.6B**), suggesting that the lesion detection algorithm used for the point-to-point NIR reflectance image matches well with the CP-OCT 2D projection image of the initial lesion depth. CP-OCT images were taken again after treatment with the integrated laser scanning system and previously established CP-OCT lesion detection algorithms indicate that the lesion was removed (**Figure**

7.6D). Visible depth composition digital microscopy (DCDM) images were taken before (**Figure 7.6C**) and after (**Figure 7.6E**) laser treatment also indicate complete removal. The white demineralization is apparent on the visible occlusal surface (**Figure 7.6C**) and it extended a bit beyond the initial laser incisions marking the 4 x 4 mm windows (**Figure 7.6C**, red-dashed box). The demineralization within the window is absent in the final image after removal (**Figure 7.6E**).

The sum of the pixels within the 4 x 4 mm windows on the 2D depth maps was calculated to determine the total volume ablated, initial lesion volume, and final lesion volume. The average volume ablated is 0.602 mm^3 , whereas the average initial lesion volume was 0.411 mm^3 . Thus, 0.191 mm^3 of excess sound tissue was removed, which equates to roughly to a mean $11.9 \text{ }\mu\text{m/voxel}$ of excess enamel removed over the entire 4 x 4 mm window. CP-OCT images taken after laser removal indicate that the average remaining volume of demineralization is $2.02 \times 10^{-5} \text{ mm}^3$, roughly 99% of the initial lesion was removed using the coaxial NIR/CO₂ laser ablation system.

7.5 DISCUSSION

The ultimate objective is to develop an image-guided laser system that can be used for the selective removal of dental caries. The developed system removed over 99% of the demineralization with a mean loss of a layer of only $11.9 \text{ }\mu\text{m}$ of sound tissue. This degree of depth selectivity likely exceeds what would be achievable with the hand-held dental drill.

The point-to-point NIR imaging system is a less expensive alternative than current extended InGaAs cameras and allows integration with a CO₂ laser for image-guided

caries removal. Furthermore, the point-to-point NIR laser scanning system yielded images comparable to ones previously taken with an InGaAs camera.

Previous lesion detection algorithms relied on the user setting a global threshold to identify lesions (Tom et al., 2016). This was not ideal as it subjects the selective caries removal to user judgment and bias. An adaptive thresholding method (Otsu's method) and developed controllable variables were used for accurately detecting occlusal lesions in a non-biased manner. This method is desirable for automating a selective caries ablation system for future studies, since it does not require user input in between every NIR reflectance image. Although, the selective caries ablation system performed well in removing occlusal demineralization, factors including noise, object size, mean differences, contrast and variances between the object and background can affect this segmentation technique (S. U. Lee, Yoon Chung, & Park, 1990). More avenues of lesion detection, including machine learning, are to be explored in the future.

In previous selective ablation experiments, the CO₂ laser caused surface roughening which caused higher reflectivity in irradiated areas and ultimately led to unnecessary tissue removal (Tom et al., 2016). However, the CO₂ laser did not cause any significant surface roughening that interfered with the NIR reflectance images ([Section 7.3.3](#)) as indicated in the final visible images (**Figure 7.6E**). This is consistent with previous CO₂ laser studies indicating that there were no significant changes in the contrast of sound enamel at NIR wavelengths after laser irradiation and suggests that the previous surface roughening was likely caused by alignment issues between the CO₂ laser and the NIR reflectance camera (LaMantia et al., 2014).

An XY stage to scan the tooth to acquire the NIR images. This was required to scan the entire occlusal surface in addition to a scattering reference (maximum 14 x 14 mm imaging window). Further integration will be needed for a practical clinical system. A single scanning system will be required for both lasers that can encompass the entire area of the tooth that is fast enough for rapid acquisition of NIR images. Large area micro-electromechanical systems (MEMS) mirrors are available that can handle the relatively low single pulse energies (< 20 mJ pulses) utilized in this study. The use of multiple fiberoptic cables is a compact method for collecting and delivering backscattered light to the photodetector and this approach can sample a larger scanning area and acquire signals that may be obstructed by the convoluted occlusal topography. The Access CO₂ laser used is unique in that it is compact and does not require water-cooling which is advantageous for use in the dental clinic. The IPG Photonics NIR fiber laser used for this study will need to be replaced with a more compact diode laser or LED source. The next step is to produce a fully integrated CO₂/NIR image-guided laser ablation system that is compact enough to be fitted into a dental handpiece. A fully integrated CO₂ spectral-guided laser system (**Chapter III**) for the selective removal of composite restorations from tooth surfaces and that system is currently being used in a clinical study (Jang et al., 2017).

A secondary goal of this study was to demonstrate that PS-OCT could be used to assess the lesion volume and measure the volume of tissue ablated. A previously established PS-OCT lesion detection program for nondestructively quantifying lesion volume and severity was used to verify and compare to a new method of analyzing tissue removed (R. C. Lee et al., 2014). There were some challenges to overcome in

measurement of tissue removal volume. Most noticeably, in the 3D OCT registration of the initial and final surfaces, the surrounding edges of the occlusal surface did not align well and produced artifacts within the 2D ablation depth map (**Figure 7.6A**). This can be attributed to slightly different angles during PS-OCT imaging and/or the detection of surface edges prior to 3D registration. However, multiple registrations of different PS-OCT scans of the same tooth demonstrated that this method can be reliably used to quantify tissue volume loss. This same approach can be used to evaluate conventional mechanical dental cavity preparations.

In future studies, micro-computed tomography (μ CT) can be used to further evaluate the lesion and tissue removal volume. The primary advantage of using μ CT is that lesions of any size can be imaged prior to removal, in contrast to OCT that has limited penetration in the tooth. However, in contrast to OCT, μ CT cannot be used *in vivo* to assess the volume of tissue removed.

In conclusion, we found that this integrated selective caries ablation system is highly selective in removing demineralization. The correlation between the tissue removed and initial lesion volume demonstrates the high selectivity of this system.

7.6 FIGURES AND FIGURE LEGENDS

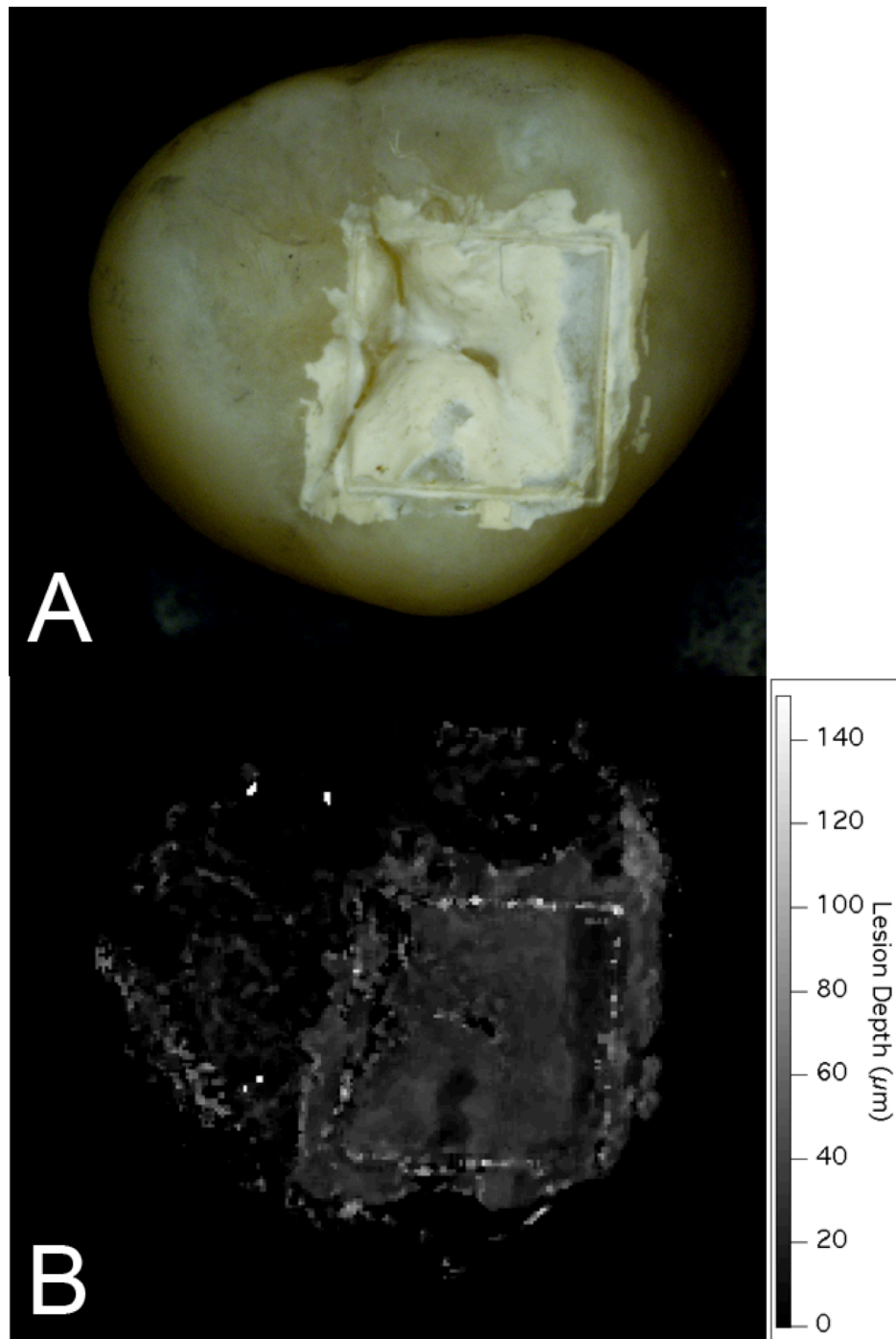


Figure 7.1: (A) Depth composition digital microscopy image of one of the 4 x 4 mm windows with demineralization taken at 25x magnification. (B) 2D projection image of the lesion depth of the same sample generated from cross polarization – optical coherence tomography (CP-OCT) scans.

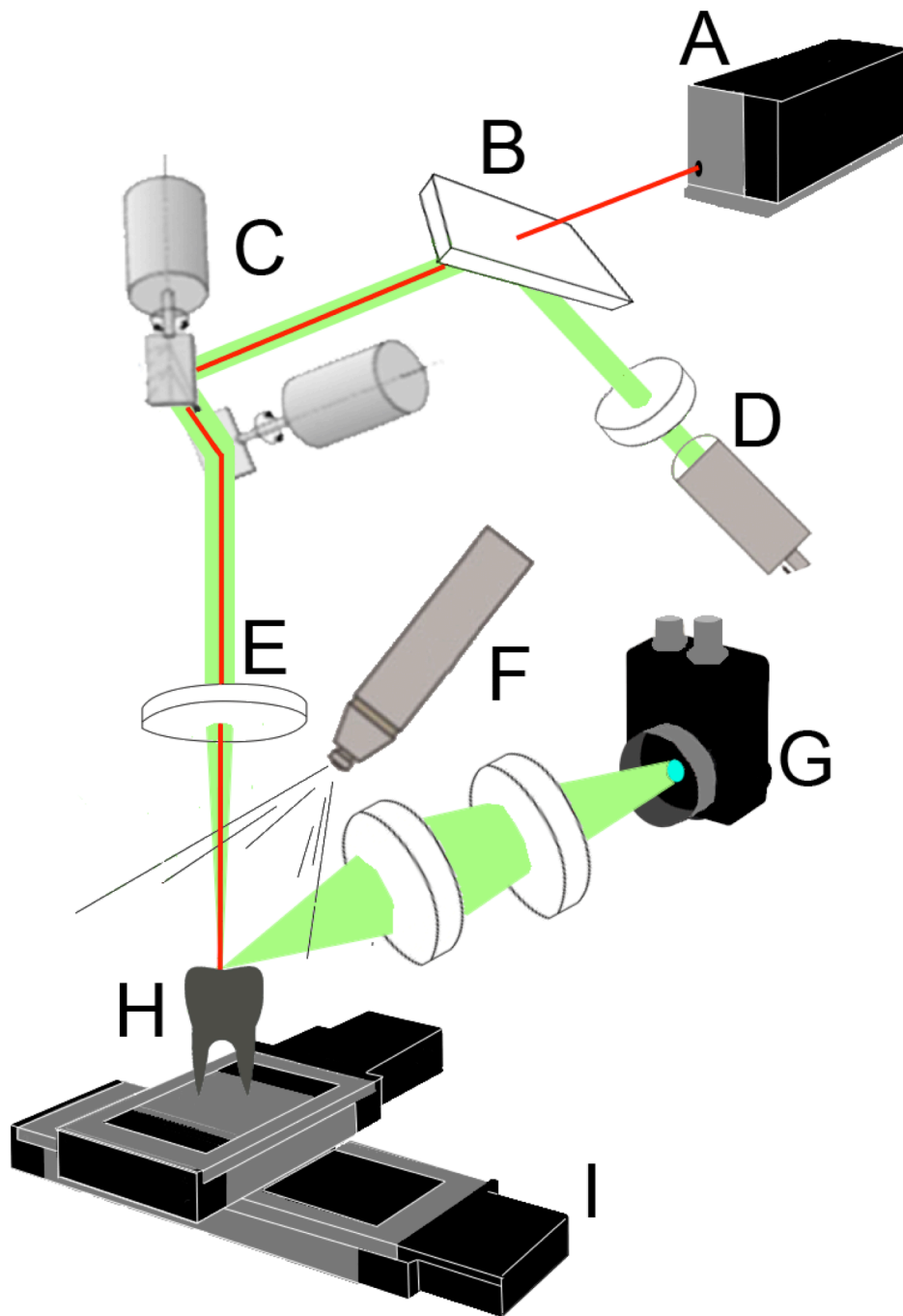


Figure 7.2: Diagram of the NIR/CO₂ laser scanning system with (A) CO₂ laser; (B) beamsplitter; (C) XY galvanometer scanner; (D) NIR fiber laser with polarizer; (E) ZnSe scanning lens; (F) water-spray nozzle; (G) InGaAs detector; (H) tooth sample; and (I) XY stages.

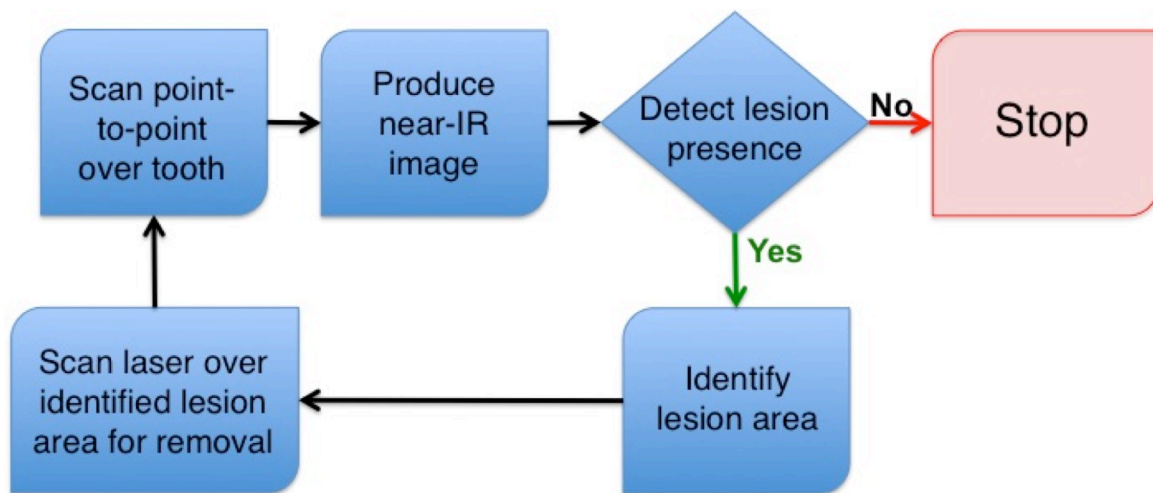


Figure 7.3: Flow-chart outlining selective caries ablation procedure.

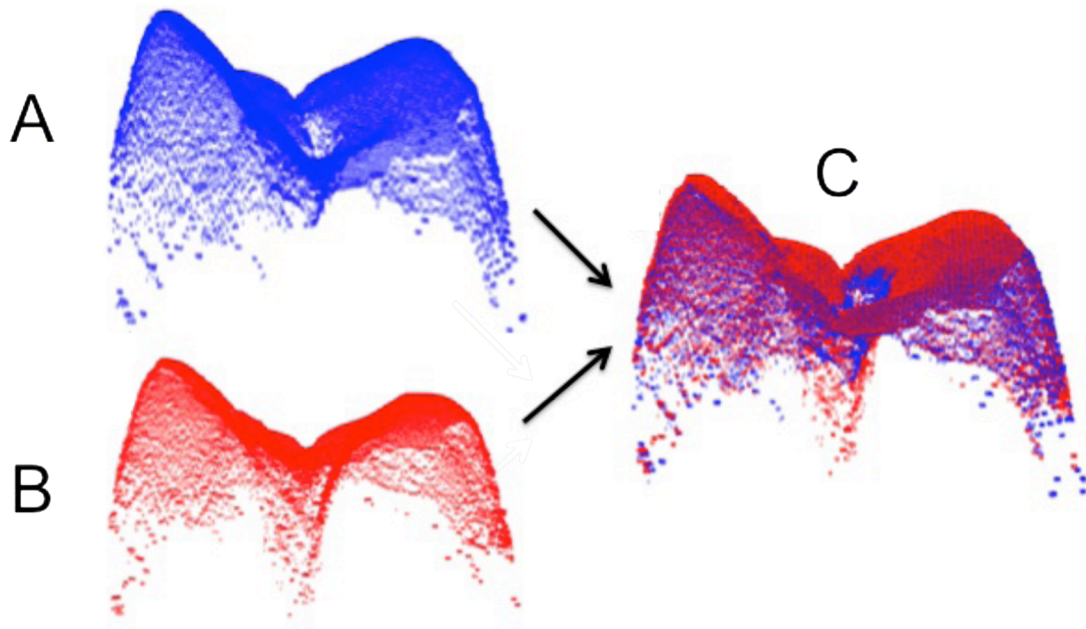


Figure 7.4: 3D surfaces imaged with co-polarization optical coherence tomography. (A) 3D pre-ablation surface; (B) 3D post-ablation; (C) Pre-/post-

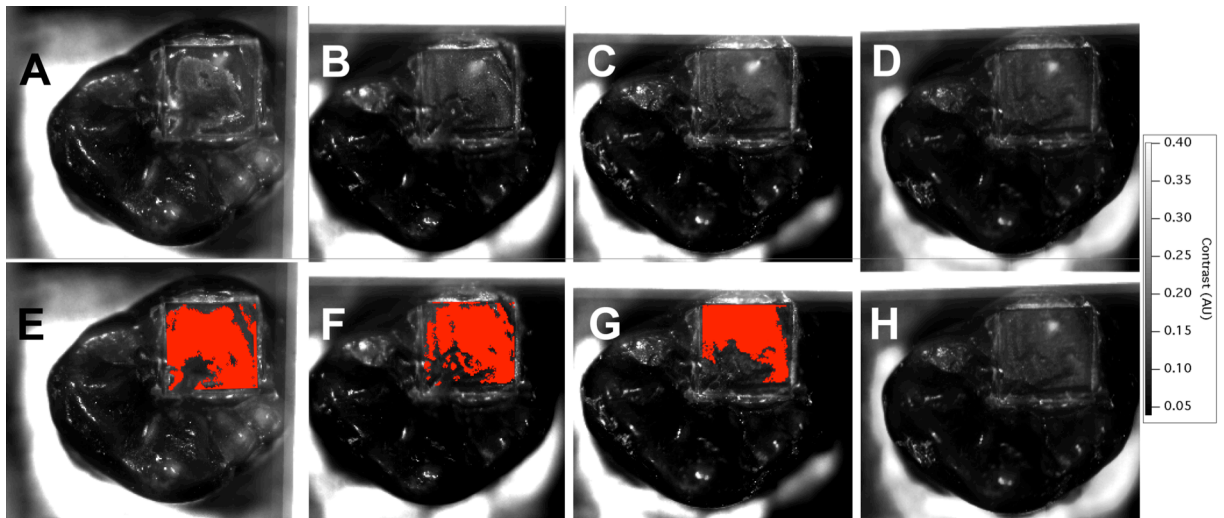


Figure 7.5: (A – D) Sequential near-infrared (NIR) reflectance images generated by the point-to-point NIR scanning system. (E – H) Look-up table (LUT; in red) overlaid on top of the acquired NIR reflectance images. (D, H) Final NIR point-to-point reflectance image of the sample. After 8 iterations (H), demineralization can no longer be detected, suggesting the lesion was completely removed within the 4 x 4 mm window.

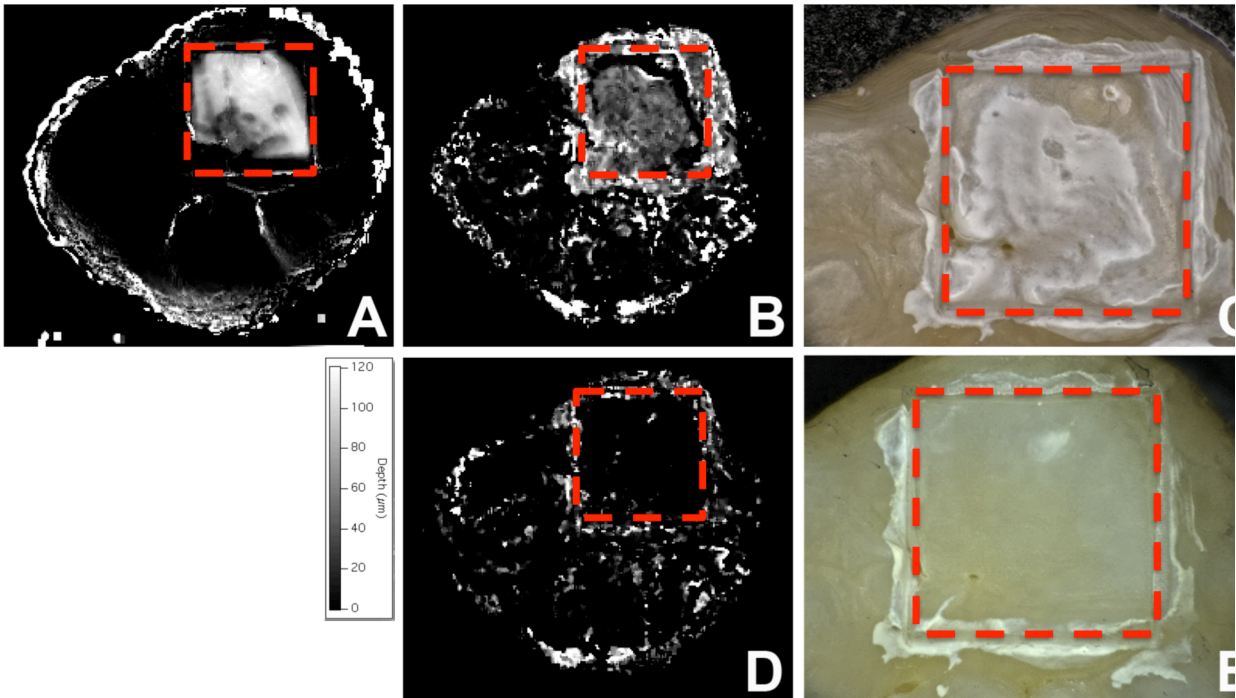


Figure 7.6: (A) 2D ablation depth map created by registering and subtracting the initial and final surfaces derived from co-polarization OCT scans showing the area ablated by the laser. (B) Initial 2D lesion depth map created from cross-polarized OCT. The area of ablation in (A) correlates well with the initial lesion area in (B). (C) Depth composition digital microscopy (DCDM) image of the artificially generated lesion before treatment (50x). The white chalky demineralization is visible on the occlusal surface. (D) Final 2D lesion depth map taken after selective caries ablation. The absence of bright pixels within the 4 x 4 mm window (outlined by the red dotted square) indicates lesion removal. (E) DCDM image of the occlusal surface after selective removal (50x). Note the absence of the white chalky demineralization.

7.7 REFERENCES

Almaz, E. C., Simon, J. C., Fried, D., & Darling, C. L. (2016). Influence of stains on lesion contrast in the pits and fissures of tooth occlusal surfaces from 800-1600-nm. *Proc SPIE Int Soc Opt Eng*, 9692.

Brezinski, M. (2006). *Optical Coherence Tomography: Principles and Applications*. London: Elsevier.

Bush, J., Davis, P., & Marcus, M. A. (2000). *All-Fiber Optic Coherence Domain Interferometric Techniques*. Paper presented at the Fiber Optic Sensor Technology II.

Chan, K. H., Chan, A. C., Fried, W. A., Simon, J. C., Darling, C. L., & Fried, D. (2015). Use of 2D images of depth and integrated reflectivity to represent the severity of demineralization in cross-polarization optical coherence tomography. *Journal of biophotonics*, 8(1-2), 36-45

Chan, K. H., & Fried, D. (in press). Multispectral cross-polarization reflectance measurements suggest high contrast of demineralization on tooth surfaces at wavelengths beyond 1300-nm due to reduced light scattering in sound enamel. *Journal of Biomedical Optics*.

Duplain, G., Boulay, R., & Belanger, P. A. (1987). Complex index of refraction of dental enamel at CO₂ wavelengths. *Appl. Optics*, 26, 4447-4451.

Dye, B. A., Tan, S., Lewis, B. G., Barker, L. K., Thornton-Evans, T. G., Eke, P. I., . . . Li, C. H. (2007). Trends in oral health status, United States, 1988-1994 and 1999-2004. *Vital Health Stat 11. 2007;(248):1-92*, 248, 1-92.

Eberhard, J., Bode, K., Hedderich, J., & Jepsen, S. (2008). Cavity size difference after caries removal by a fluorescence-controlled Er:YAG laser and by conventional bur treatment. *Clinical oral investigations*, 12(4), 311-318.

Eberhard, J., Eisenbeiss, A. K., Braun, A., Hedderich, J., & Jepsen, S. (2005). Evaluation of selective caries removal by a fluorescence feedback-controlled Er:YAG laser in vitro. *Caries Res*, 39(6), 496-504.

Featherstone, J. D., Barrett-Vespone, N. A., Fried, D., Kantorowitz, Z., & Seka, W. (1998). CO₂ laser inhibitor of artificial caries-like lesion progression in dental enamel. *Journal of dental research*, 77(6), 1397-1403.

Featherstone, J. D. B., Glena, R., Shariati, M., & Shields, C. P. (1990). Dependence of *in vitro* demineralization and remineralization of dental enamel on fluoride concentration. *J. Dent. Res.*, 69, 620-625.

Featherstone, J. D. B., & Nelson, D. G. A. (1987). Laser effects on dental hard tissue. *Adv. Dent. Res.*, 1(1), 21-26.

Fejerskov, O., & Kidd, E. (Eds.). (2003). *Dental Caries: The Disease and its Clinical Management*. Oxford: Blackwell.

Fowler, B., & Kuroda, S. (1986). Changes in heated and in laser-irradiated human tooth enamel and their probable effects on solubility. *Calcif. Tissue Int.*, 38, 197-208.

Fried, D., Featherstone, J. D., Le, C. Q., & Fan, K. (2006). Dissolution studies of bovine dental enamel surfaces modified by high-speed scanning ablation with a $\lambda = 9.3\mu\text{m}$ TEA CO₂ laser. *Lasers Surg Med*, 38(9), 837-845.

Fried, D., Featherstone, J. D. B., Darling, C. L., Jones, R. S., Ngaotheppitak, P., & Buehler, C. M. (2005). Early Caries Imaging and Monitoring with Near-IR Light. *Dental Clinics of North America - Incipient and Hidden Caries*, 49(4), 771-794.

Fried, D., Xie, J., Shafi, S., Featherstone, J. D. B., Breunig, T., & Lee, C. Q. (2002). Early detection of dental caries and lesion progression with polarization sensitive optical coherence tomography. *J. Biomed. Optics*, 7(4), 618-627.

Fried, W. A., Darling, C. L., Chan, K., & Fried, D. (2013). High Contrast Reflectance Imaging of Simulated Lesions on Tooth Occlusal Surfaces at Near-IR Wavelengths. *Lasers Surg. Med*, 45, 533-541.

Hevinga, M. A., Opdam, N. J., Frencken, J. E., Bronkhorst, E. M., & Truin, G. J. (2007). Microleakage and sealant penetration in contaminated carious fissures. *J Dent*, 35(12), 909-914.

Hsu, D. J., Darling, C. L., Lachica, M. M., & Fried, D. (2008). Nondestructive assessment of the inhibition of enamel demineralization by CO₂ laser treatment using polarization sensitive optical coherence tomography. *Journal of Biomedical Optics*, 13(5), 054027.

Jang, A. T., Chan, K. H., & Fried, D. (2017). Automated ablation of dental composite using an IR pulsed laser coupled to a plume emission spectral feedback system. *Proc SPIE Int Soc Opt Eng*, 10044.

Jepsen, S., Acil, Y., Peschel, T., Kargas, K., & Eberhard, J. (2008). Biochemical and morphological analysis of dentin following selective caries removal with a fluorescence-controlled Er:YAG laser. *Lasers in Surgery and Medicine*, 40(5), 350-357.

Kidd, E. A. (2004). How 'clean' must a cavity be before restoration? *Caries Res*, 38(3), 305-313.

Kuroda, S., & Fowler, B. O. (1984). Compositional, structural and phase changes in *in vitro* laser-irradiated human tooth enamel. *Calcif. Tissue Int.*, 36, 361-369.

LaMantia, N. R., Tom, H., Chan, K. H., Simon, J. C., Darling, C. L., & Fried, D. (2014). *High contrast optical imaging methods for image guided laser ablation of dental caries lesions*. Paper presented at the Lasers in Dentistry XX.

Law, M. W., & Chung, A. C. (2009). Efficient implementation for spherical flux computation and its application to vascular segmentation. *IEEE transactions on image processing : a publication of the IEEE Signal Processing Society*, 18(3), 596-612.

Lee, R. C., Kang, H., Darling, C. L., & Fried, D. (2014). Automated assessment of the remineralization of artificial enamel lesions with polarization-sensitive optical coherence tomography. *Biomed Opt Express*, 5(9), 2950-2962.

Lee, S. U., Yoon Chung, S., & Park, R. H. (1990). A comparative performance study of several global thresholding techniques for segmentation. *Computer Vision, Graphics, and Image Processing*, 52(2), 171-190.

Lee, Y. K., & Rhodes, W. T. (1990). Nonlinear image processing by a rotating kernel transformation. *Opt Lett*, 15(23), 1383-1385.

Nelson, D. G. A., Jongebloed, W. L., & Featherstone, J. D. B. (1986). Laser irradiation of human dental enamel and dentine. *NZ. Dent. J.*, 82, 74-77.

Nguyen, D., Chang, K., Hedayatollahnajafi, S., Staninec, M., Chan, K., Lee, R., & Fried, D. (2011). High-speed scanning ablation of dental hard tissues with a $\lambda=9.3 \mu\text{m}$ CO₂ laser:

adhesion, mechanical strength, heat accumulation, and peripheral thermal damage. *J. Biomed. Opt.*, 16(7), 071410:071411-071418.

Otsu, N. (1979). A Threshold Selection Method from Gray-Level Histograms. *IEEE Trans. Syst. Man Cybern.*, 9(1), 62-66.

Powell, G. L., & Whisenant, B. K. (1991). Comparison of three lasers for dental instrument sterilization. *Lasers Surg Med*, 11(1), 69-71.

Rogowska, J., Bryant, C. M., & Brezinski, M. E. (2003). Cartilage thickness measurements from optical coherence tomography. *J Opt Soc Am A Opt Image Sci Vis*, 20(2), 357-367.

Simon, J. C., Chan, K. H., Darling, C. L., & Fried, D. (2014). Multispectral near-IR reflectance imaging of simulated early occlusal lesions: Variation of lesion contrast with lesion depth and severity. *Lasers Surg Med*, 46(3), 203-215.

Tao, Y. C., & Fried, D. (2009). Near-infrared image-guided laser ablation of dental decay. *Journal of Biomedical Optics*, 14(5), 054045.

Tom, H., Chan, K. H., Darling, C. L., & Fried, D. (2016). Near-IR Image-Guided Laser Ablation of Demineralization on Tooth Occlusal Surfaces. *Lasers Surg Med*, 48(1), 52-61.

Vila Verde, A., Ramos, M. M., & Stoneham, A. M. (2009). Benefits in cost and reduced discomfort of new techniques of minimally invasive cavity treatment. *Journal of dental research*, 88(4), 297-299.

Zuerlein, M., Fried, D., Featherstone, J., & Seka, W. (1999). Optical properties of dental enamel at 9 - 11 μm derived from time-resolved radiometry. *Special Topics IEEE J Quant. Elect.*, 5((4)), 1083-1089.

CHAPTER VIII

CONCLUDING REMARKS

8.1 CONCLUDING REMARKS

These studies have demonstrated that lasers can be guided using feedback mechanisms for removing dental lesions and pre-existing restorations with high selectivity. The developed feedback laser systems have the potential of replacing conventional methods. Furthermore, new methods were developed for selectivity and although these studies were done *in vitro*, these methods can be effortlessly translated for *in vivo* clinical procedures i.e. evaluating *in vivo* cavity preparations and/or composite replacement procedures.

8.1.1 Spectral – guided composite ablation

Previous experiments demonstrated that lasers can be used for removing various restorative filling materials (Hibst & Keller, 1991). Furthermore, Dumore et al. has demonstrated that the optical emission spectra of the luminous plasma plume produced during composite and enamel ablation can be used to differentiate between enamel and composite ablation (Dumore & Fried, 2000). The study presented in **Chapter II** was to develop an autonomous spectral – guided feedback system and demonstrate its high selectivity. In the next **Chapter (III)**, the composite removal system was further investigated to determine the safety and efficacy of composite removal by measuring the pulpal temperature during laser treatment and surface modulation post treatment. Pulpal temperatures remained well within the safe levels and post-ablative microscopy and 3D tomographic scans determined the high selectivity of composite ablation. **Chapter IV** demonstrated that a composite removal system is clinical feasible by developing a miniaturized system using a set of less expensive but higher throughput set of photodetectors filtered at wavelengths specific to the emission lines of composite

and enamel. The average excess enamel removed (0.03 mm^3) with the laser demonstrates higher selectivity compared to the conventional handpiece.

8.1.2 Near – Infrared image guided caries ablation

Previous studies have shown that near – infrared (NIR) images at 1450-nm produce high contrast images of dental caries and these images were used to guide a CO₂ laser for selective caries ablation (Chan & Fried, 2012; Tom, Simon, Chan, Darling, & Fried, 2014). However, it was challenging to evaluate its selectivity without obtaining the lesion volume prior to removal. **Chapter IV** researched methods of quantifying the lesion volume *in vivo* using optical coherence tomography and projecting lesion depth and severity onto 2D images to be easily compared with lesion images captured at varied wavelengths. In addition, detecting lesions with NIR reflectance can be improved with higher lesion contrast. The study in **Chapter V** investigated the use of wavelengths beyond 1450-nm for lesion detection and found that longer wavelengths had significantly higher contrast. Imaging using wavelengths beyond 1700-nm was evaluated and it was determined that improved lesion contrast correlated with lower enamel scattering and the best performance came from 1950-nm reflectance imaging. Previous image – guided laser ablation methods relied on two separate systems consisting of a caries imaging setup and a scanning laser, and caused alignment issues. **Chapter VI** discusses an integrated system, where imaging and scanning lasers were integrated into a combined system. The ablation laser and the imaging laser were coaxially aligned so that the light scattering signal emanating from the lesion is precisely positioned for subsequent laser scanning ablation. Point-to-point NIR images is an improvement in terms of signal throughput and cost over previously used NIR InGaAs

cameras. We have also employed polarization – sensitive optical coherence tomography (PS-OCT) for evaluating the selectivity of caries removal and this can be done *in vivo*.

PS-OCT is advantageous in determining the initial lesion volume and the removal volume. Using, PS-OCT, we found that 99% of the artificially generated lesion was removed using the image-guided approach.

8.2 FUTURE WORK

Further research is required to evaluate the clinical feasibility of these feedback techniques *in vivo*. The spectral guided ablation system in **Chapter IV** introduced a design utilizing fiberoptic bundles. These same fiberoptic bundles can be used to acquire NIR images and direct the laser scanning of caries lesions. The convoluted topography of the tooth can obscure the imaging of occlusal pits and fissures, but with an arrangement of multiple fibers, the system is able to visualize the tooth structure from multiple vantage points simultaneously.

Further *in vitro* measurements can be made between the PS-OCT and μ CT scans for further verification of selective laser removal. The lesion detection and removal volume algorithms created for PS-OCT can be translated for μ CT measurements. Additionally, these *in vivo* methods developed for evaluating the selectivity of caries removal can be used to monitor the inadvertent removal of sound structure from calculus debridement, tooth polishing and whitening. NIR images have also been shown to detect calculus and root caries lesions with high contrast and developing image – guided approaches for selective removal would be straightforward. This research can potentially advance the standard of healthcare with an emphasis in increased conservative care.

8.3 REFERENCES

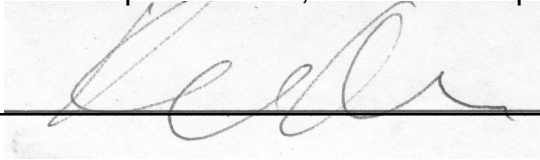
- Chan, K. H., & Fried, D. (2012). Selective Removal of Demineralization Using Near Infrared Cross Polarization Reflectance and a Carbon Dioxide Laser. *Proceedings - Society of Photo-Optical Instrumentation Engineers*, 8208.
- Dumore, T., & Fried, D. (2000). Selective ablation of orthodontic composite by using sub-microsecond IR laser pulses with optical feedback. *Lasers in Surgery and Medicine*, 27(2), 103-110.
- Hibst, R., & Keller, U. (1991). *Removal of dental filling materials by Er:YAG laser radiation*. Paper presented at the Lasers in Orthopedic, Dental, and Veterinary Medicine.
- Tom, H., Simon, J. C., Chan, K. H., Darling, C. L., & Fried, D. (2014). Near-infrared imaging of demineralization under sealants. *J Biomed Opt*, 19(7), 77003.

Publishing Agreement

It is the policy of the University to encourage the distribution of all theses, dissertations, and manuscripts. Copies of all UCSF theses, dissertation, and manuscripts accessible to the public and will preserve these to the best of their abilities, in perpetuity.

I hereby grant permission to the Graduate Division of the University of California, San Francisco to release copies of my thesis, dissertation, or manuscript to the Campus Library to provide access and preservation, in whole or in part, in perpetuity.

Author Signature _____

A handwritten signature in black ink, appearing to be 'K. Lee', written over a horizontal line.

Date 12/3/2018